Genetic profiling of a cone-dominated retina and cone photoreceptor subtypes

Vincent P. Kunze

Date of birth

June 8, 1986

Place of birth

Kempten (Allgäu)

Accepted thesis

Doctor rerum naturalium (Dr. rer. nat.)

Institute for Biology and Environmental Sciences

Carl von Ossietzky Universität Oldenburg

First examiner:	Prof. Dr. Karl-Wilhelm Koch
Second examiner:	apl. Prof. Dr. Karin Dedek
Date of thesis defense:	December 18, 2017

Abstract

Mammals have two major types of sensory neurons in the retina: rods, specialized for vision in dim-light, and cones for vision in well-lit conditions and the perception of color. In my thesis, I characterized features of cone photoreceptor subtypes and the cone-dominated retinae of the tree shrew and the thirteen-lined ground squirrel.

In tree shrew, I described morphological and transcriptomic changes during development. Compared to mice, the general morphology of the developing retina was similar. There were subtle differences in the onset of transcription factors and in the relative timepoints of photoreceptor genesis. The transcriptomic analysis revealed and onset Wif1-expression after birth, a gene that could potentially suppress rod development in the tree shrew.

Furthermore, I looked at molecular differences in cone photoreceptor subtypes. Most mammals have two cone types, namely S- and M-cones. They diverge in their sensitivity to different wavelengths of light, based on their expression of different light-sensitive proteins: S-opsin for blue light and M-opsin for green light. Until now, cones have been classified mostly by the opsin they express. The purpose of this project was to identify genetic differences in cones and, more specifically, to find genes that are involved in cone synapse formation. For this study, I used the thirteen-lined ground squirrel that, in contrast to mouse, is diurnal and has a cone-dominated retina. The two cone types are morphologically indistinguishable, so I developed a protocol to dissociate and label live cells with an antibody targeting the extracellular domain of S-opsin. I then manually collected single cells for next-generation sequencing. The analysis of the transcriptome revealed differentially expressed genes that define cone identity beyond their expression of S- or M-opsins. I presented immunohistochemical evidence for the applicability of my data and, additionally, I identified synapse-specific genes in S-cones: Flna and Cadm1. They are known to play roles in synapse assembly in the brain. In addition, I tested AAV-delivered GFP-expression in the squirrel retina. This laid the groundwork for functional studies in the ground squirrel.

At last, I looked at differences in mRNA expression in photoreceptors of the hibernating ground squirrel. Photoreceptors undergo large morphological changes in this phase. I concluded that the phototransduction machinery is not affected by hibernation. In addition, I identified differentially expressed genes that may play roles in the adaptive changes of photoreceptor morphology during hibernation: Pebp1, Ctnnd1 and Slitrk3.

Zusammenfassung

Säugetiere haben zwei Haupttypen von sensorischen Neuronen in der Netzhaut: Stäbchen, die auf das Sehen bei schwachem Licht spezialisiert sind und Zapfen für das Sehen in gut beleuchteten Zuständen und für die Wahrnehmung von Farbe. In dieser Arbeit habe ich Eigenschaften der einzelnen Zapfentypen und den zapfendominierten Retinae des Spitzhörnchens und des Dreizehnstreifen-Hörnchens charakterisiert.

Im Spitzhörnchen habe ich morphologische und transkriptomische Veränderungen während der Entwicklung analysiert. Im Vergleich zu Mäusen war die Morphologie der sich entwickelnden Retina ähnlich. Es gab geringe zeitliche Unterschiede in der Expression von Transkriptionsfaktoren und bei den relativen Zeitpunkten der Entstehung der Photorezeptoren. Die transkriptomische Analyse zeigte eine starke Wif1-Expression nach der Geburt. Dieses Gen könnte die Stäbchenentwicklung im Spitzhörnchen unterdrücken.

Des Weiteren habe ich molekulare Unterschiede in den Zapfentypen untersucht. Die meisten Säugetiere besitzen zwei Zapfentypen, nämlich S- und M-Zapfen. Sie unterscheiden sich in ihrer Empfindlichkeit gegenüber verschiedenen Wellenlängen des Lichts, basierend auf ihrer Expression von verschiedenen lichtempfindlichen Proteinen: S-Opsin für blaues Licht und M-Opsin für grünes Licht. Bislang wurden Zapfen meist allein durch das Opsin klassifiziert, das sie exprimieren. Das Ziel dieses Projekts war es, genetische Unterschiede in Zapfen zu identifizieren und Gene zu finden, die an der Bildung von Zapfensynapsen beteiligt sind. Für diese Studie wurde das Dreizehnstreifen-Hörnchen untersucht, das im Gegensatz zur Maus tagaktiv ist und über eine zapfendominierte Retina verfügt. Die beiden Zapfentypen sind morphologisch nicht unterscheidbar, deswegen habe ich ein Protokoll entwickelt, um lebende Zellen zu dissoziieren und mit einem Antikörper zu markieren, der an die extrazelluläre Domäne von S-Opsin bindet. Anschließend habe ich manuell einzelne Zellen für die RNA-Sequenzierung isoliert. Die Analyse zeigte differenziell exprimierte Gene, welche die unterschiedliche Identität der S- und M-Zapfen definieren. Immunhistochemische Belege zeigten die

Anwendbarkeit meiner Daten. Des Weiteren habe ich Synapsen-spezifische Gene in S-Zapfen identifiziert: Flna und Cadm1. Von denen ist bekannt, dass sie bei der Synapsenbildung im Gehirn eine Rolle spielen. Zusätzlich habe ich die AAV-transduzierte GFP-Expression in der Retina des Dreizehnstreifen-Hörnchens getestet. Damit wurde der Grundstein für funktionelle Untersuchungen in diesem Modell gelegt.

Abschließend habe ich Unterschiede in der mRNA-Expression in Photorezeptoren des Dreizehnstreifen-Hörnchens während des Winterschlafs untersucht. Photorezeptoren zeigen große morphologische Veränderungen in dieser Phase. Ich kam zu dem Schluss, dass die Expression von Phototransduktionsgenen nicht durch den Winterschlaf beeinflusst wurde. Zudem habe ich differentiell exprimierte Gene identifiziert, die bei den adaptiven Veränderungen der Photorezeptormorphologie während des Winterschlafs eine Rolle spielen könnten: Pebp1, Ctnnd1 und Slitrk3.

List of Contents

List of Figures

List of Tables

Abbreviations

AAV	Adeno-associated virus
AC	Amacrine cell
ACUC	Animal Care and Use Committee
ARAC	Animal Research Advisory Committee
AVMA	American Veterinary Medical Association
BSA	Bovine serum albumin
bp	base pairs
Ca^{2+}	Calcium ions
CB	Cell body
cDNA	Complementary DNA
cGMP	Cyclic guanosine monophosphate
ChAT/Cht	Choline O-acetyltransferase
CMV	Cytomegalovirus
CNG	Cyclic nucleotide-gated
CRISPR	Clustered regularly interspaced short palindromic repeats
DAPI	4',6-diamidino-2-phenylindole
dim1	Dimension 1
DKO	Double knockout
DNA	Deoxyribonucleic acid
E[n]	Embryonic day [n]
ECM	Extracellular matrix
EDTA	Ethylenediaminetetraacetic acid
eGFP	Enhanced green fluorescent protein
FH	Fiber of Henle
g	Gram
GC	Ganglion cell
GCL	Ganglion cell layer
GEO	Gene Omnibus
GFP	Green fluorescent protein
GPCR	G-protein-coupled receptor
HBSS	Hank's balanced salt solution
HC	Horizontal cell
IHC	Immunohistochemistry
ILM	Inner limiting membrane

IPL	Inner plexiform layer
IS	Inner segment(s)
KO	Knock-out
logFC	log-fold change
LSM	Laser-scanning microscopy
MDS	Multidimensional scaling
misc.	Miscellaneous
mg	Milligram
µL	Microliter
mL	Milliliter
mm	Millimeter
NADPH	Nicotinamide adenine dinucleotide phosphate
NBL	Neuroblastic layer
NEI	National Eye Institute
NFL	Nerve fiber layer
NIH	National Institutes of Health
OLM	Outer limiting membrane
OPL	Outer plexiform layer
OS	Outer segment(s)
P[n]	Postnatal day [n]
PBS	Phosphate-buffered saline
PBST	PBS-Triton X-100
PCR	Polymerase chain reaction
PDE	Phosphodiesterase
PFA	Paraformaldehyde
PKC	Protein kinase C
Rcv/Rcvrn	Recoverin
RGC	Retinal ganglion cell
RNA	Ribonucleic acid
RNA-seq	RNA-sequencing
RT	Room temperature
SCBC	S-cone bipolar cell
Sop	S-opsin
TBS	Tris-buffered saline

1 Introduction

1.1 The mammalian retina

The retina is the neural tissue at the back of the eye that signals to the brain in response to light (figure 1). The cell bodies of the retinal neurons are organized in three layers (Dowling, 1987): the outer nuclear layer (ONL), the inner nuclear layer (INL), and the ganglion cell layer (GCL). In between these nuclear layers are two synaptic layers: the outer and the inner plexiform layer (OPL, IPL).

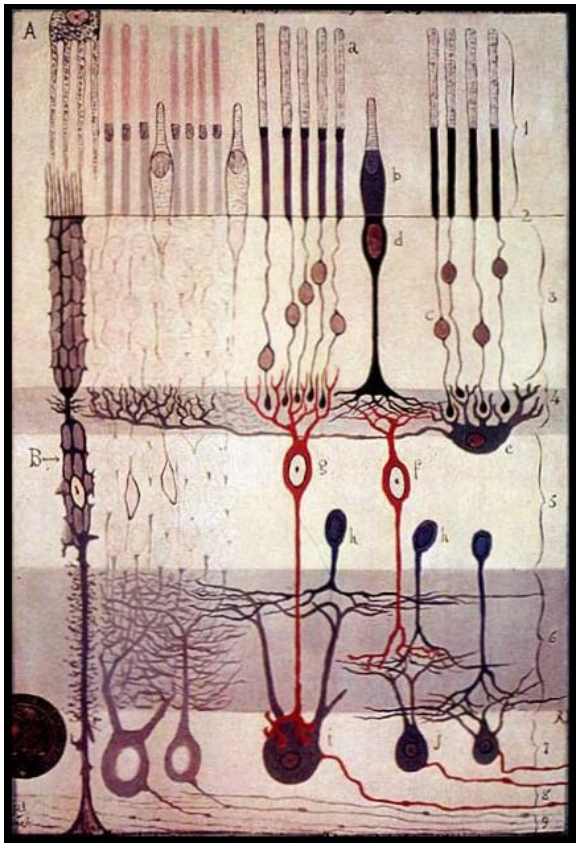

Figure 1 Structure of the mammalian retina. A drawing by Santiago Ramon y Cajal (1900). 1. Inner and outer segments. 2. Outer limiting membrane. 3. Outer nuclear layer. 4. Outer plexiform layer. 5. Inner nuclear layer. 6. Inner plexiform layer. 7. Ganglion cell layer. 8. Nerve fiber layer. 9. Internal limiting membrane. A. Pigmented cells. B. Müller cell. a. Rods. b. Cones. c. Rod nucleus. d. Cone Nucleus. e. Horizontal cell f. Cone-associated bipolar cell. g. Rod-associated bipolar cell. h. Amacrine cells. i/j. Ganglion cells. Image under public domain.

The cell bodies of photoreceptors are localized in the ONL. Photoreceptors express light-sensitive proteins of the opsin family, and their activation starts the process of transforming light information into chemical signals that are relayed to cells in the INL (Kolb, 2005; Lamb, 2007).

The INL contains horizontal cells, bipolar cells and amacrine cells. Horizontal cells contact multiple photoreceptors in the OPL. They integrate and modulate signals from distal photoreceptors through feedback inhibition. Bipolar cells transfer the signal vertically to the IPL, where they synapse onto amacrine cells and ganglion cells (RGCs). Amacrine cells are also lateral neurons and they have their processes in the IPL. They integrate and modulate signals to shape transmission to RGCs by providing inhibitory feedback to synaptic terminals of bipolar cells or ganglion cell dendrites (Kolb, 2005b).

The GCL contains displaced amacrine cells and retinal ganglion cells. RGCs integrate the information they receive and relay it to higher brain regions through spike trains. Different types encode a variety of visual features, e.g., contrast, size, movement, color. There are also non-image-forming RGCs that control the pupillary reflex or the circadian clock (Güler et al., 2008; Hatori et al., 2008).

In addition to the described neurons, there are also Müller glial cells that span across all layers of the retina. They play a supportive role, as they form an architectural support of the retina. Among other functions, they maintain the homeostasis of the retina and recycle neurotransmitters (Reichenbach and Robinson, 1995)

1.2 Photoreceptor cells

Mammals have two major types of photoreceptors in the retina: Rod photoreceptors, specialized for dim-light conditions, and cone photoreceptors for bright light and the perception of color (Kolb, 2005). Cone types differ in their sensitivity to different wavelengths of light, based on the expression of different opsin proteins (figure 2). Most mammals are dichromats. They have S-cones that express short-wavelength opsin (blue or S-opsin) and M-cones that express medium-wavelength

opsin (green or M-opsin). Some primates are trichromats and carry an additional L-cone that expresses long-wavelength opsin (red or L-opsin).

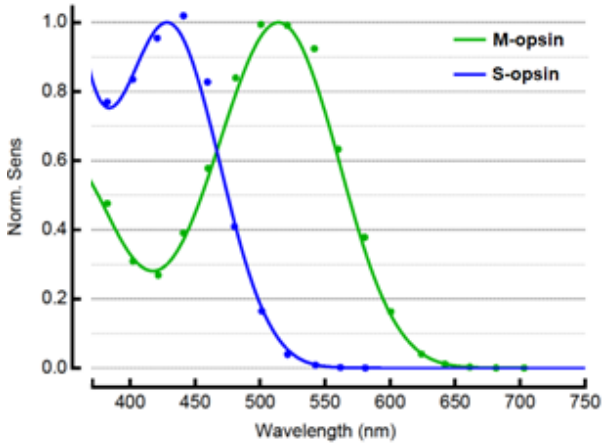

Figure 2 Spectral sensitivity curves of cone opsins found in the retina of the golden-mantled ground squirrel (*Callospermophilus lateralis*). The opsins expressed in M- and S-cones show different sensitivities to light of varying wavelengths. Image provided by Juan Angueyra (National Eye Institute, NIH) based on data from Kraft, 1988.

Structurally, photoreceptors consist of the outer segment (OS), the inner segment (IS), the cell body that contains the nucleus, and the synaptic terminal (figure 3). Rod outer segments are generally thinner and longer than cone OS. Rhodopsin is embedded in disks, enclosed membrane organelles that are densely packed in the rod OS. Cone opsins on the other hand are embedded in the “open” disk-like structures, formed by foldings of the plasma membrane of cones (Mustafi et al., 2009). Inner segments contain mitochondria, ribosomes and membranes. In cones of the tree shrew, mitochondria are organized in a single large ellipsoid (Foelix et al., 1987). Cone synaptic terminals are called cone pedicles, they are generally larger than rod terminals, the rod spherules. The synaptic terminals of both types are filled with synaptic vesicles, close to the synaptic ribbons. Each rod spherule has one to two ribbons, whereas each cone pedicle has dozens (Migdale et al., 2003; Mustafi et al., 2009).

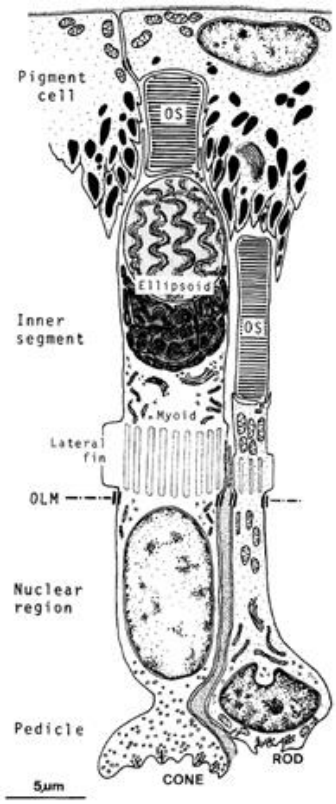

Figure 3 Depiction of a cone and a rod photoreceptor in the adult tree shrew retina. Compared to other mammals, tree shrew cones have relatively small cone outer segments and a large ellipsoid filled with mitochondria. OLM: outer limiting layer; OS: outer segment. From: Foelix et al. (1987). Reprint permission was obtained from the publisher. © Springer

The process of phototransduction is similar in both rods and cones (Lamb, 2013). The transformation of light information into chemicals signals begins in the outer segments of photoreceptors (figure 3). Photons that hit the chromophore 11-*cis*-retinal in the receptor protein opsin cause the photoisomerization to all-*trans*-retinal. This triggers a series of conformational changes in the opsin part. Opsins belong to the large family of G-protein coupled receptors (GPCR). After activation by light, they couple to G-proteins, which are named rod or cone transducin, where they catalyze the exchange of GDP to GTP. The activated G-protein α-subunit removes the inhibitory γ-subunits of the effector enzyme phosphodiesterase 6 (PDE6). Upon activation, PDE6 hydrolyzes cGMP that is bound to the cyclic nucleotide gated (CNG) channel. This causes the CNG channels to close, thus

stopping the influx of Na^+ and Ca^{2+} (the “dark current”), which changes the membrane potential of the photoreceptor. This eventually leads to a reduced release of glutamate at the synapse, the signal received by the downstream neurons (Luo et al., 2008).

Cones and rods express different isoforms of the same proteins for the phototransduction process (Fu and Yau, 2007; Lamb, 2013). The different isoforms lead to the different characteristics of rods and cones: rods are much more sensitive to light, they can respond to a single photon (Korenbrot, 2012; Tachibanaki et al., 2001; Kefalov et al., 2005; Luo et al., 2008). Cones require more light to become activated, and photoresponses in cones are faster, which provides a higher temporal resolution. In addition, cones can hardly be saturated.

Molecular differences between S- and M-cones are harder to identify. Until now, cone subtypes have been classified mostly by the opsin they express. Aside from the opsins, S- and M-cones share the same phototransduction machinery (Lamb et al., 2007). There were reports of subtype-specific, differential protein expression in different species, e.g., carbonic anhydrase in human S-cones, the calcium channel α_{1D}-subunit in tree shrew M-cones, rod arrestin and NADPH diaphorase in tree shrew S-cones (Nork et al., 1990; Morgans, 1999; Müller et al., 1989; Petry and Murphy, 1995).

In addition, we know that S- and M-cones are wired differently in the outer plexiform layer. S-cones for example synapse onto the S-cone bipolar cells, which was originally described by Mariani et al. (1984) in primates. Later this was confirmed in other species (ground squirrel, Puller et al., 2011; rabbit, Liu and Chow, 2007; mouse, Haverkamp et al., 2005). This type is not contacted by rods or M-cones.

1.3 Development of the retina

Retinal cells originate from multipotent progenitors in a specific order. This order is highly conserved across vertebrate species (Lamb et al., 2007). Birthdating

studies have revealed when individual cell types are born, i.e., exit the cell cycle (Sidman, 1961; Young, 1985). In these studies, mice were injected with ^{3}H-thymidine at different time points. Cells that have exited the cell cycle retain the label permanently, which allowed the investigators to examine the labeled cells after the animals were mature. These experiments showed that retinal cells are born in two waves, with ganglion cells, amacrine cells, horizontal cells and a subtype of cone photoreceptors exiting the cell cycle first. In the second wave, Müller cells and bipolar cells are born. Rods are different because they appear over nearly the whole time course, starting to develop shortly after the onset of the first wave (Cepko et al., 1996; figure 4).

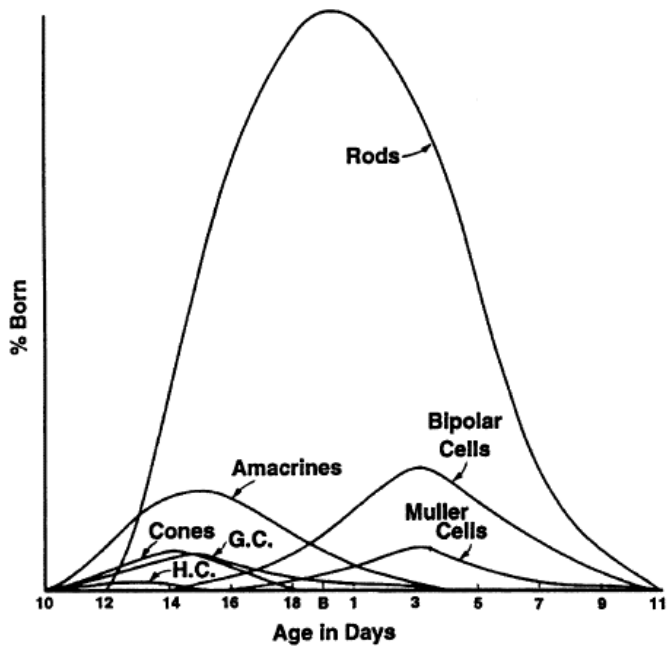

Figure 4 Order of birth of retinal cells in the mouse retina. Birthdating studies with ^{3}H-thymidine revealed the order of cell type genesis. GC: Ganglion cells; HC: amacrine cells.
Modified by Cepko et al., 1996 from Young et al., 1985. Reprint permission for both versions were obtained from the publishers (© National Academy of Sciences, © Wiley)

1.4 Photoreceptor development

The fate of a cell progenitor is determined by the combinatorial code of transcription factors. In the retina, the earliest steps in the development of photoreceptors are mediated by the notch receptor and its downstream targets (Yaron et al., 2006; Jadhav, 2006). Inhibition of this receptor, that keeps cells in the cell cycle, drives a progenitor cell to commit to becoming a photoreceptor precursor. The exact mechanisms for this step are still unknown. Once the cell has become a photoreceptor precursor, six transcription factors determine if it differentiates into a rod, an S-cone or an M-cone (figure 5; Swaroop et al., 2010).

Otx2 is expressed in all cells that commit to the photoreceptor cell fate. Experiments in KO mice have shown that these mice lose all photoreceptors, as well as bipolar cells and horizontal cells (Nishida et al., 2003).

Crx acts downstream of Otx2 and is also important for all photoreceptor types. Crx-deficient mice develop photoreceptors, but they fail to express a number of photoreceptor-specific genes. They also lack outer segments, which leads to retinal degeneration (Furukawa et al., 1999).

Nrl is the key transcription factor for rod development. Nrl-KO mice do not have any rods; instead, the majority of photoreceptors in these mice are S-cone-like (Mears et al., 2001).

Nr2e3 is a downstream target of Nrl (Swaroop et al., 2010) and acts as a suppressor of cone genes. Mutant mice have been reported to express cone genes in rods (Chen et al., 2005).

Rorβ is expressed in both cones and rods and may play a role upstream of Nrl. Rorβ-deficient mice fail to develop rod photoreceptors, instead they have a high number of S-cone-like photoreceptors. At the same time, it shares characteristics with Crx, because all remaining photoreceptors do not have outer segments (Jia et al., 2009).

Trβ2, a nuclear receptor, is a thyroid hormone-regulated transcription factor. Its activation induces M-cone gene expression. KO-mice do not express M-opsin. Instead, all cones express S-opsin (Ng et al., 2001; Forrest and Swaroop, 2012).

The deletion of certain transcription factors (Nrl, Trβ2, Rorβ) leads to an absence of rods or M-cones and to an increase in S-cone-like photoreceptors. This observation gave rise to the hypothesis that the S-cone cell fate could be the default pathway (Swaroop et al., 2010). This means, if Nrl or Trβ2 are not induced in a developing photoreceptor, the cell becomes an S-cone.

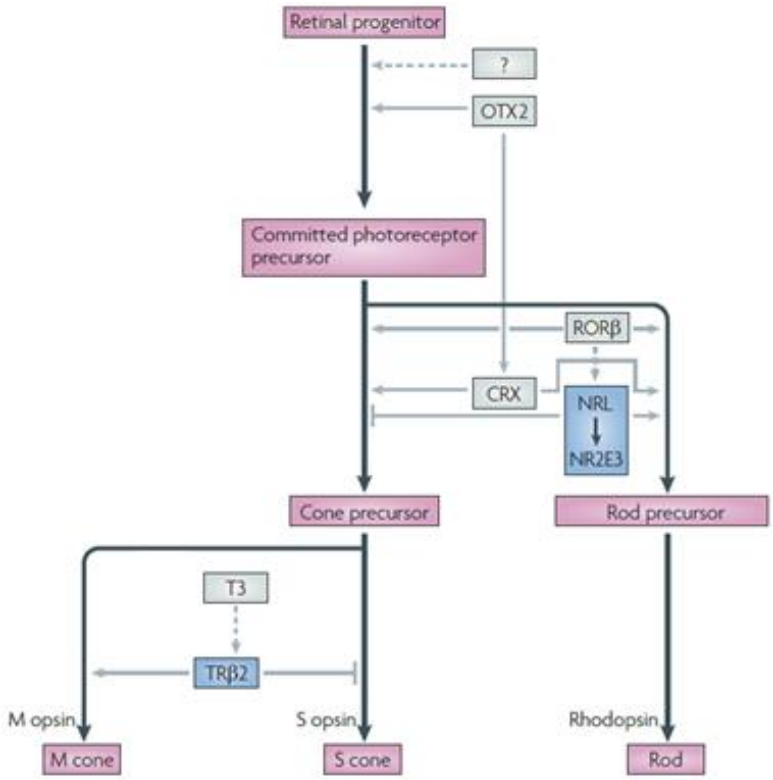

Figure 5 Transcription factors in photoreceptor development. The differential expression of transcription factors determines the cell fate of a photoreceptor progenitor. Adapted by permission from Macmillan Publishers Ltd: Nature Neuroscience Reviews. Swaroop et al., 2010.

1.5 The tree shrew and the thirteen-lined ground squirrel as model organisms for cone-dominated vision

Tree shrew

Tree shrews (*Tupaia belangeri*) are diurnal animals that are native to southeast Asia (figure 6). They have been placed in close taxonomic relationship to primates; its exact position is still under debate (Fan et al., 2013; Springer and Gatesy, 2016). However, their retina is different from primates, as they do not have L-cones or a fovea. Tree shrews have a cone-dominated retina with a photoreceptor ratio of approx. 83% M-cones, 10% S-Cones and 7% rods. The density of cones ranges from 14,300 cells/mm^2 to 35,300 mm^2 (Petry et al., 1993).

Figure 6 Photograph of a tree shrew (*Tupaia belangeri*). Image rights: CC BY-SA Author: Cymothoa exigua. Wikimedia Commons.

Thirteen-lined ground squirrel

The thirteen-lined ground squirrel (*Ictidomys tridecemlineatus*) is a diurnal, omnivorous animal and belongs to the order Rodentia (figure 7). It is native to North America. This squirrel has a cone-dominated retina, it is estimated to consist of 80% M-cones, 6% S-cones and 14% rods. The density of photoreceptors ranges from

40,000 cells/mm^2 around the optic nerve head to 90,000 cells/mm^2 in the visual streak (Kryger et al., 1998; Sajdak et al., 2016).

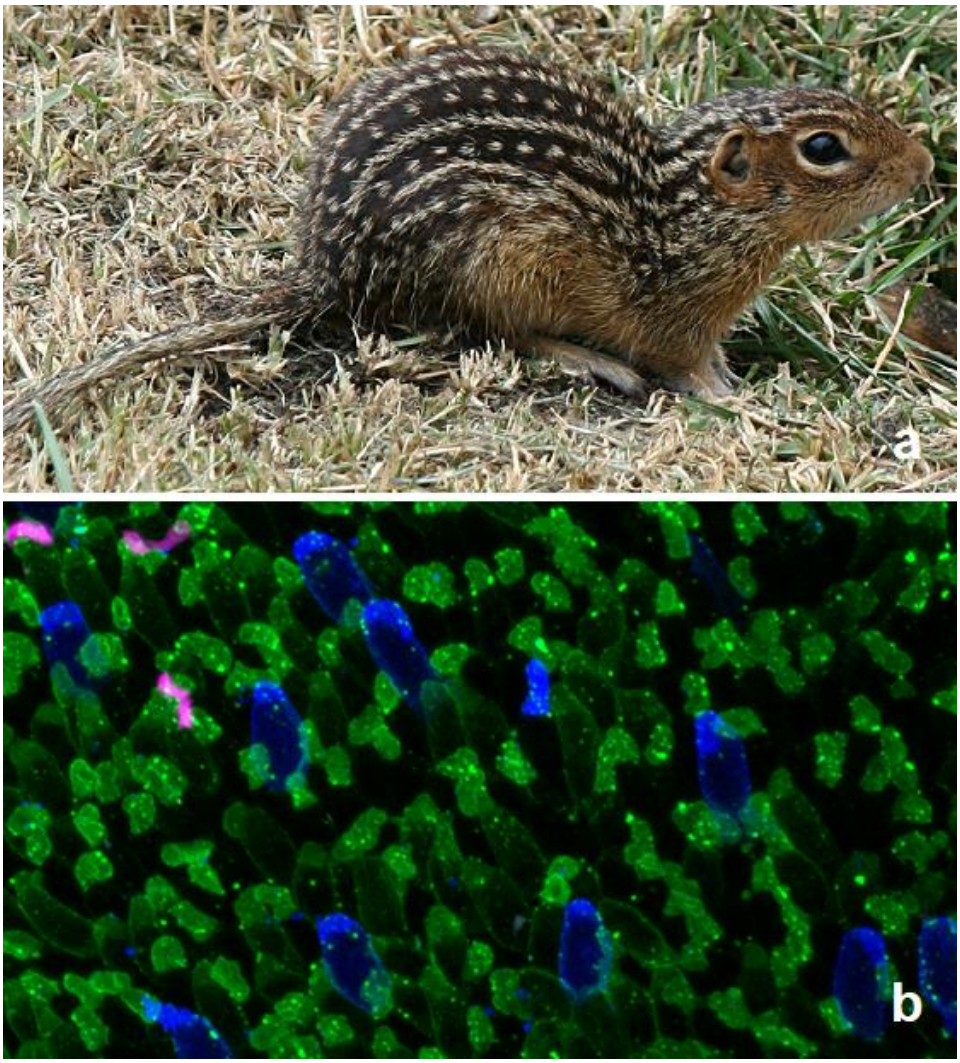

Figure 7 The thirteen-lined ground squirrel. **a** Photograph of an adult thirteen-lined ground squirrel (*Ictidomys tridecemlineatus*). **b** The cone-dominated retina of a thirteen-lined ground squirrel. Flat-mount; inner and outer segments. Labeled are S-cones (blue, anti-S-opsin), M-cones (green, anti-M-opsin) and rods (magenta, anti-rhodopsin).
Image rights for a): CC BY Marit & Toomas Hinnosaar, flickr.com

The ground squirrel is a hibernating species. When entering torpor, its catabolism switches from carbohydrates to lipids (van Breukelen and Martin, 2015) and the body temperature lowers from 38 °C to the surrounding temperature which could be as low as 0 °C. Its heart rate is reduced to approx. 5% of the normal rate and it

breathes about once every 30 min. Every 1-2 weeks, the torpor is interrupted by interbout arousals, a period of 12 – 24 h in which the body temperature rises back to 38 °C. The mechanisms behind the circannual rhythm of the squirrel are not entirely clear yet (Merriman et al., 2016).

During hibernation, the retina of the squirrel undergoes adaptive changes. Cone outer segments are shortened, the number and size of the ellipsoid mitochondria is reduced, the ribbons in the synaptic terminals are dramatically smaller or detached, and the number of synaptic vesicles is reduced (Kuwabara, 1975; Gruber et al., 2006, Mehta et al, 2013; Merriman et al., 2016). The changes show an appearance similar to cone degeneration in a rabbit model for retinitis pigmentosa (Jones et al., 2011).

1.6 The S-cone specific bipolar cell synapse

Parts of this thesis try to answer questions about differences in S- and M-cone photoreceptors. These subtypes are mostly classified by the opsin they express. There were only a handful of reported differences (see section 1.2). The majority of cones in mice express both S- and M-opsin (Applebury et al., 2000). “True” S-cones that only express S-opsin form specific synapses with S-cone bipolar cells (SCBCs; Haverkamp et al., 2005). Li Jia (National Eye Institute, NIH) investigated if the alteration of opsin-expression affects the S-cone to SCBC synapse. She crossed S-opsin-KO- and Thrb-KO mice with Clomeleon mice (Kuner and Augustine, 2000). S-opsin-KO mice do not express S-opsin, Thrb-KO mice lack M-opsin expression. Thrb is a key transcription factor for M-cone development. The majority of cones in Thrb-KO mice express only S-opsin (Ng et al., 2001). Clomeleon mice express a chloride-sensitive fluorescent protein under the Thy1 promoter. The protein labels ganglion cells, a few amacrine cells and SCBSs (Haverkamp et al., 2005). The label in SCBCs also labels their dendrites. Combined with a fluorescent anti-cone arrestin-antibody that labeled all cone pedicles, she studied possible changes in S-cone to SCBC-synapse interactions. Li Jia examined the number of SCBC dendritic branches and the number of cells that are contacted by SCBCs in these mice (figure

8; unpublished results). Besides looking at the S-opsin- (panel b) and the Thrb-KO mice (c), she also tested double-KO mice (d) that lacked all cone opsins. In her analysis, she concluded that there was no significant change (e, f). Genetic disruption of the normal S- and M-opsin expression pattern did not alter the specific connections between S-cone photoreceptors and SCBCs in the mouse retina. In addition, she found that the expression of cone arrestin is downregulated in Thrb-KO- or double-KO mice (figure 8, panels c, d)

Li Jia's findings were a key factor for me to investigate differences in gene expression in S- and M-cones, because I learned from her experiments that the opsins are not the sole determiners of S- or M-cone identity, as demonstrated by the S-cone specific wiring.

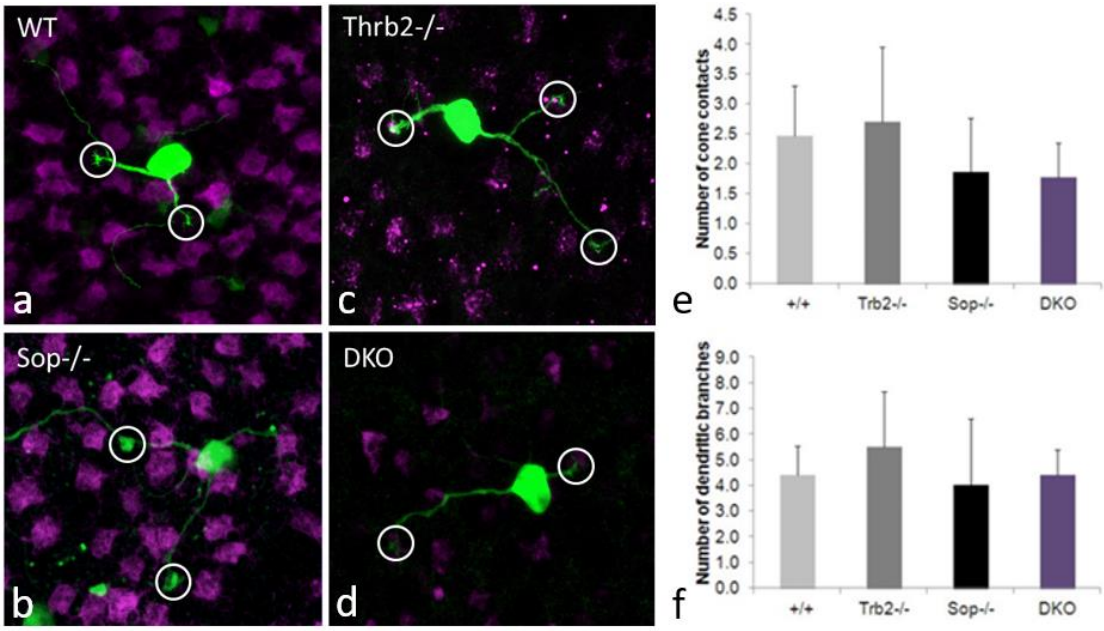

Figure 8 S-cone to S-cone-bipolar cell synapses in mice that lack opsin-expression (S, M, or both). Cone pedicles were stained with anti-cone arrestin antibody (magenta). S-cone bipolar cells express a fluorescent protein (green; Clomeleon-mouse (Kuner and Augustine, 2000). Data provided by Li Jia (NIH), unpublished.

1.7 Research objectives

Many studies on the visual system focused on nocturnal animals like the mouse. This led to enormous knowledge about features of the rod-dominated retina. In this thesis, my goal was to investigate characteristics of the cone-dominated retina. For this I planned to use the thirteen-lined ground squirrel and the tree shrew as model organisms. New findings might provide useful information on human vision. The photoreceptor distribution in these animals is comparable to the photoreceptor distribution in the macular area of the human retina, though, they do not have a fovea.

First, I wanted to investigate the development of the tree shrew retina in a morphological and a genetic approach. This might provide clues if genetic differences during early development could explain the cone dominance in the tree shrew retina.

Secondly, I wanted to explore the molecular identity of S- and M-cone photoreceptors of the ground squirrel. To identify molecular signatures, I planned to develop a method to collect S- and M-cone single cells, so I could analyze their transcriptome. Differentially expressed genes should be validated. Further, I planned to explore ways to study the function of newly identified genes. The injection of an adeno-associated virus (AAV) should be tested as a way to genetically alter gene expression in the squirrel retina. At the same time, this should be used as a tool to label rod photoreceptors. This would allow to complete the transcriptomic analysis of all photoreceptor types in the squirrel.

At last, I wanted to identify differences in mRNA expression in photoreceptors of the hibernating ground squirrel. Photoreceptors undergo large morphological changes in this phase. I wanted to explore the genetic background of these adaptive changes.

2 Materials and Methods

2.1 Materials

2.1.1 Chemicals

B27 supplement; *ThermoFisher*
Bovine serum albumin (BSA); *Sigma*
DAPI (4',6-Diamidino-2-Phenylindole); *ThermoFisher*
Dulbecco's Modified Eagle Medium (DMEM); *Gibco*
EDTA; *Sigma*
Ethanol 200 proof; *Warner Graham*
Fetal calf serum; *Gibco*
Glutamax; *ThermoFisher*
Hibernate-A culture medium; *ThermoFisher*
HBSS (Hank's balanced salt solution); *Fisher Scientific*
L-cysteine; *Sigma*
L-glutamine; *Sigma*
Low Input Library Prep Kit v2; *Clontech*
Methanol; *Sigma*
Nail polish; *Electron Mircoscopy Sciences*
Normal Goat Serum (NGS); *Jackson ImmunoResearch*
Papain; *Worthington*
Paraformaldehyde (16 %); *Electron microscopy sciences*
PBS (1x); *Gibco*
PBS (10×); *Quality Biological*
ProLong Gold Mountant; *Fisher Scientific*
Protease Inhibitor Cocktail; *Sigma*
Qubit dsDNA HS Assay Kit; *ThermoFisher*
Sucrose; *Sigma*
SimplyBlue SafeSatain (Coomassie G-250)*; ThermoFisher*
SMART-Seq v4 Ultra® Low Input RNA Kit for Sequencing; *Clontech*
Sodium azide; *Sigma*
Sodium chloride; *Sigma*
Streptavidin/penicillin solution; *ThermoFisher*
TBS (10x); *Crystalgen*
O.C.T.- compound; *Tissue-Tek*
Qubit High Sensitivity DNA Analysis Kit; *Agilent*
Tris (Tris(hydroxymethyl)-aminomethan); *Sigma*
Triton X-100; *Sigma*

Tween 20; *Sigma*
Vectashield; *Vector Laboratories*

2.1.2 Consumables

1.5 mL microcentrifuge tubes; *USA scientific*

15 mL centrifuge tubes; *Corning*

50 mL centrifuge tubes; *Corning*

55 mm Glass bottom dish w/ 30 mm micro-well #0 cover glass; *Cellvis*

Micropipettes for injections; *Eppendorf*

NuPAGE Blot membranes; *Invitrogen*

NuPAGE SDS-gels; *Invitrogen*

Superfrost Plus slides; *Fisherbrand*

TipOne Pipette tips 10, 100, 1000; *USA scientific*

2.1.3 Instruments

<u>Confocal microscopy</u>

LSM 510 confocal microscope; *Zeiss*

LSM 780 confocal microscope; *Zeiss*

Plan-Neofluar 20x/0.50 Ph2 objective; *Zeiss*

Plan-Apochromat 63x/1.40 Oil DIC M27 objective; *Zeiss*

<u>Single cell picking</u>

Evos cell imaging system; *ThermoFisher*

Axiovert 100; *Zeiss*

Transferman 4r micromanipulator; *Eppendorf*

CellTram microinjector; *Eppendorf*

<u>RNA-seq</u>

Bioanalyzer 2100; *Agilent*

Qubit Fluorimeter; *ThermoFisher*

HiSeq 2500; *Illumina*

Centrifuges

Biofuge primo; *Sorvall*

Biofuge fresco; *Heraeus*

Misc. tools

Surgical instruments; Fine Science Tools

Surgical instruments; Roboz

Pipetman G pipettes; Gilson

Reference 2 pipettes; Eppendorf

Neodymium Block Magnets for magnetic beads collection; K&J Magnetics

Injection syringe; *Hamilton*

2.1.4 Software

RNA-seq analysis

R; *The R Foundation*

Bioconductor; Gentleman et al., 2004; Huber et al, 2015

Deseq2; Love et al., 2014

edgeR; Robinson et al., 2010

gplots, Warnes et al., 2016

HTseq; Anders et al., 2017

Limma; Ritchie et al., 2015

pcaExplorer; Marini, 2017

STAR; Dobin et al., 2013

Tximport; Soneson et al., 2015

Voom; Law et al., 2014

Supercomputer: NIH Biowulf2 cluster; *NIH HPC Facility*

Microscopy

Zen; *Zeiss*

Fiji; Schindelin et al., 2012

ImageJ2; Schindelin et al., 2015

GIMP; *gimp.org*

2.1.5 Antibodies

Primary antibodies

Anti-Cadm1 PA5-24196, 1:100; *ThermoFisher*

Anti-ChAT AB144, 1:100; *Millipore*

Anti-Filamin A #4762, 1:100; *Cell signaling*

Anti-L/M-Opsin EDK101, 1:100; *Kerafast*

Anti-opn1sw (S-opsin), 1:200; *Santa Cruz*

Anti-PKCα P5704, 1:1000; *Sigma*

Anti-recoverin AB5585, 1:1000; *Millipore*

Anti-rhodopsin MAB5316, 1:200; *Chemicon*

Anti-rod arrestin (SAG) 23546-1-AP, 1;200; *Proteintech*

Secondary antibodies

Donkey-anti-goat Alexa 488, 1:500; *ThermoFisher*

Donkey-anti-mouse-Cy5, 1:500; *Jackson ImmunoResearch*

Donkey-anti-rabbit-Cy3, 1:500; *Jackson ImmunoResearh*

2.2 Methods

2.2.1 Tissue preparation

For all animal procedures, the guidelines of the Animal Research Advisory Committee (ARAC), the American Veterinary Medical Association, and the Animal Care and Use Committee (ACUC) were adhered.

Postnatal tree shrews (*Tupaia belangeri*) and ground squirrels (*Ictidomys tridecemlineatus*) were euthanized by using isoflurane following decapitation. Tree shrew fetuses were removed from euthanized dams and decapitated. Eyes were enucleated by sharp dissection following preparation of the retina.

For whole-retina RNA-sequencing, tree shrew retinae were immediately flash frozen in liquid nitrogen and stored at -80 °C until RNA extraction. All other procedures are described below.

2.2.2 Cryosections

Dissected pieces of ground squirrel and tree shrew retina were incubated in PBS with 4 % PFA for 3 hours (room temperature, RT). After five washes with PBS (10 min at room temperature) the retina was incubated in increasing amounts of sucrose in PBS (10% - 20% - 30%, 30 min steps). After 16 h in 30 % Sucrose (4°C), the tissue was embedded in Tissue-Tek O.C.T. compound and flash frozen in dry ice. After 2h at -20 °C, the embedded tissue was sectioned using a Leica 3050S cryostat and transferred to Fisherbrand Superfrost Plus slides.

2.2.3 Immunohistochemistry

Slides containing retinal sections were washed twice in PBST (PBS, 0.5% Triton X-100) and incubated with blocking solution (4% donkey serum in PBST) for 1 hour (RT). The tissue was covered with primary antibody solution (dilutions listed in section 2.1.5.; in blocking solution) and incubated for 14-16 hours at 4 °C. After three washes (PBST, 10 min), secondary antibody coupled to a fluorophore (Alexa 488, ThermoFisher; Cy3 or Cy5; Jackson ImmunoResearch) was applied to the sample (1:500 in blocking solution) for 2.5 h at room temperature. After three washes, the samples were mounted with Vectashield mounting medium with DAPI (Vecta Laboratories). The tissue was imaged using a Zeiss LSM 780 or a Zeiss LSM 510 confocal microscope and ZEN imaging software (Zeiss).

2.2.4 Live-labeling and isolation of cone subtypes for RNA-seq

The eyes of sacrificed ground squirrels were removed and dissected. After removal of the pigment epithelium, a 10 mm^2 piece of retina was incubated in digestion buffer (5 U/mL papain, 0.667 mg/mL L-cysteine, 1 mM EDTA in Hank's balanced salt solution (HBSS)) for 20 min at 37 °C. The retina was washed twice with Hib-A (Hibernate-A medium, 2% B27, 1 % streptavidin/penicillin, 0.25 % Glutamax, 0.25 % L-glutamine, 10 mM NaCl) followed by incubation with goat-anti-S-opsin, (1:50 in Hib-A) for 45 min (4 °C). After two additional washes, the retina was incubated with Donkey-anti-goat antibody (Alexa Fluor 488), 1:50 in Hib-A, 45 min at 4 °C. The tissue was triturated using a 1000 µL pipette (5-10 times) to dissociate the cells. The suspension was filtered through a cell strainer and centrifuged to remove debris (2000 x g, 3 min, 4 °C). The cells in the pellet were carefully resuspended in 500 µL Hib A and placed on an inverted microscope (Evos cell imaging system or Zeiss Axiovert 100). S-opsin-positive cells (presumably S-cones) and negative cells with cone morphology (presumably M-cones) were separately collected using glass micropipettes connected to a micromanipulator (Eppendorf TransferMan 4r) and transferred into 8 µL lysis buffer (Clontech

SMARTer Ultra Low Input RNA Kit for Sequencing - v3). For each sample, 16–20 single cells were pooled. Samples were flash frozen in dry ice and stored at -80 °C until use.

2.2.5 RNA-sequencing of ground squirrel single cells

RNA-extraction of single cell samples and generation of double stranded cDNA was performed using the Clontech SMARTer Ultra Low Input RNA Kit. For the construction of the library, the Low Input Library Prep Kit v2 (Clontech) was used. The quality of the cDNA was analyzed with the Agilent 2100 BioAnalyzer. Concentrations were measured with the Qubit dsDNA HS (high sensitivity) assay. Up to eight samples with different Illumina barcodes were pooled in one lane of a flow cell (Illumina HiSeq 2500). The read length was set to 50 bp in single-end mode. All kits were used as instructed by their manufacturers.

2.2.6 Data analysis of squirrel RNA-seq data

The ground squirrel genome and annotation in version GCA_000236235.1 were used to align the reads in STAR (Dobin et al., 2013) on the Biowulf2 NIH supercomputer. HTseq (Anders et al., 2017) was used to count and annotate the reads. The output of this process was used for the data normalization and differential expression analysis with the DESeq2 package (Love et al., 2014) for *R* 3.3.1. For this step, a protocol by Love et al., (2017) was used. The pcaExplorer package (Marini, 2017) was used for data visualization.

2.2.7 Data analysis of tree shrew RNA-seq files

The reads were aligned and counted with Kallisto (Bray et al., 2016) on the Biowulf2 NIH supercomputer. The transcriptome and the annotation file were

retrieved from the NCBI database (accession number GCF_000334495). Count data were analyzed using a protocol by Law et al. (2016). For this, the count files were imported into edgeR (Robinson et al., 2010) using the package tximport (Soneson et al., 2015). In edgeR, counts were normalized using the TMM function (Trimmed mean of M-values). The output was used to create time-course graphs of gene expression. MDS-plots for unsupervised clustering were created in edgeR with the plotMDS function. Differentially expressed genes were determined with Limma/voom (Ritchie et al., 2015; Law et al., 2014). Heatmaps were created using the gplots package (Warnes et al., 2016).

3 Results

3.1 Development of a cone-dominated retina

To study the development of a cone-dominated retina, I collaborated with Prof. Yong-Gang Yao from the Kunming Institute of Zoology. At his facility, I had the opportunity to work with tree shrews (*Tupaia belangeri*), which have a cone proportion of approximately 93%. I collected samples from animals at different stages of development, from E25 (embryonic day 25), to P30 (postnatal day 30). I also included tissue from five-year old (Y5) animals to look at effects of aging. I wanted to look at the development on two different levels: genetic changes (RNA-seq) and morphological changes (tissue sections and immunohistochemistry).

3.1.1 Morphology of the developing tree shrew retina

To study the morphology of the developing tree shrew retina, I collected samples at nine different time points: embryonic days E30, E40, postnatal days P0, P6, P9, P12, P21, P27 and 5 years (Y5) after birth. Important events during development are birth after 44 days of gestation (E44/P0), eye opening at around P22 and weaning at P30. The average life span is only described for animals in captivity, which is nine to twelve years (Fuchs and Corbach-Söhle, 2010). After retinal dissection, I fixed, froze and subsequently sectioned the samples on a cryostat. I then used the various sections for immunohistochemical stainings. To highlight stages of development, I used different markers to identify retinal cell types: anti-recoverin (red) for all photoreceptor types and bipolar cells, mainly type 2 (Milam et al., 1993; Haverkamp et al., 2003); anti-choline acetyltransferase (ChAT, green) for cholinergic amacrine cells and the two distinctive ChAT bands in the inner plexiform layer (IPL); anti-protein kinase C α (PKCα, blue) for rod bipolar cells and a subset of cone bipolar cells (Puller et al., 2011). I used DAPI (not shown in the merged images) to stain nuclei.

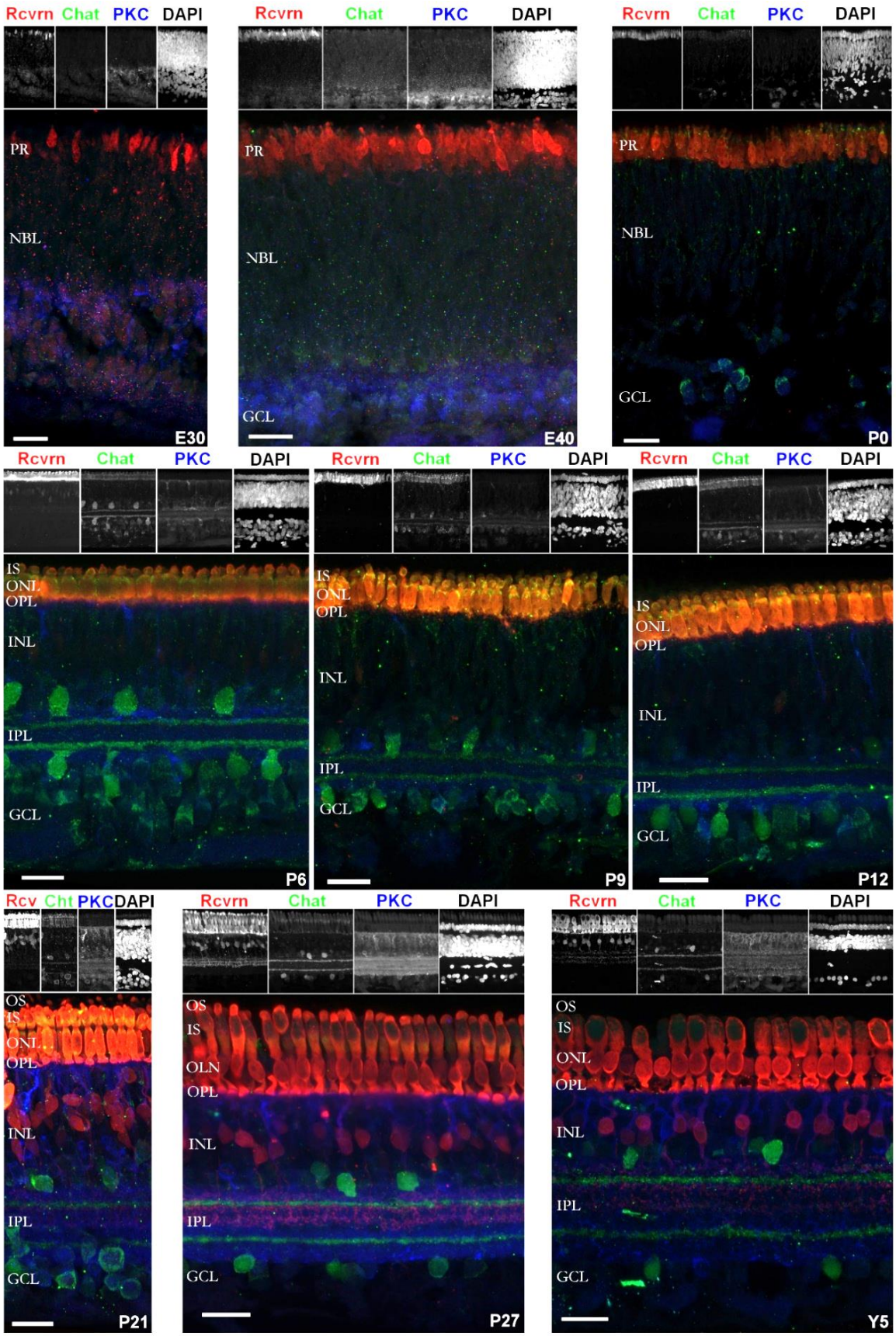
Rcvrn Chat PKC DAPI
PR
NBL
GCL
E30
E40
P0
IS
ONL
OPL
INL
IPL
P6
P9
P12
Rcv Cht PKC DAPI
OS
OLN
P21
P27
Y5

Figure 9

Figure 9 Retinal development of the tree shrew. Immunostainings at embryonic days E30, E40, postnatal days P0, P6, P9, P12, P21, P27, and after five years (Y5). Antibodies: anti-recoverin (red); anti-choline acetyltransferase (ChAT, green); anti-protein kinase C α (PKCα, blue); DAPI (not shown in merged images).
Settings for the laser-scanning confocal microscope were optimized for each section to best represent emerging cell types; intensities of the colors do not represent stronger or weaker expression between different time points. Scale bars: 20 µm

At embryonic days E30 and E40 a recoverin signal was located in the outermost layer of the developing retina (figure 9). The nuclei were not distinguishable from nuclei in the neuroblastic layer (NBL), as seen in the DAPI channel (top right of each panel). Only the recoverin label seemed to distinguish those cells, which were most likely developing photoreceptors. These cells had small apical protrusions that might resemble early inner segments. At E30 the labeling was sparse, but the number of positive cells increased in this sublayer at E40. Interestingly, a few cells showed a stronger signal, compared to other positive cells in the same row. Choline acetyltransferase (ChAT) was not detected at E30, but sparsely at E40 in the putative future ganglion cell layer (GCL). I detected faint PKCα-signals at E30 in half of the section, closer to the vitreal surface. At E40 many positive cells were located in the GCL.

On the day of birth (P0), the morphology of recoverin-positive photoreceptors did not change. However, the recoverin signal was more evenly distributed across all cells of this layer. Also, this layer became more distinguished, as I could observe a small gap, the putative outer plexiform layer, between photoreceptors and the developing cells in the neuroblastic layer (DAPI channel). ChAT and PKCα signals were limited to cells in the ganglion cell layer, their signals were co-localized in numerous cells.

At P6 I observed various changes. All main layers of the retina were visible at this time point. The recoverin label showed further development of photoreceptor inner segments and the photoreceptor nuclei were now arrayed in one single row. I

observed multiple small extensions that indicated the development of photoreceptor synaptic terminals. I detected faint recoverin-positive cells, most likely bipolar cells, in the inner nuclear layer (INL). ChAT-positive cells, putatively amacrine cells, were localized outside both sides of the IPL, with two distinct ChAT bands within the IPL. Interestingly, photoreceptors also showed a ChAT-signal. I found PKCα to be expressed in the GCL and in the INL, at about the same positions as ChAT-positive cells in these layers. In addition, I found a few PKCα-positive cells located more towards the outer retina, close to the recoverin-positive bipolar cells. These were most likely PKCα-positive bipolar cells (Negishi et al., 1988; Greferath et al., 1990). In the IPL, three PKCα-bands were visible.

I observed small changes at P9 and P12. The size of the GCL seemed reduced, the number of cell rows has decreased from 5 – 6 down to 3 – 4. At the same time, the size of the INL has expanded, likely due to more differentiating bipolar cells.

At P21 I discovered photoreceptor outer segments labeled by recoverin. The morphology of the photoreceptor terminals was also more distinguished, although they had not reached their mature appearance yet. The shape of the photoreceptors looked more elongated compared to previous time points. I did see an increased number of recoverin- and PKCα-positive bipolar cells, as well as an increase in PKCα-bands in the IPL. The exact number was hard to determine, because the bands were not as clear as the ChAT-bands. Some of the bipolar cells showed a co-localized recoverin- and PKCα-label.

At P27 the tree shrew was close to its weaning age. The photoreceptors were further elongated and had grown full outer segments and synaptic terminals. In the inner segments, I could see large ellipsoids that contained the mitochondria and filled about half of the inner segments. The nuclei became more round. Nuclei seen within the OPL and IPL were putative microglial cells that migrated into these layers (compare Hume et al., 1983). When I looked at the distribution of all layers, I saw a further decrease in INL and GCL size. At this time point, the ChAT signal in photoreceptors has almost vanished, a clear signal was only observed in in the ChAT bands and in cells in the INL and GCL. I still saw a strong PKCα-signal in putative bipolar cells in the INL and putative amacrine cells or ganglion cells. In contrast to P0, only a few cells showed a co-localized signal for PKCα- and ChAT.

In the aged tree shrew retina (5 years) I observed a few changes. Outer segments were not detected, they were most likely lost during tissue preparation. The diameter of the photoreceptor somata and inner segments of cones looked bigger compared to the previous age. In addition, the size of the IPL has further expanded.

To take a different perspective on the development, I stained retinal sections of tree shrew retina for S-opsin, M-opsin and rhodopsin (figure 10). At P0 (not shown), no opsin-signals were visible. The next stage I tested was P6 (panel **a**). Here, all opsins were detectable. Most of the signals were concentrated at the tip of each labeled cell, hinting to outer segment development. This detail was not detected with recoverin-staining (figure 9). In addition to that, all opsins showed a dim signal in the membrane throughout every cell. At P12 and P18 (panels **b, c**), the expression of the opsins did not reveal any changes. For P12, I also prepared a flat-mounted tissue sample (panel **e**). This view displayed a uniform pattern of M- and S-opsin-labeled cells. Interestingly, the S-opsin channel of this image (panel **f**) revealed lateral processes, possibly in search for postsynaptic binding partners. These could be telodendrites that contact neighboring cones through gap junctions. At P27, the outer segments of S- and M-cones became defined and distinguishable from the inner segments. In addition, the rhodopsin-staining showed a clear difference in the morphology of rod outer segments compared to their cone counterparts (compare figure 3).

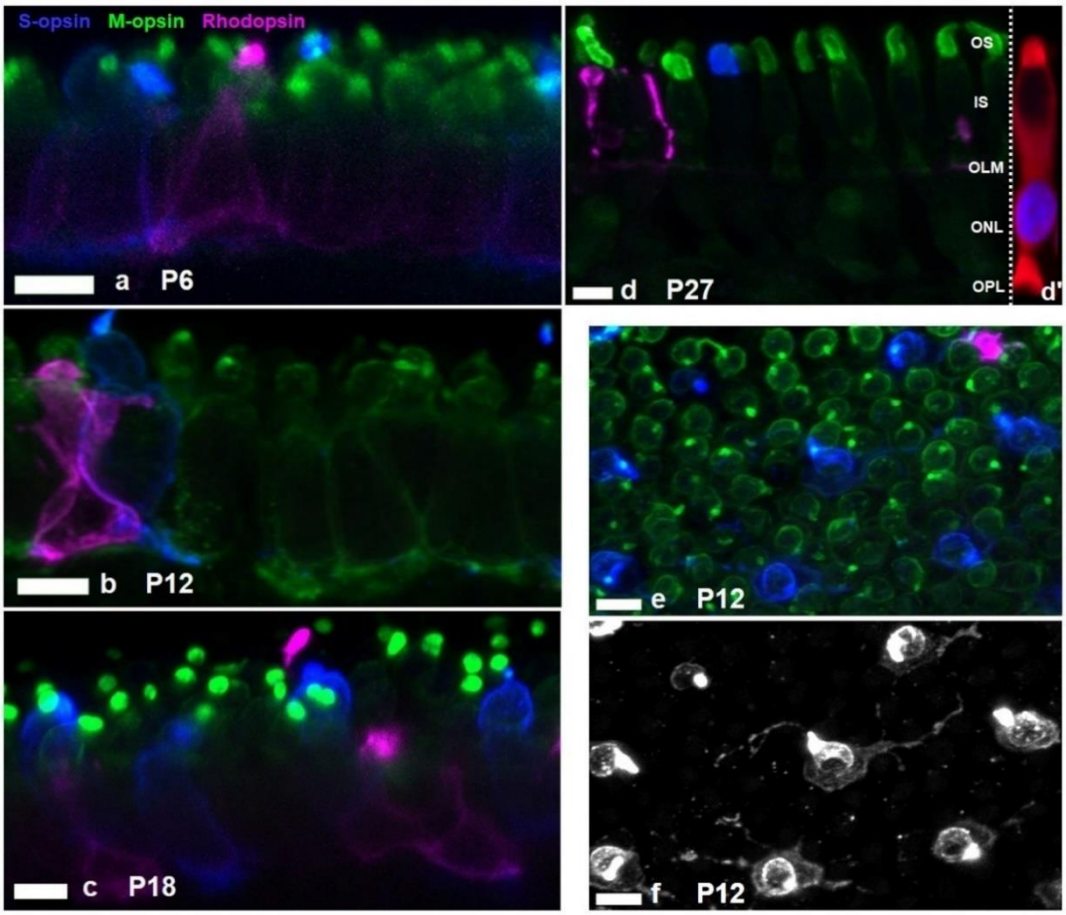

Figure 10 Opsin expression in the developing tree shrew retina. The tissue was stained for S-opsin (blue), M-opsin (green) and Rhodopsin (magenta). **a-d** Cross sections at different stages of development. **d'** A recoverin (red)/DAPI (blue)-stained cone (P27) was inserted for morphological comparison **e** Flat-mounted tree shrew retina at P12. **f** Same as in e; only the S-opsin channel is shown to highlight the S-cone processes.
OS: outer segments; IS: inner segments; OLM: outer limiting membrane; ONL: outer nuclear layer; OPL: outer plexiform layer. Scale bars: 5 µm.

3.1.2 Gene expression in the developing tree shrew retina

After studying morphological changes during the development of the tree shrew retina, I wanted to explore how these changes are reflected on gene expression level. I collected whole retinae from tree shrews at embryonic days E25, E30, E40, postnatal days P0, P9, P18, P24, P30 and at Y5 (five years); two animals per time point. I collected the samples in Prof. Gao's facility in Kunming, China. Zhi Xie's

group (Sun Yat-sen University, Guangzhou, China) sequenced the samples and passed the raw sequencing files to me for analysis (details are described in the methods section).

First, I created a multidimensional scaling plot (MDS) to visualize quantitative estimates of similarity among the samples in an unsupervised manner. The plot is shown in figure 11. Each sample pair clustered together, this meant that the variance per time point was low. Furthermore, dimension 1 (dim1), which explains most of the observed variance, sorted the samples (unsupervised) by age. This indicated that the developmental progression was reflected in the measured gene expression.

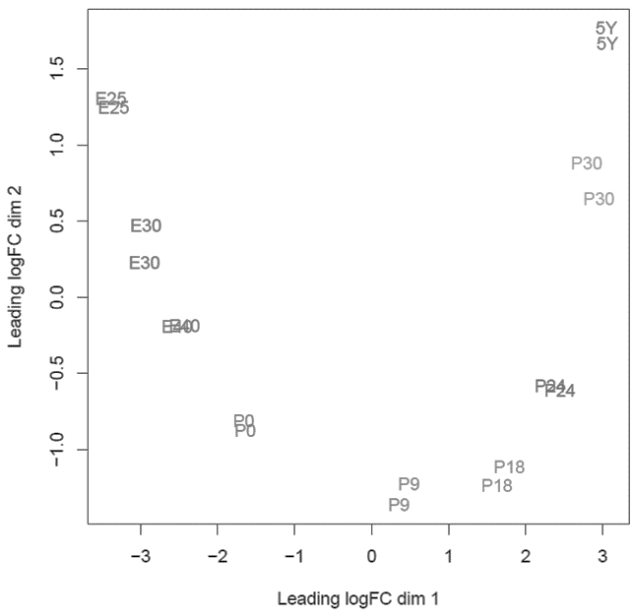

Figure 11 Unsupervised clustering of tree shrew RNA-seq samples (MDS plot). The first dimension represents the leading-fold-change that best separates samples and explains the largest proportion of variation in the data. Samples found in the same cluster have a high similarity. Dimension 1 (dim1) sorted the samples (unsupervised) by age, an indicator that the development was reflected in the measured gene expression.

3.4.2.1. Transcription factors for photoreceptor differentiation

In the next step, I explored the transcription factor expression in the tree shrew dataset. In order to compare the expression to a rod-dominated species, I received RNA-seq data of mouse (*Mus musculus*) from Douglas Forrest's laboratory (NIDDK/NIH). The data were collected from wildtype mice retinae of mixed C57BL/6J × 129/Sv-background at embryonic day E16 and postnatal days P1, P3, P7, P14 and P28. They used pools of six to twelve retinae per sample; one sample per time point. The mouse dataset (Ng et al., 2017) is publicly available on the NCBI Gene Omnibus (GEO) server (ncbi.nlm.nih.gov/geo/), accession number GSE95016.

First, I looked at the expression of opsins as marker for photoreceptor type differentiation during development (figure 12, first row). I normalized all expression values to allow an easier comparison. In tree shrew, I detected a strong onset of S-opsin (Opn1sw) and rhodopsin (Rho) between birth (P0) and P9. S-opsin showed a slightly higher increase in this phase, before both reached their peak expression at P18, shortly before eye opening at P22. Compared to these, M-opsin (Opn1mw) expression began later, with a milder onset between P0 and P9, and a further increase before reaching a plateau between P24 and P30. The retinae from five-year-old animals showed the highest M-opsin expression. In mouse, I observed an onset of S-opsin expression around the day of birth (P1), whereas expression of rhodopsin began later between P3 and P7. M-opsin was the last opsin in the group, starting after P7, with a very strong expression at P14, the day of eye opening. At this stage, Rhodopsin and S-opsin have not reached their peak yet, they further increased until P28.

After investigating the opsin expression, I focused on transcription factors that lead to the differentiation of photoreceptor types. In tree shrew, I observed an onset of Nrl, an important factor for rod differentiation, at E30, and peak expression at E40, a few days before birth (figure 12, second row). Between P0 and P18, the expression was stable, but slightly decreased compared to the peak. At later stages (P24 – Y5) I saw a further decrease in expression. Nrl expression in mouse began after birth at P1 and continuously rose until P28.

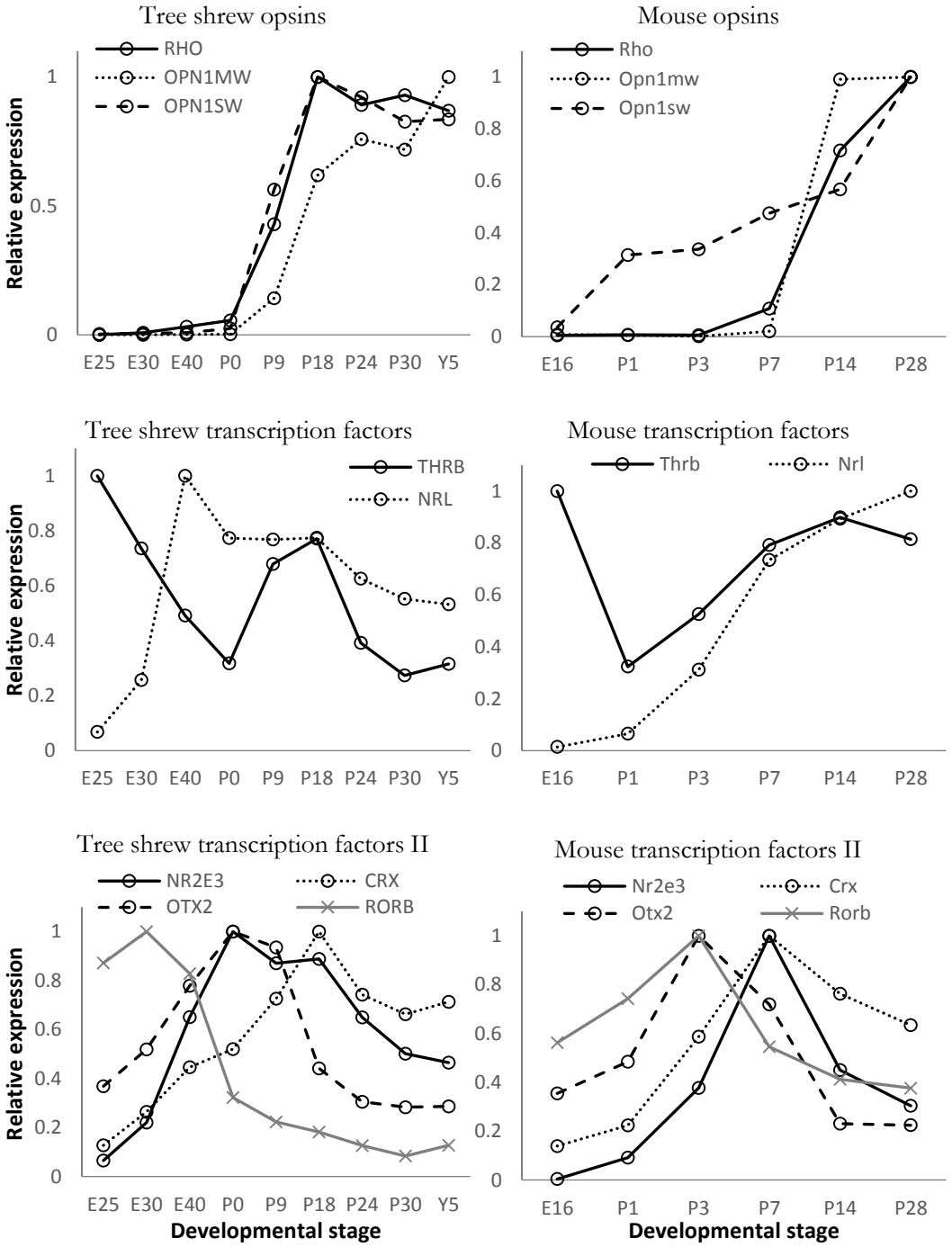

Figure 12 Comparison of gene expression in the developing retinas of tree shrew and mouse. I collected and sequenced tree shrew retinae at nine different ages. Mouse data were provided by D. Forrest. Expression values were normalized for each gene.
First row: comparison of opsin expression. Second row: transcription factors important for rod- (Nrl) and M-cone- (Thrb/Trβ2) differentiation. Third row: additional transcription factors for photoreceptor differentiation.

Thrb, the gene that encodes Trβ2 (the key factor for M-cones), showed a strong expression at the earliest stage (E25) in tree shrew and decreased before rising again at P0. From there it rose until P18 and decreased after eye opening (P24). In mouse, the curve for Thrb showed a similar shape, with a high expression at the beginning (E16), followed by a dip at birth. It then peaked again at the day of eye opening (P14).

In the third row of figure 12 I am showing additional transcription factors. Otx2, an early degerminator of general photoreceptor cell fate, was one of the first transcription factors I observed in both tree shrew and mouse retina. In both species, the gene was moderately expressed at the earliest stages tested and peaked at or around birth (P0 in tree shrew, P3 in mouse).

Crx acts downstream of Otx2 and is also important for all photoreceptor types. The expression of Crx correlated with that of Otx2. But compared with Otx2, the peak of Crx was shifted to P18 in tree shrew and P7 in mouse. In both animals, expression decreased around the day of eye opening (P22 in trees shrew, respectively P14 in mouse).

In Tree shrew, Nr2e3, a downstream target of Nrl, followed the Nrl pattern. The only difference was a slightly delayed peak that occurred at P0. In mouse, the case was different. The onset of Nr2e3 was comparable to Nrl, but instead of continuously rising, it peaked at P7 and decreased at later stages.

Rorβ, another downstream target of Nrl, had an early peak at E30 in tree shrew. From there it continuously decreased. The strongest decline was observed right before birth, between E40 and P0. Interestingly, in mouse it reached its highest expression after birth at P3, before it also fell.

3.4.2.2 Differential gene expression in tree shrew retinal development

In the previous section I explored genes that are known to play an important role in photoreceptor development. After that I wanted to focus on all genes that showed a significant change in expression over the course of retinal development. This could

help to find new genes that might be important during retinal development. To look at the RNA-seq data, I chose to look at key time points during development. Here, I wanted to study changes that occur after birth. For this, I listed genes that show the highest change in expression between P0 and P9. I created a heatmap that showed the top genes and their expression at all time points (figure 13).

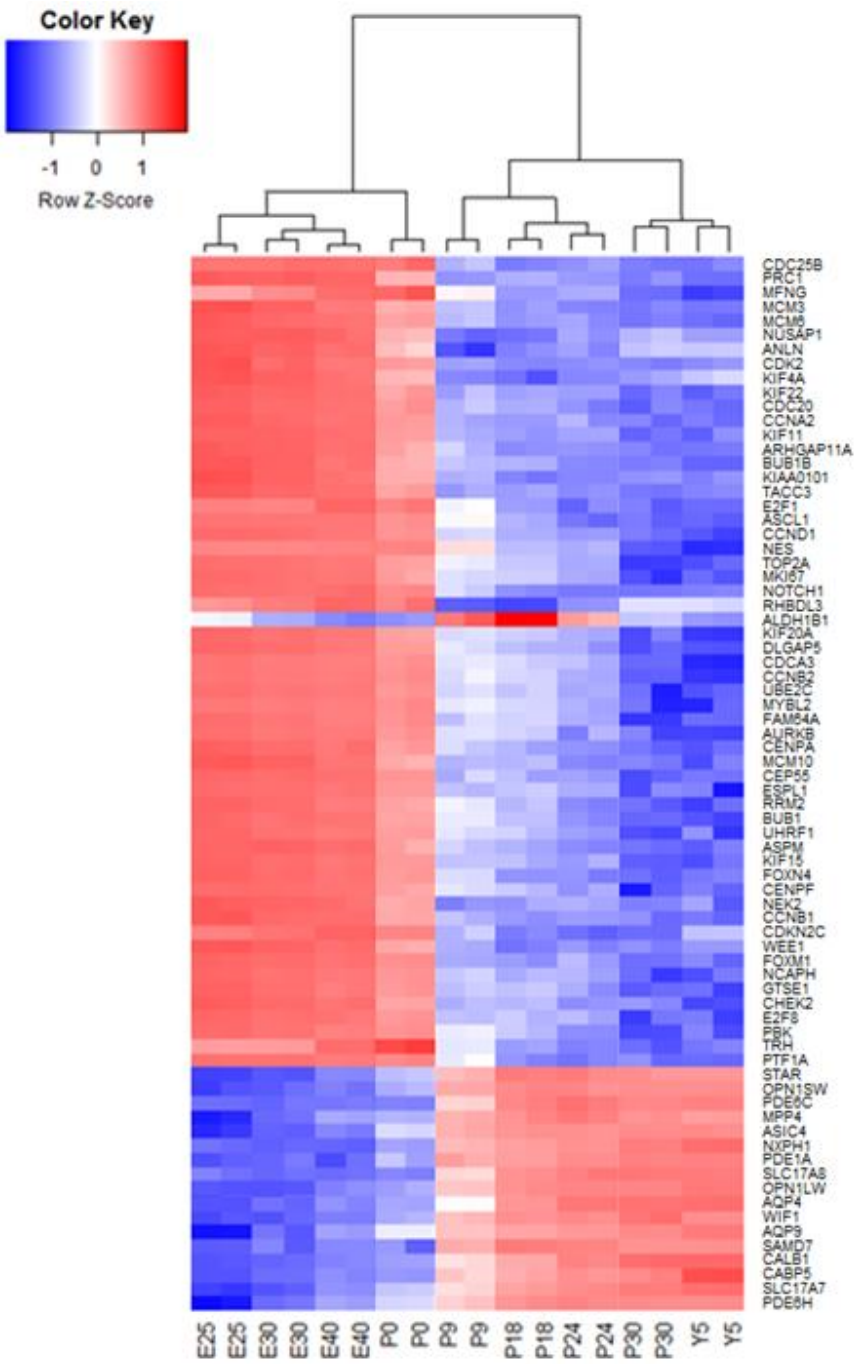

Figure 13 Differentially expressed genes in tree shrew retinal development. The heatmap shows genes that had the highest log2fold change between P0 and P9. Blue coloring indicates a lower expression compared to other stages, red indicates a higher expression.

In the first part of the heatmap, I observed many genes that were highly expressed at early embryonic stages (E25 – P0), before their expression dropped right after birth (P9 – Y5). The majority of these genes were involved in various stages of the cell cycle. Two of them were important for directing the differentiation for retinal cells, like Foxn4 and Ptf1a, which lead to differentiation of progenitors towards horizontal and amacrine cell fates (Fujitani et al., 2006).

A different gene, not involved in the cell cycle, was Rhbdl3. This gene encodes rhomboid-3, an intramembrane serine protease. Its function is unknown, other family members have been reported to take part in growth factor and cytokine signaling, quality control of proteins and trafficking (Freeman, 2016).

Further genes I found were Notch1 and Mfng. Both act in the notch receptor pathway during embryonic development. In the retina, Notch1 regulates photoreceptor and ganglion cell differentiation by controlling genes that repress differentiation (Riesenberg et al., 2009). It occurs earlier than the transcription factors discussed in the previous section.

There were also genes that were upregulated after P9. Samd7 is reported to be controlled by the transcription factor Crx (Hlawatsch et al., 2013) and it silences non-rod genes in rod photoreceptors (Omori et al., 2017).

At P9 I saw a number of genes involved in cone phototransduction: PDE-subunits Pde6c, Pde6h and the opsin genes Opn1sw, Opn1mw. Slc17a7 (or Vglut1) is expressed in the synaptic terminals of photoreceptors and bipolar cells, where it sequesters glutamate into synaptic vesicles (Johnson et al., 2007). Its expression after P0 was an indicator for photoreceptor synapse formation. Other indicators for that were Mpp4 and Nxph1. Mpp4 encodes the membrane palmitoylated protein-4. It is a retina-specific scaffolding protein that may organize presynaptic protein complexes in the photoreceptor ribbon synapse (Yang et al., 2007). Nxph1 (neurexophilin 1) forms a tight complex with alpha neurexins, a group of proteins that promote adhesion between dendrites and axons (Petrenko et al., 1996).

Aldh1b1 encodes aldehyde dehydrogenase 1 family member B1, active in alcohol metabolism. Recently, this gene was reported to be a immunohistological marker for colorectal cancer (Matsumoto et al., 2017). In human, it is ubiquitously expressed (proteinatlas.org).

I also discovered two genes of the aquaporin family. Aqp4 was reported to be primarily expressed in Müller cells, where it contributes to water homeostasis in the retina. Aqp9 is found in ganglion cells and might facilitate the uptake of lactate or glycerol (Tran et al., 2017).

One of the lesser known genes I found was Wif1. Effects of Wif1-expression in the retina have been studied by Hunter et al. in 2004. The authors claim that it might regulate rod production. This could have interesting implications for the development of a cone-dominated retina.

3.2 Genetic profiling of cone photoreceptor subtypes

Mammals have two major types of photoreceptors in the retina: rod photoreceptors, specialized for dim-light conditions, and cone photoreceptors for bright light and the perception of color. Until now, cone subtypes have been classified mostly by the opsin they express. Aside from the opsins, S- and M- cones share the same phototransduction machinery (Lamb et al., 2007). There are isolated reports of subtype-specific protein expression. We know that there are differences in how S- and M-cones are wired in the mammalian retina. S-cones exclusively contact the S-cone bipolar cell (SCBC; Haverkamp et al., 2005). I hypothesized there should be a molecular basis behind the specificity. If that is true, it would mean that M- and S-cones do not share the same molecular identity, or transcriptome. Li Jia answered the question if opsin molecules solely define the identity by investigating the specific SCBC synapse. She studied this specific synapse in mice with an S-opsin or M-opsin deletion (see section 1.6). She concluded that the genetic disruption of the normal S- and M-opsin expression pattern did not alter the specific connections between S-cone photoreceptors and SCBCs in the mouse retina.

This motivated me to analyze the mRNA expression in S- and M-cones. This would allow me to create and compare, for the first time, the gene expression profiles of these highly related cell types.

For this work, I decided against working with mice, because their cones are different from most other mammals. Particularly, because most mouse cones co-express both S- and M-opsin (Haverkamp et al., 2005). Instead, I decided to work with tissue from the thirteen-lined ground squirrel. The squirrel has a cone-dominated retina, and there is no co-expression of different opsins in one and the same photoreceptor type (figure 7).

3.2.1 Live Labeling of S-Cone Photoreceptors

First, I developed a way to identify and isolate individual S- and M-cones, because whole-tissue samples, as used in section 3.1.2, were not sufficient for this task.

I modified a protocol from Liu Hong (NIDDK, NIH) to dissociate small pieces of squirrel retina (approx. 10-15 mm^2). In short, the tissue was kept in Hibernate-A cell medium and digested with papain, followed by carefully triturating the tissue (see methods for details). The protocol was adjusted until I received a suspension with a high abundance of single cells that retained their cell morphology (cone outer segments and synaptic terminals). An example for a successful dissociation is shown in figure 14.

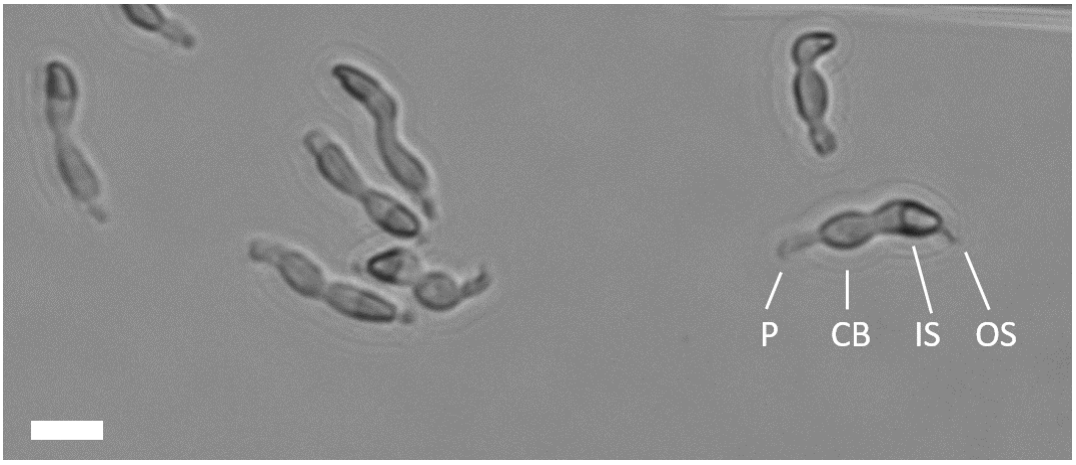

Figure 14 Photoreceptors of the ground squirrel after dissociation. The protocol allowed a dissection that kept most cells morphologically intact. The cell on the right is an example for an intact cell. The synaptic terminal, the inner segment (with its large ellipsoid) and the small outer segment are still present. P: cone pedicle, CB: cell body, IS: inner segment, OS: outer segment. Scale bar: 20 µm.

After the dissociation protocol was optimized, I developed a way to identify individual cone subtypes. Dissociated cone photoreceptors of the thirteen-lined ground squirrel retina have a very distinct morphology and are therefore easy to identify. However, cone subtypes were not morphologically distinguishable. In

contrast to mice, no genetically altered reporter squirrels were available. Inspired by ideas from Christian Puller (Carl von Ossietzky Universität Oldenburg) and Juan Angueyra (NEI/NIH), I used an antibody that specifically targeted the N-terminus of S-opsin. Since opsins are transmembrane proteins, parts of the protein, like the N-terminus, are located on the extracellular surface within the disk-like structures of the outer segment. Therefore, the antibody should be able to reach the antigen in live tissue.

First, I tried this method on a non-dissociated retina sample. Figure 15 (a) shows a live flat-mounted piece of a retina (that has not been fixed or permeabilized) after antibody treatment (goat-anti-S-opsin and Alexa 488-anti-goat). I observed a distinct staining pattern, similar to S-opsin staining in fixed tissue (figure 7b). I concluded that the S-opsin-staining of live cells worked.

To label single cells, I modified my dissociation protocol. I first treated the retina with papain to digest intercellular connections, but I did not triturate the tissue immediately. This allowed me to replace the cell medium by carefully using a pipette. I wanted to avoid multiple centrifugation steps that would be necessary if I had dissociated cells at this point. Centrifugal forces might stress the cells and change their morphology. After washing the sample by replacing the papain solution multiple times with fresh cell medium, I incubated it with the primary and secondary antibody. After this, I triturated the pre-digested tissue and evaluated the labeling.

Figure 15 (b, c) shows the antibody-treated cells with transmitted light (b) and at 470 nm excitation (c). This example shows one S-opsin-positive cell (arrowhead) and two photoreceptors that were not labeled (arrows), putative M-cones. This method allowed me to separately collect S- and M-cones samples for RNA-sequencing.

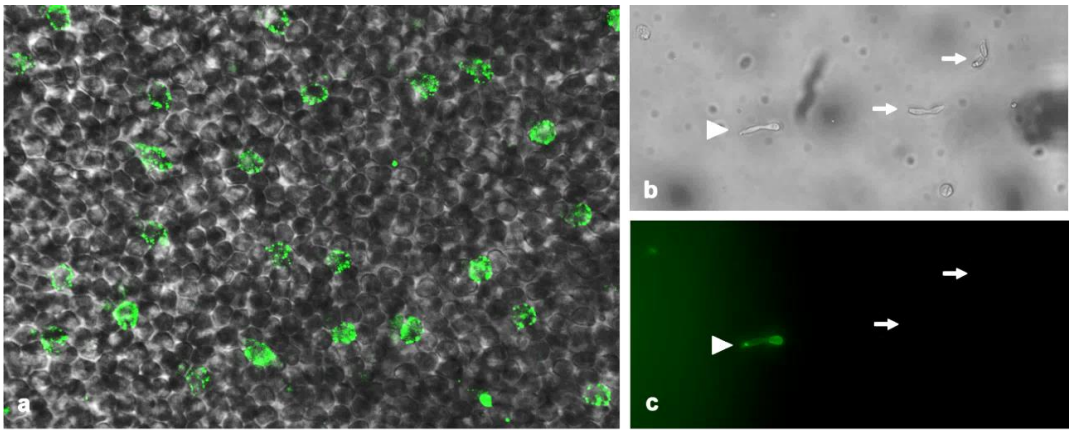

Figure 15 Live labeling of S-cone photoreceptors. Live, non-permeabilized, non-fixed ground squirrel retina was incubated with primary goat-anti-S-opsin antibody and secondary green-fluorescent anti-goat antibody. **a** Labeling of S-opsin (green) in flat mount retina shows a pattern of S-cones. **b, c** Dissociated retinal neurons after antibody treatment under transmitted light b) and excitatory light c) conditions. One S-opsin-positive cell (arrowhead) was detected and manually collected. Unlabeled cells with cone morphology (arrow) were most likely M-cones.

3.2.2 Single cell RNA-sequencing

To collect S- and M-cones for the transcriptome analysis, I used my previously described live-labeling method. The dish that contained the cells was placed on an inverted microscope with fluorescence illumination. I picked the cells manually by using a glass pipette that was connected to a micromanipulator. For each sample, I pooled 16-20 cells of one cone subtype. I picked cells from a total of 13 adult ground squirrels. During the summer, I collected five S-cone and three M-cone samples from awake ground squirrels. In the winter months, I collected two S-cone and three M-cone samples from squirrels that were hibernating. Subsequently, I extracted and processed the RNA to prepare the sequencing library.

In short, samples were lysed and double strand cDNA was synthesized using the SMARTer cDNA synthesis kit that was optimized for low input amounts of RNA. After PCR amplification of the cDNA, I had to ensure that the original RNA was not degraded by ribonucleases (RNases). The quality of each sample was tested on a 2100 Bioanalyzer. The samples were treated with fluorescent dye that can be

detected by the device. The device electrophoretically separated the fragments and measured the retention time. A size-standard allowed me to determine the length (in base pairs; bp) of my fragments. As an example, five samples are shown in figure 16. The analysis showed that my samples were in a size-range of 700 – 10,000 bp. The average mRNA length in mammals is 2,200 bp (Griffiths et al., 2005). The assay confirmed that I successfully extracted and amplified the mRNA molecules, since no degradation was observed.

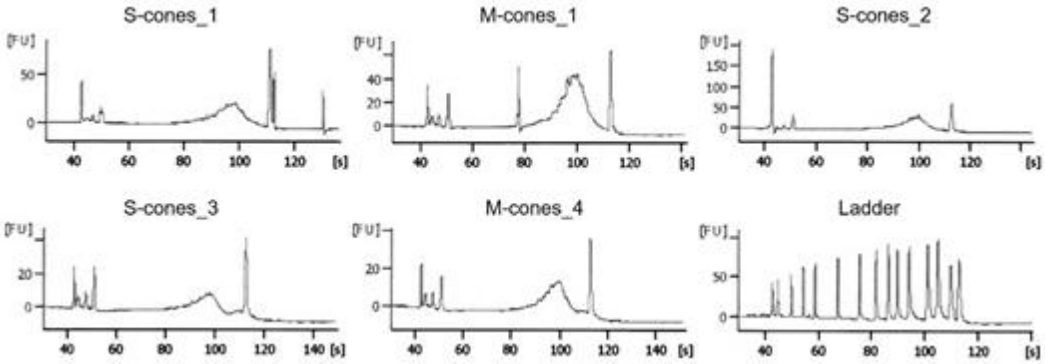

Figure 16 Quality analysis (I) of single cell samples (electropherogram). After first-strand synthesis and cDNA-amplification of each RNA extract, samples were analyzed for fragment size and amount of DNA. The device measures the amount of DNA (in fluorescence units (FU)) over the retention time (s). The ladder allows the determination of fragment sizes. Shown are five examples and the bp-ladder. Fragment sizes in all samples were in the range of 700 – 10,000 bp.
Fragment-size of each ladder-peak: 1) 35 bp, 2) 50 bp, 3) 100 bp, 4) 140 bp, 5) 200 bp, 6) 300 bp. 7) 400 bp. 8) 500 bp, 9) 600 bp, 10) 700 bp, 11) 1000 bp, 12) 2000 bp, 13) 3000 bp, 14) 7000 bp, 14) 10,380 bp.

Before the final library synthesis, the cDNA had to be fragmented by sonication to get an average length of 300 bp per fragment. This was to ensure that sequencing reads would not be limited to the 5’- and 3’-ends of each mRNA transcript. The samples were analyzed again to check for successful fragmentation (figure 17). All samples were in the range of 200 – 2,000 bp.

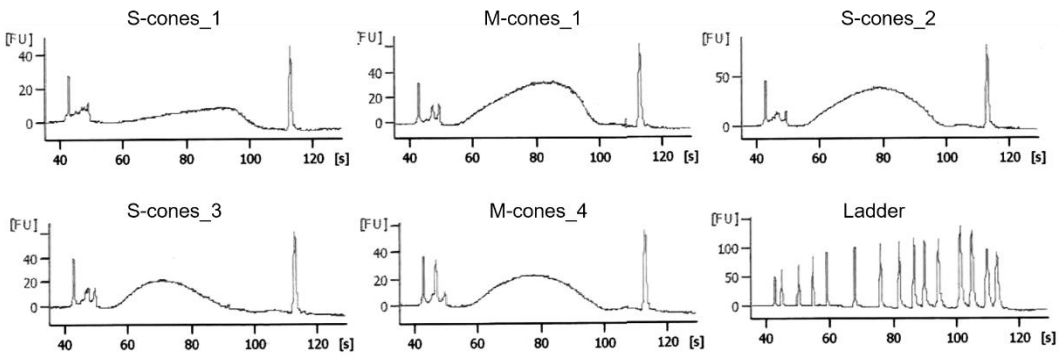

Figure 17 Quality analysis (II) of single cell samples after fragmentation (electropherogram). Before the final library synthesis, the sample had to be fragmented to an average length of 300 bp. This is to ensure that sequencing reads would not be limited to the 5'- and 3'-ends of each mRNA transcript. The samples were analyzed again to check for successful fragmentation. All samples were in the range of 200 – 2,000 bp.
Fragment-size of each ladder-peak: 1) 35 bp, 2) 50 bp, 3) 100 bp, 4) 140 bp, 5) 200 bp, 6) 300 bp. 7) 400 bp. 8) 500 bp, 9) 600 bp, 10) 700 bp, 11) 1000 bp, 12) 2000 bp, 13) 3000 bp, 14) 7000 bp, 14) 10,380 bp.

After this, each sample received its unique molecular barcode (a sequence of six bp) and the sequencing adapters, followed by PCR amplification. The sample concentrations were measured (Qubit fluorescence assay) and equimolarly pooled. I sequenced my cone library on the Illumina HiSeq 2500 platform. The device was operated by the NIDDK Genomics Core (NIH).

3.2.3 RNA-seq: Phototransduction genes in S- and M-cones

I analyzed the reads with RNA-STAR, HTseq and DESeq2 (for *R*) on the NIH Biowulf2 supercomputer. In short, each 50 bp read was aligned to the genome file of the thirteen-lined ground squirrel and the genes were identified using the gene annotation file of the squirrel. Then, the total number of counts per gene per sample was determined and statistically analyzed.

I detected reads from a total of 10,160 different genes that were present in at least one of the samples (out of 13). Out of those, 9,415 genes were found in at least six or more of my samples. In figure 18, I am showing an overview of all genes that

were detected, sorted by the number of counts (x-axis). The position on the y-axis (log fold change) indicates an enrichment in M-cones (high values) or in S-cones (low values). We can see that most of these genes -represented by dots- were expressed at similar levels in both cone types. The position of S- and M-opsin (black, respectively grey circle) in their respective quadrants agree with my expectations and show a successful separation of both cone types during sample collection.

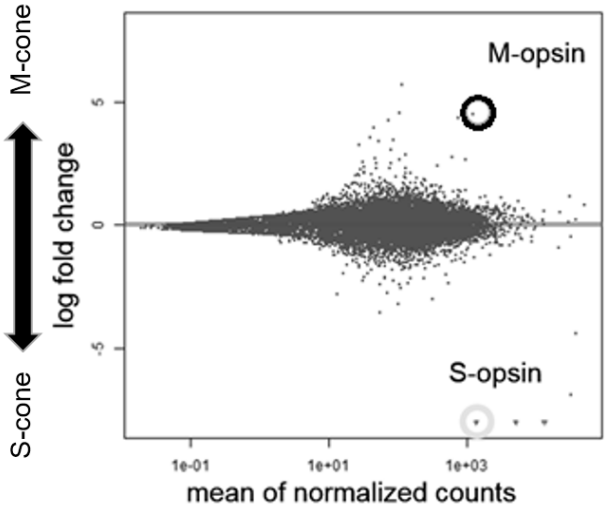

Figure 18 Differential gene expression in S- and M-cones. Negative log fold change values below the grey line represent S-cone enriched genes, positive numbers above the line represent M-cone enriched genes. 10,160 different genes were detected in at least one of the samples, 9,415 genes were found in at least six or more samples. The position of S- and M-opsin (black, respectively grey circle) in their respective quadrants agree with the expectations and show a successful separation of these cone types during sample collection.

First, I checked my sequencing data for signs of rod contamination. For this, I extracted the average expression values of known rod-markers in my samples (table 1). The rod-specific rhodopsin (Rho) was detected in both cone types at low levels (117.06 reads in S- and 138.13 in M-cones), whereas other rod-specific genes like rhodopsin kinase (Grk1), rod transducin$_{\alpha}$ (Gnat1) and the rod-inducing transcription factor Nrl showed negligible read numbers. This implied I had no or close to no contamination by rods.

Table 1 Mean reads for rod and cone genes in M- and S-cone samples

Gene	Counts (mean) S-cone samples		M-cone samples	
Rho (rhodopsin)	117.06	±264.71	138.13	±317.38
Nrl	0.00	±0.00	12.35	±30.25
Gnat1 (rod transducin$_\alpha$)	0.00	±0.00	0.06	±0.14
Grk1 (rhodopsin kinase)	0.00	±0.00	0.00	±0.00
Opn1sw (S-opsin)	24219.91	±11400.27	10.27	±5.63
Opm1mw (M-opsin)	44.74	±53.03	2606.54	±711.94
Gnat2 (cone transducin$_\alpha$)	2953.34	±2016.39	5057.80	±2489.38
Grk7 (receptor kinase 7)	1514.72	±840.61	1644.50	±399.63

To further verify the consistency of my data, I analyzed the expression of the opsins and known cone genes that I would expect to find in both subtypes (figure 19). I found that the number of reads for S-opsin (Opn1sw) was much higher in S-cone samples compared to M-cone samples (24,220 reads vs. 10 reads on average). The opposite was found for M-opsin (Opn1mw), which was highly enriched in M-cones (2,607 vs. 45 in S-cones). To compare genes that both cone types should have in common, I looked at genes that are involved in cone phototransduction: cone-transducin$_\alpha$ (Gnat2), receptor kinase 7 (Grk7), GCAP1 (Guca1a) and the cone-specific CNG-channel subunits (Cnga3, Cngb3). Except for cngb3, which showed slightly elevated reads in S-cones, all genes were expressed at similar levels.

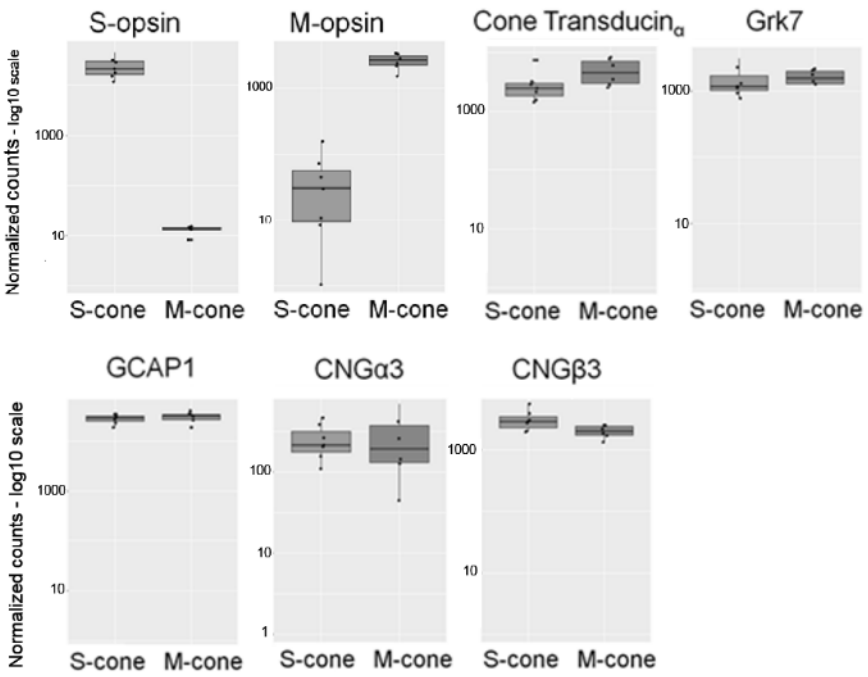

Figure 19 Commonly expressed genes in both cone types. S- and M-opsin were enriched in their respective dataset. Known markers for both cone types, namely cone transducinα (Gnat2), receptor kinase 7 (Grk7), guanylate cyclase activating protein 1 (Guca1a) and the CNG-channel subunits α3 and β3 (Cnga3, Cngb3), had similar expression values in both cone types.

3.2.4 Differentially expressed genes in S- and M-cones

After I confirmed reliable read numbers of general cone phototransduction genes, I wanted to focus on differentially expressed genes in the different cone subtypes. The analysis was done using DESeq2 for *R*, a tool that can estimate the variance-mean dependence in count data from RNA-seq experiments and test for differential expression based on a model using the negative binomial distribution (Love et al., 2014).

Including S- and M-opsin, my differential expression analysis showed a total of 34 genes significantly (P_{adj}<0.05) enriched in S-cones and 14 genes significantly enriched in M-cones. Table 2 and table 3 provide an overview of those genes, sorted by difference ("log2fold change"). Smaller numbers in Table 2 indicate a higher number of counts in S-cone samples, whereas larger numbers indicate more reads in M-cone samples.

Table 2 List of S-cone enriched genes. RNA-seq results based on mRNA expression in seven S-cone and six M-cone samples.

S-cone genes

Gene	Description	log2Fold Change	p_{adj}	Counts (mean) in S-cone samples		Counts (mean) in M-cone samples	
Opn1sw	opsin 1 (cone pigments), short-wave-sensitive	-10.15	7.97E-204	24219.91	±11400.27	10.27	±5.63
Ccdc136	coiled-coil domain containing 136	-9.58	1.10E-142	9348.85	±3901.57	9.74	±12.83
Nrxn3	neurexin III	-9.42	3.56E-104	2486.05	±1265.18	0.77	±0.54
Calu	calumenin	-6.88	5.74E-124	58027.24	±11017.21	379.52	±167.75
Sag	S-antigen, rod arrestin	-4.42	6.85E-12	68019.29	±25157.49	841.98	±1380.65
Snx7	sorting nexin 7	-3.56	3.13E-06	100.69	±57.66	1.29	±2.11
Flna	filamin, alpha	-3.23	8.23E-05	184.05	±166.83	3.10	±3.57
Ell2	elongation factor RNA polymerase II 2	-3.03	1.35E-05	563.19	±390.37	35.48	±28.62
Phldb1	pleckstrin homology like domain, family B, member 1	-2.80	3.35E-03	48.70	±60.68	0.09	±0.21
Anks1b	ankyrin repeat and sterile alpha motif domain containing 1B	-2.75	5.31E-03	130.60	±120.53	0.10	±0.25
Cadm1	cell adhesion molecule 1	-2.55	7.56E-03	198.48	±191.99	11.40	±19.95
LOC106145164	uncharacterized LOC106145164	-2.44	2.33E-02	99.95	±44.19	4.63	±5.29
Bicd1	bicaudal D homolog 1	-2.41	2.73E-02	193.42	±156.44	7.43	±12.39
Cpne3	copine III	-2.38	2.19E-02	242.72	±159.09	16.05	±17.14
Lnp1	leukemia NUP98 fusion partner 1	-2.38	1.78E-02	955.97	±586.60	76.71	±100.64
LOC101956933	uncharacterized LOC101956933	-2.19	2.81E-02	402.15	±188.64	48.67	±50.40
Gnb2	guanine nucleotide binding protein (G protein), beta 2	-2.18	1.78E-02	105.39	±48.74	15.66	±13.55
Acbd6	acyl-Coenzyme A binding domain containing 6	-1.80	2.97E-03	381.29	±115.51	91.31	±50.55
Atg7	autophagy related 7	-1.70	1.73E-02	523.49	±181.72	138.85	±103.07
Spag9	sperm associated antigen 9	-1.41	3.19E-02	1010.37	±508.57	347.84	±192.69
LOC101975357	histone H2B type 1	-1.31	1.63E-04	1761.88	±649.18	685.71	±117.78
Pet100	PET100 homolog	-1.24	6.49E-03	371.78	±99.33	143.87	±41.79

Table 3 List of M-cone enriched genes. RNA-seq results based on mRNA expression in seven S-cone and six M-cone samples.

M-cone genes

Gene	Description	log2Fold Change	p_{adj}	Counts (mean) in S-cone samples		Counts (mean) in M-cone samples	
Chst3	carbohydrate (chondroitin 6/keratan) sulfotransferase 3	5.66	5.15E-20	0.24	±0.33	245.19	±148.35
Tjp2	tight junction protein 2	4.55	1.37E-10	0.22	±0.30	228.19	±202.87
Opn1mw	medium-wave-sensitive opsin 1-like	4.50	1.67E-13	44.74	±53.03	2606.54	±711.94
Tex28	testis expressed 28	4.34	1.63E-09	7.30	±17.94	1626.75	±495.15
Arntl2	aryl hydrocarbon receptor nuclear translocator-like 2	4.26	5.16E-09	0.10	±0.19	156.28	±136.01
Isl2	insulin related protein 2 (islet 2)	3.95	1.88E-07	0.00	±0.00	98.98	±61.20
Shkbp1	Sh3kbp1 binding protein 1	3.54	1.19E-05	0.30	±0.52	85.64	±58.72
Rapgef5	Rap guanine nucleotide exchange factor (GEF) 5	3.46	1.59E-05	3.32	±6.03	183.97	±194.94
Ephx1	epoxide hydrolase 1, microsomal	3.39	4.73E-05	0.37	±0.84	115.05	±78.95
CUNH6 orf132	chromosome unknown C6orf132 homolog	3.27	8.23E-05	0.46	±0.61	59.67	±67.65
Rassf4	Ras association (RalGDS/AF-6) domain family member 4	3.06	7.29E-04	0.05	±0.13	170.41	±180.32
Bco1	beta-carotene oxygenase 1	2.87	1.87E-03	8.03	±13.68	267.42	±128.69
Ankrd33	ankyrin repeat domain 33	2.77	6.21E-05	104.42	±90.07	1193.02	±549.04
Acvrl1	activin A receptor, type II-like 1	2.72	6.07E-03	1.40	±3.70	98.02	±92.42
Oat	ornithine aminotransferase	2.66	3.46E-05	193.64	±181.81	1822.90	±832.62
CUNH1 orf226	chromosome unknown C1orf226 homolog	2.64	4.62E-03	14.54	±23.83	215.93	±222.62
Cables2	CDK5 and Abl enzyme substrate 2	2.51	1.89E-02	0.96	±2.01	104.44	±111.19
Kcnj14	potassium inwardly-rectifying channel, subfamily J, member 14	2.51	1.87E-02	0.00	±0.00	169.77	±139.74
Glt1d1	glycosyltransferase 1 domain containing 1	2.38	2.62E-03	88.35	±63.64	717.13	±459.84
Inca1	inhibitor of CDK, cyclin A1 interacting protein 1	2.33	4.12E-02	0.19	±0.51	69.18	±63.87

Crmp1	collapsin response mediator protein 1	2.31	4.98E-02	5.41	±9.10	161.37	±66.03
Itgb5	integrin beta 5	2.30	3.19E-02	19.25	±39.00	255.55	±177.90
Sipa1l1	signal-induced proliferation-associated 1 like 1	2.29	3.19E-02	6.70	±7.14	98.84	±90.42
Slc25a25	solute carrier family 25 (mitochondrial carrier, phosphate carrier), member 25	2.12	3.19E-02	31.14	±36.44	243.60	±160.91
Nxn	nucleoredoxin	2.09	1.86E-02	42.24	±39.04	279.21	±246.70
Gtf3c1	general transcription factor III C 1	1.73	2.73E-02	90.79	±61.59	373.45	±122.86
Gabarapl 1	gamma-aminobutyric acid (GABA) A receptor-associated protein-like 1	1.59	3.35E-03	110.94	±60.45	359.92	±162.59
Pitpnb	phosphatidylinositol transfer protein, beta	1.59	3.19E-02	146.97	±79.96	516.48	±219.48
Fkbp4	FK506 binding protein 4	1.57	3.89E-02	140.90	±44.81	492.62	±357.05
Psmd11	proteasome (prosome, macropain) 26S subunit, non-ATPase, 11	1.49	7.85E-03	208.82	±88.23	635.12	±278.07
Sgk1	serum/glucocorticoid regulated kinase 1	1.43	1.75E-02	501.57	±248.34	1498.69	±586.96
Ckb	creatine kinase, brain	1.17	2.69E-03	18701.22	±6343.74	43698.70	±12809.95
Prnp	prion protein	1.09	2.81E-02	2030.25	±911.35	4539.32	±1052.81
Guk1	guanylate kinase 1	0.55	2.73E-02	10680.18	±965.25	15736.68	±2559.87

The differential gene expression analysis detected **opn1sw** (S-opsin) as the top gene in S-cones. The second-most expressed S-cone gene was **Ccdc136** (coiled coil domain containing 136). The gene has previously been described as novel marker for S-opsin-positive cells in mice (Smiley et al., 2016).

Calu (calumenin) is a Ca^{2+}-binding EF-hand protein and is thought to play a role in protein folding and sorting. However, close examination showed that this gene was a false-positive result. A closer look at the reads that were aligned to this locus, revealed that those reads most likely belonged to opn1sw. On the genome, those two genes are located next to each other (more details are provided in the

supplement, 6.1; this was also true for an M-cone enriched gene that is localized next to opn1mw (M-opsin). Opn1mw-reads were falsely aligned to Tex28).

Sag encodes the protein rod arrestin, an important member of the rod phototransduction cascade. Rod arrestin in S-cones has been reported before (Müller et al., 1989; Craft et al., 2014). Nevertheless, it is still generally considered to be a rod gene (Lamb, 2013) which made this finding surprising (continued in section 3.2.5.).

Cpne3 (copine 3) is a member of Ca^{2+}-binding proteins that translocate from the cytoplasm into the membrane at high Ca^{2+}-concentrations (Perestenko et al., 2010). Because they also have a domain for protein-protein interactions, they may target other proteins to the membrane. Interestingly, other members of this protein family are specifically expressed in other retinal cell types. Copine 9 has been reported as a new marker for S-cone bipolar cells (Shekhar et al., 2016). Their function is not known yet.

Gnb2 is a G-protein$_\beta$ subunit. In cones, Gnb3 is thought to be the transducin$_\beta$ subunit in the phototransduction cascade (Lamb, 2013). To investigate if there could be a difference between S- and M-cones, I also looked at the expression values of Gnb3. Gnb3 is highly expressed in both S- and M-cones, so that seemed unlikely. However, in 1992, Peng and colleagues immunolabeled primate retina with antibodies against different β-subunits. They found Gnb2 in amacrine cells and in the OPL.

Interestingly, a group of genes found in this dataset shared a common characteristic. **Spag9**, **Ccdc136**, **Atg7** and **Cadm1** are all expressed in testes or spermatozoa (Jagadishet al., 2005; Geng et al., 2016; Wang et al., 2014; Surace et al., 2006). Some of these are associated with infertility of male mice.

In addition, I found three genes that could play a role in synapse formation in S-cones: Nrxn3, Flna and Cadm1. These discoveries were especially interesting considering the specific S-cone bipolar cell synapse.

- **Nrxn3** is a member of the neurexin family of cell-adhesion molecules. Studies showed that neurexins are expressed in presynaptic terminals and

they form trans-synaptic complexes with members of the neuroligin family (Ichtchenko et al., 1995). Early studies suggested they could play a role in synapse formation (Dean et al., 2003). Later, the group around Südhof demonstrated that Neurexin is rather required to enhance signaling at the synapse and to keep it functional (Südhof, 2008).

- **Flna** has been reported to play a role in axon guidance of UV-sensitive photoceptors in *Drosophila* (Oliva et al., 2015).
- The deletion of **Cadm1** in a mouse model resulted in processes of horizontal cells sprouting into the ONL (Ribic et al., 2014).

Because of these reports I decided to take a closer look at Flna and Cadm1 (see sections 3.2.6 and 3.2.7).

3.2.5 Rod arrestin is highly expressed in S-cones

One of the genes enriched in S-cones was rod arrestin (Sag; 68,019 reads in S-cones vs. 841 reads in M-cones), a typical rod marker. To verify this result, I labelled ground squirrel retina with rod arrestin antibody and co-stained with anti-rhodopsin and anti-S-opsin to identify rods and S-cones (figure 20). As predicted by the RNA-seq data, I found strong localization of rod arrestin (green) in S-opsin-positive cells (blue). As expected, rhodopsin-positive cells (magenta) were also immunoreactive for rod arrestin. The protein was not detected in M-cones, which are the most common type of photoreceptors in the squirrel retina (~ 80 %). This result was important because it confirmed my mRNA-based prediction on protein-level. Craft et al. (2014) and Müller et al. (1989) reported a similar staining in monkey and tree shrew retinas. However, the function of rod arrestin in S-cone photoreceptors is not entirely understood yet.

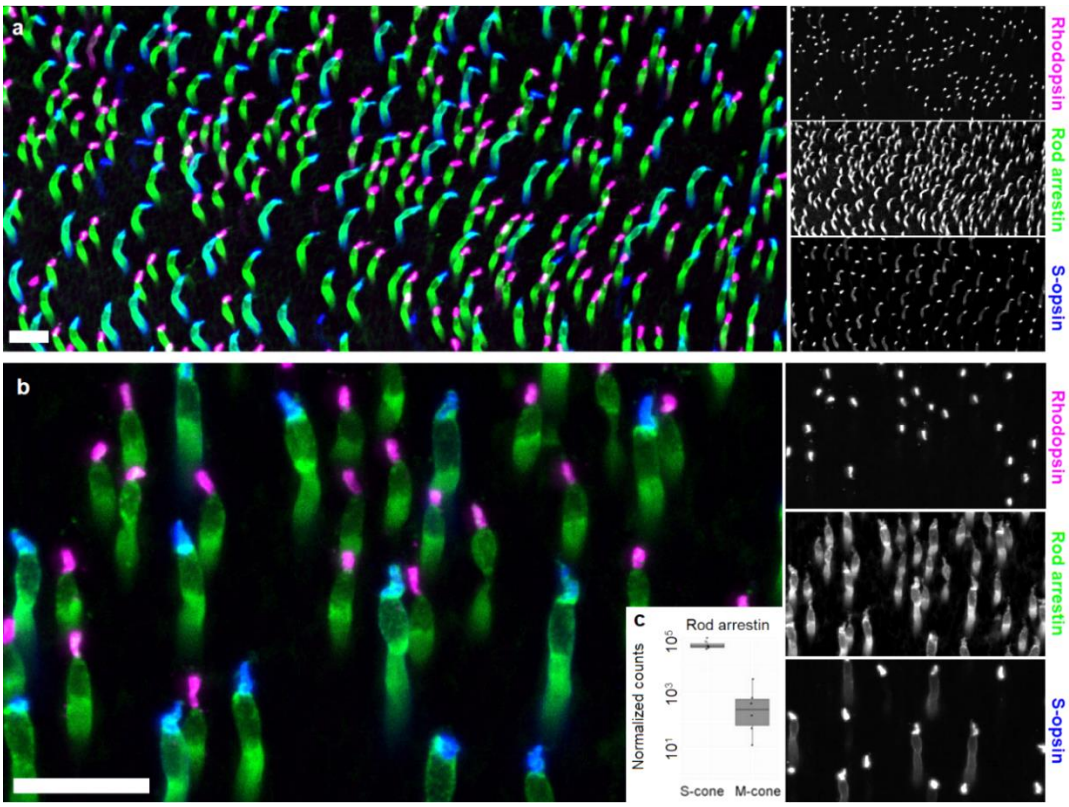

Figure 20 Expression of rod arrestin in rod and S-cone photoreceptors of the ground squirrel at different magnifications. Based on the high RNA expression values of rod arrestin (sag) in S-cones, a flat-mounted ground squirrel retina was stained with anti-rod arrestin (green), rhodopsin (magenta) and S-opsin (blue). Co-labeling of rod arrestin and S-opsin confirmed my RNA-seq findings on protein level. Scale bars: 20 µm.

3.2.6 Filamin A expression in the ground squirrel retina

According to my RNA-seq, data, filamin A (Flna) was highly enriched in S-cones. I chose to further investigate this gene because it could potentially play a role in S-cone synapse formation based on these previous findings: Filamin A is an actin-binding protein. It helps to form cell-cell contacts in the cardiovascular system in mice (Feng et al., 2006) and regulates axon regeneration (Cho et al., 2015). Most interestingly, it is involved in axon guidance of the UV-sensitive R7-cell in *Drosophila* (Oliva et al., 2015).

To test the prediction, I investigated its expression on protein level. Figure 21 shows a tissue section of the ground squirrel after immunostaining with filamin A (green), S-opsin (blue), and rhodopsin (magenta).

Filamin A signals were observed in the OPL, OLM and in putative blood vessels of the ground squirrel. No cell bodies were labeled and there was no co-localization with rhodopsin or S-opsin, so I could not determine in which cells filamin A was expressed. However, comparing the filamin A-signal in the OPL to that of the nuclei (panel b), it seemed to be closer localized towards the INL. It is possible that the observed puncta arose from dendrites of horizontal cells or bipolar cells.

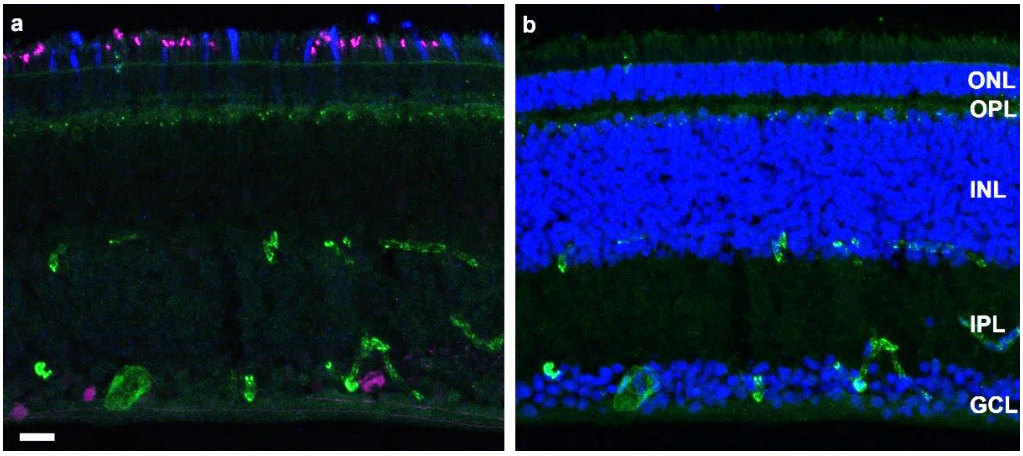

Figure 21 Filamin A expression in the ground squirrel retina. The RNA-seq analysis predicted differential expression of filamin A in S-cones. **a** A tissue section was stained with antibodies against filamin A (green), S-opsin (blue), and rhodopsin (magenta). Filamin A labeled the OPL and blood vessels in the inner retina. A faint signal was detected in the OLM **b** Filamin A staining (green) and nuclei (DAPI, blue) in the same section. Close localization of filamin A to nuclei of the INL could indicate expression in horizontal cells or bipolar cells. Scale bar: 20 µm.

3.2.7 Cadm1 expression in the ground squirrel

Cadm1 (cell adhesion molecule 1) was predicted to be differentially expressed in S-cones (198 reads in S-cones compared to 11 reads in M-cones). This transmembrane protein was especially interesting because it plays a role in synapse formation in the brain (Biederer et al., 2002) and in the outer plexiform layer of the retina. In a previous KO-mouse study, the authors observed dendrites of horizontal cells that sprouted into the outer nuclear layer (Ribic et al., 2014).

To evaluate the protein expression of Cadm1 I stained retinal sections and flat-mounted tissue of the ground squirrel (figure 22). I detected distinct Cadm1-puncta (green) in the outer and inner segments of S-opsin- (blue) and rhodopsin-positive photoreceptors (panels a-d). Although the signal in those segments looked highly distinct, it was also detected in presumably all cell bodies of the retina. The plexiform layers were not labeled (panels e-f).

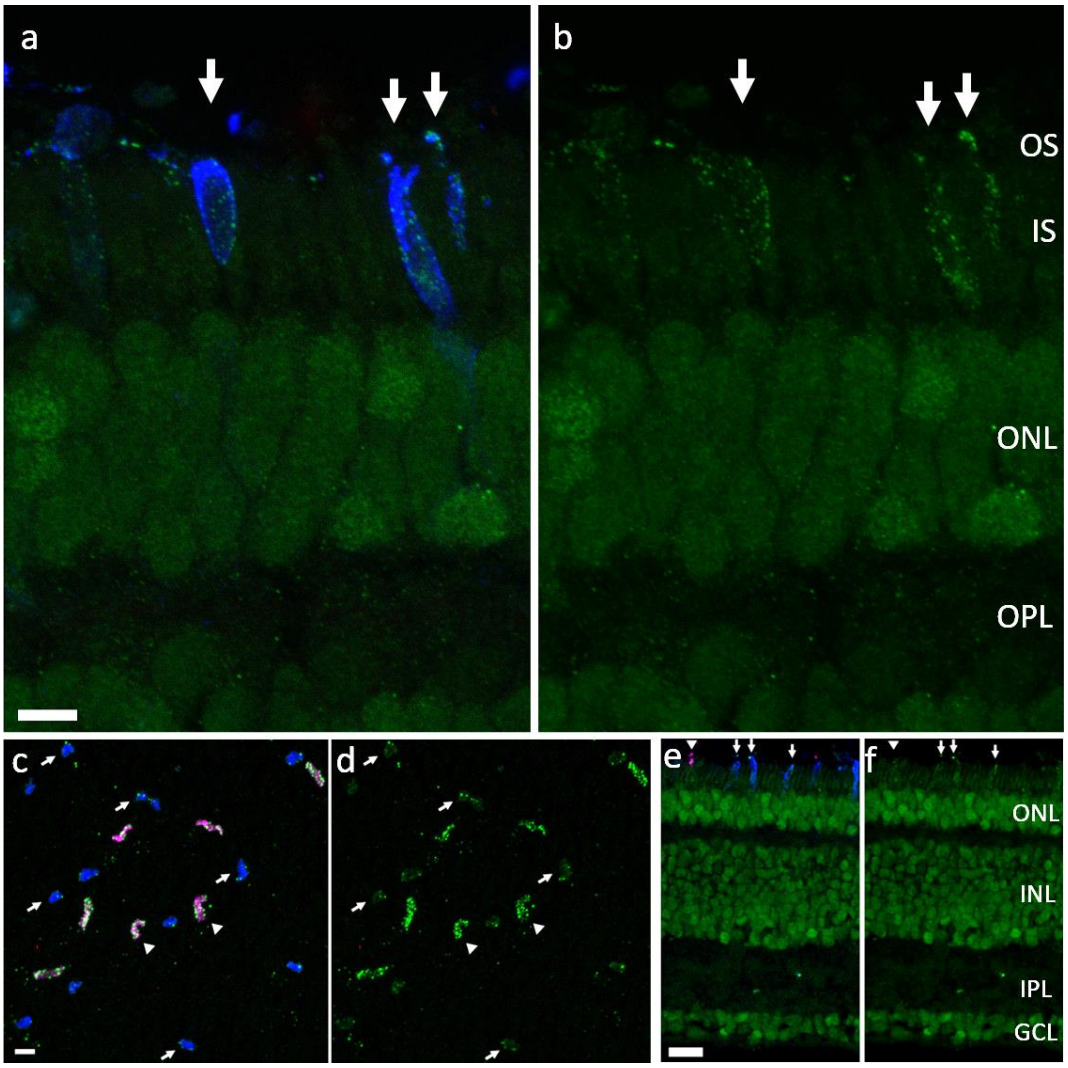

Figure 22 Cadm1 expression in the ground squirrel retina. Tissue was stained with antibodies against Cadm1 (green), S-opsin (blue) and rhodopsin (magenta). Distinct Cadm1-puncta were detected in inner and outer segments of S-cones (arrows) and rods (arrowheads). A signal in cell bodies was detected in all nuclear layers and the GCL. **a-b** Photoreceptors (section; (a) merged, (b) Cadm1 only). **c-d** Photoreceptor outer segments (flat-mount; (c) merged, (d) Cadm1 only) **e-f** All layers at low magnification (section; (e) merged, (f) Cadm1 only. Scale bars a-d:5 µm, e-f: 20 µm

3.3 AAV mediated GFP-expression in the ground squirrel

The comparison of the M- and S-cone transcriptome identified differentially expressed genes for which we do not know what function they may have in these cells. Genetic tools that allow the overexpression or a knockdown of an unknown gene *in vivo*, could help to identify the function. Therefore, I tested the adeno-associated virus (AAV)-mediated delivery of a reporter vector in the ground squirrel. I used AAV serotypes 2 and 8 in different animals. AVV8 has previously been reported to efficiently transduce mouse photoreceptors (Allocca et al., 2007). The AAVs for this experiment were kindly provided by Zhijian Wu (Ocular Gene Therapy Core, NEI/NIH). Tantai Zhao, a surgeon in Dr. Wei Li's laboratory (NEI/NIH), performed the injections (subretinal and intravitreal). All plasmids contained eGFP (enhanced green fluorescent protein) under control of the ubiquitous CMV promoter to test which cells I could transduce with these serotypes. I harvested, fixed and cryosectioned the retinae six weeks after injection.

Figure 23 shows selected cells that expressed GFP after the intravitreal injection of AAV2. No antibodies were used, the signal (green) originated from the expressed GFP. The density of transduced cells was sparse, but it was observed in a variety of retinal cells. I found putative horizontal cells (panel a), Müller cells (b), photoreceptors (c), bipolar cells (d) and ganglion cells (e).

AAV2 could successfully be used to transduce cells in the ground squirrel retina. However, to achieve cell specificity, a cell type-specific promoter would be deemed necessary, since this serotype did not show a preference for specific cell types.

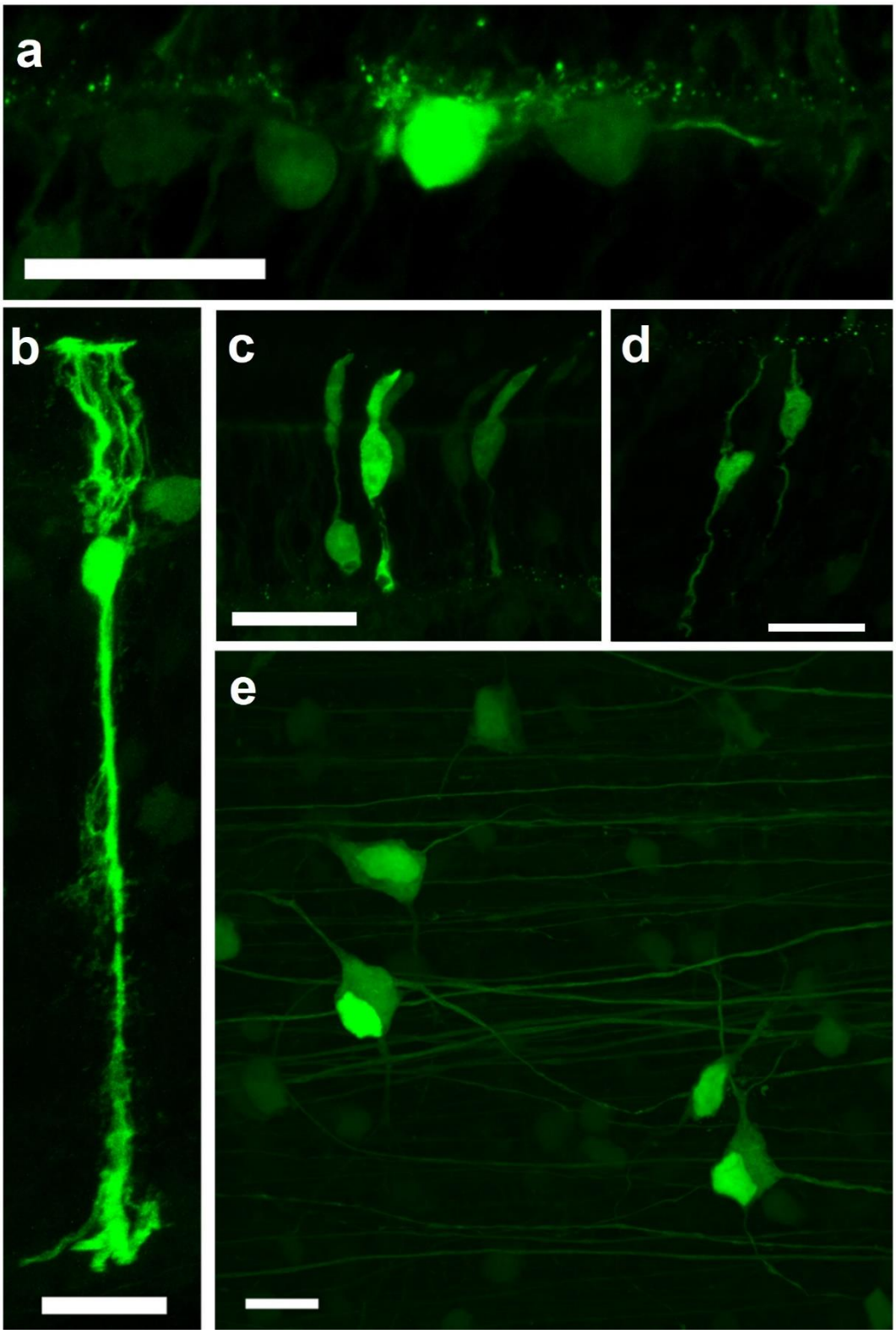

Figure 23 AAV2-mediated GFP-expression in cells of the ground squirrel retina (cryosections). An adeno-associated virus, serotype 2, with CMV-GFP was intravitreally injected in one eye of a ground squirrel. The virus transduced different cell types: **a** Putative horizontal cells. **b** Müller cell. **c** Photoreceptors. **d** Bipolar cells. **e** Ganglion cells (flat mount). Scale bars: 20 µm.

Figure 24 shows a cryosection of a retina after subretinal injection of AAV8. I found a strong signal in the photoreceptor layer, close to the site of injection. Other layers were not labeled. The results indicated that the subretinal injection of serotype 8 could be used as a tool to specifically target photoreceptor cells.

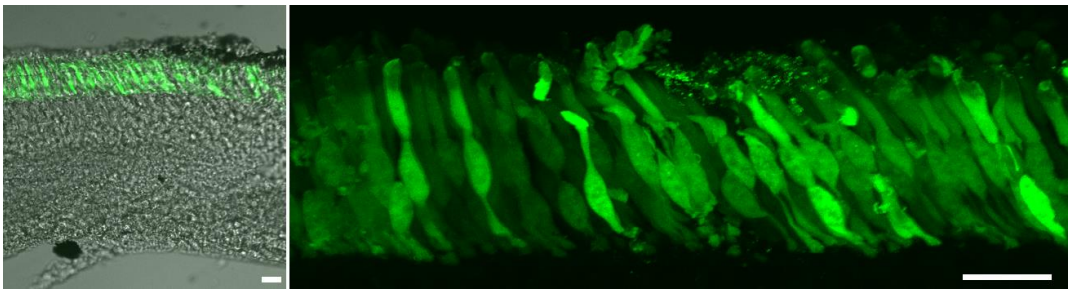

Figure 24 AAV8-mediated GFP-expression in ground squirrel photoreceptors. An adeno-associated virus, serotype 8, with CMV-GFP was subretinally injected in one eye of a ground squirrel. Left: retinal section shows GFP-expression in the photoreceptor layer around the site of injection. GFP was not detected in any other layer. Right: a magnified view on the photoreceptor layer shows GFP-signals throughout individual photoreceptor cells. Scale bar: 20 µm

3.4 Targeting rod photoreceptors for genetic profiling

The S-cone has been described as the default photoreceptor in the retina (Swaroop et al., 2010). When rod- or M-cone-fate are not induced, the photoreceptor will become an S-cone. For rods, it is mainly the expression of the transcription factor Nrl that determines its fate. In my RNA-seq experiment that determined molecular differences in cone photoreceptors, I observed a high expression of rod arrestin in rods and S-cones, but not in M-cones. This might also be true for Cadm1, which showed distinct puncta in S-cones and rods, but not in M-cones. It could be possible that rods share more genes with S-cones than we previously thought. To examine this hypothesis, I planned to examine the genetic profile of ground squirrel rods through RNA-sequencing.

3.4.1 Use of the human GRK1-promoter to target rods

First, I needed to develop a way to label rods. I tried live-labeling rods using the same protocol I used to label S-cone photoreceptors (figure 15), but with an antibody directed against rhodopsin. When I looked at the dissociated and stained single cells, I did not detect any signals (not shown). This supported the presumption, that my protocol only works for epitopes that are on the surface of the cell. Rods, as we know, have an outer membrane, that completely encloses the rhodopsin-containing disks. Since it was necessary to keep the cells in a healthy state for the RNA-extraction, I could not use detergents to permeabilize the cells. Based on my previous experience with AAV-mediated GFP transduction (section 3.3), I used an AAV-delivered vector expressing GFP under the control of the rod-specific promoter of human GRK1 (rhodopsin kinase). A comparable construct has been shown to successfully lead to GFP-expression in mouse photoreceptors (Khani et al., 2007; Yu et al., 2017). In contrast to mouse, rhodopsin kinase expression in the ground squirrel is restricted to rods. This is supported by my RNA-seq data (table 1) and by biochemical assays that studied the opsin-phosphorylation after Grk7 (cone opsin kinase)- inhibition (Liu et al., 2005).

I kindly received the packaged virus from Zhijian Wu (Ocular Gene Therapy Core, NEI/NIH). Tantai Zhao, a surgeon in Dr. Wei Li's laboratory (NEI/NIH), subretinally injected the AAV in one animal. After six weeks, I dissected the retina. I quickly identified the area penetrated by the injection needle and confirmed fluorescence signals around this site using a fluorescence microscope. I excised this part and dissociated the cells. I collected and pooled 20 GFP-positive cells (figure 25). The sample was subjected to RNA-sequencing as described (methods, 2.2.5).

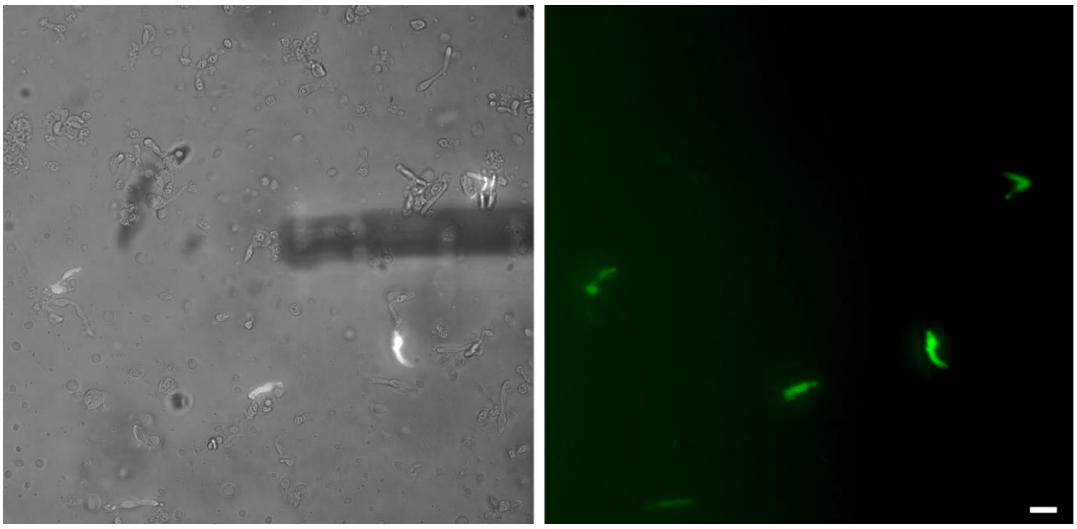

Figure 25 Dissociated cells from a ground squirrel retina six weeks after subretinal injection of an adeno-associated virus, serotype 8 (AAV8), containing GFP under control of the human GRK1 promoter. The goal was to label and isolate rod photoreceptors. The left image shows the combined DIC (differential interference contrast)- and fluorescence (470 nm excitation) view. The right image shows the same sector, but under 470 nm light only. No antibodies were used. I detected GFP-expression in a subset of dissociated cells. Scale bar 20 µm.

3.4.2 RNA-seq results of GRK1-GFP positive photoreceptors

To analyze the new sample, I compared it with three of my previously collected S-cone samples. All samples that were used for this analysis were taken from awake ground squirrels.

The analysis of the data showed zero reads for Grk1 (rhodopsin kinase). I made the same observation for other rod-specific genes: the reads for Rho (rhodopsin) and Gnat1 (rod transducin) were also low or zero (table 4). At the same time, the reads for cone genes were unexpectedly high. I found high expression of Gnat2 (cone transducin) and Grk7 (cone opsin kinase). To further identify the subtype, I looked at the expression of S- and M-cone markers. I found low expression of the S-cone-specific genes Opn1sw (S-opsin) and Sag (rod arrestin). Instead I observed high expression of M-opsin. To further examine if there were more M-cone-specific genes, I compared the new sample to the most differentially expressed M-cone genes that I identified in section 3.2.4. (table 3). Among others, I found high

expression values for Tjp2 (tight junction protein 2) and Arntl2 (aryl hydrocarbon receptor nuclear translocator-like 2), two of the highest differentially expressed genes in M-cones.

I concluded that my approach to identify rods by using human GRK1-controlled GFP-expression did not work. Instead, this approach targeted M-cone photoreceptors. Possible reasons are discussed in section 4.4.

Table 4 Gene expression in Grk1-GFP$^+$ cells. An AAV8 reporter vector was used to identify and sequence rod photoreceptors in the ground squirrel. The vector contained GFP under the control of the human GRK1 promoter. I did not observe an enrichment of rod-specific genes (Rho, Gnat1, Grk1). Instead, counts for known M-cone genes were high. The analysis of the labeled cells, compared to S- and M-cones from the previous RNA-seq experiment, suggested that I collected M-cones.

Gene expression in Grk1-GFP$^+$ cells				
Gene	**Description**	**S-cones**		**Grk1-GFP$^+$ cells***
Rho	Rhodopsin	36.38	±62.41	1.33
Opn1sw	S-opsin	58191.05	±28692.65	133.82
Opn1mw	M-opsin	80.58	±61.62	6938.58
Sag	Rod arrestin	154909.00	±65079.27	21.30
Gnat1	Rod transducin	0.00	±0.00	0.67
Gnat2	Cone transducin	7349.63	±6177.38	25637.87
Grk1	Rhodopsin kinase	0.00	±0.00	0.00
Grk7	Cone opsin kinase	3652.62	±2213.21	3874.74
Arntl2	aryl hydrocarbon receptor nuclear translocator-like 2	0.30	±0.53	315.57
Tjp2	Tight junction protein 2	0.53	±0.48	369.50

*Standard deviations for this condition are not available because only one Grk1-GFP$^+$-sample was tested

3.5 Transcriptomic changes in photoreceptors of the hibernating squirrel

Ground squirrels hibernate during the winter. The retina and the photoreceptors undergo changes during that time: synaptic ribbons are much smaller or detached, the number of synaptic vesicles is decreased, the outer of segments are shortened and number and size of the ellipsoid mitochondria is reduced (Kuwabara, 1975; Gruber et al., 200, Mehta et al, 2013; Merriman et al., 2016). I wanted to investigate how these changes are reflected on the transcriptomic level.

I analyzed the raw data files that I obtained for the S- vs. M-cone study, since photoreceptors were collected during all seasons. For this experiment, cones were grouped in two conditions: awake (8 samples) or hibernating (5 samples). In figure 26 I am showing an overview of all expressed genes that were detected. Genes were sorted by the number of counts (x-axis). The position on the y-axis indicates high expression in hibernating animals (positive numbers) or in awake animals (negative numbers). The majority of genes seemed to be equally expressed in both conditions. I found 48 genes to be significantly ($p_{adj} < 0.05$) differentially expressed.

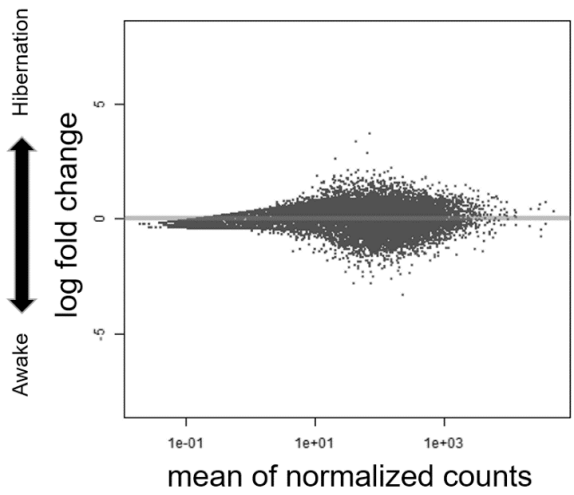

Figure 26 Differential gene expression in hibernating and awake cone photoreceptors of the ground squirrel. Each dot represents one gene. Genes with a positive log fold change-value are upregulated during hibernation, whereas negative values show genes upregulated during the awake state. Genes are sorted by their mean abundance (measured in counts, x-axis). Samples were collected from eight awake and five hibernating ground squirrels. For each sample, 16 – 20 cones were combined.

First, I looked at changes in the expression of phototransduction genes. I expected changes in these genes because of the altered morphology of outer segments in hibernating animals. Since I combined S- and M-cone samples, I included only genes that all cone subtypes have in common (figure 27). None of the analyzed genes, which include Gnat2, Guca1a, Guca1c, Cnga3, Cngb3, Grk7 and Pde6h, showed a significant difference in expression between the conditions. This indicated normal expression of phototransduction genes.

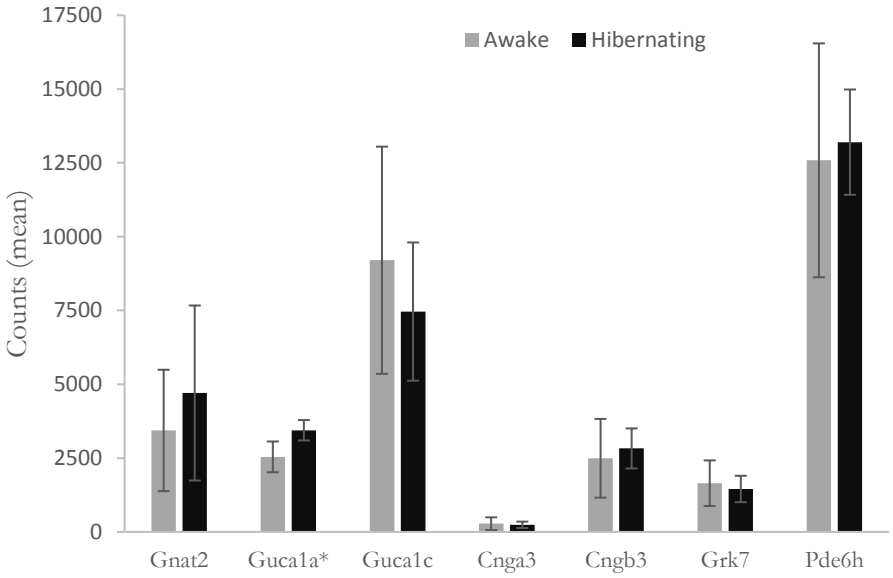

Figure 27 Phototransduction genes in cone photoreceptors of the awake and the hibernating ground squirrel. Amounts are displayed in counts (mean of all samples per condition). Hibernation did not show significant effects on expression of phototransduction genes. Gnat2: cone transducin, Guca1a: GCAP1, Guca1c: GCAP3, Cnga3: cone CNG-channel subunit α3, Cngb3: CNG-channel subunit β3, Grk7: receptor kinase 7, Pde6h: cone PDE γ-subunit. *Guca1a values were scaled to 10% to fit the diagram.

After examining components of cone phototransduction, I focused on genes that were differentially expressed (table 5 and table 6). A few of them have functions in metabolism, e.g., Ldha, Eno1 and Pdk4. This reflected changes in physiology during hibernation (van Breukelen, 2015). Furthermore, I screened the list for genes that were functionally related to outer segments and synaptic terminals. The goal

was to find genes that could explain the cone physiology during hibernation. I identified three genes that fit this description:

One of the most downregulated genes during hibernation was Slitrk3 (Slit and NTRK-like family member 3). The protein has been described as a postsynaptic adhesion-molecule that regulates the development of inhibitory synapses. Mice with a Slitrk3-deletion showed a smaller number of inhibitory synapses in hippocampal C1 neurons (Takahashi et al., 2012).

I also found Ctnnd1 (catenin δ1) to be downregulated in the hibernating animal. In neurons, it has been located at growth cones and in postsynaptic terminals. Its expression in pre-synaptic terminals is unclear. It has been reported to be involved in the regulation of synaptic density, architecture, plasticity and function (Yuan et al., 2017).

Among the genes that were upregulated during hibernation, I detected Pebp1 (or Rkip: Raf-1 kinase inhibitory protein). This protein is located in the cilium of photoreceptors. A study by Murga-Zamalloa et al. (2011) showed that it interacts with Cep290, a protein that modulates cilium formation. In their experiments on zebrafish, an accumulation of Pebp1 resulted in perturbed photoreceptor outer segment development.

Possible effects of the up- or downregulation of these genes in the context of hibernation are discussed in section 4.5.

Table 5 Upregulated genes in photoreceptors of the hibernating squirrel

Upregulated genes in the hibernating squirrel

Gene	Description	log2Fold Change	P_{adj}	Counts (mean) in awake samples		Counts (mean) in hibernating samples	
Dedd	death effector domain-containing	3.68	8.45E-06	4.04	±5.23	172.96	±74.34
Znf10	NA	3.37	4.63E-04	0.00	±0.00	113.11	±89.81
Adssl1	adenylosuccinate synthetase like 1	2.85	7.42E-03	3.03	±8.37	160.82	±181.72
Csdc2	cold shock domain containing C2, RNA binding	2.19	4.28E-02	42.15	±43.72	333.77	±120.28
Mapk9	mitogen-activated protein kinase 9	2.07	2.36E-02	45.19	±30.13	282.79	±240.49
Smg9	smg-9 homolog, nonsense mediated mRNA decay factor (C. elegans)	1.99	4.60E-02	41.24	±27.26	250.43	±175.24
LOC101960640	HLA class I histocompatibility antigen, B-40 alpha chain-like	1.78	1.91E-02	239.58	±190.72	992.20	±378.45
Tubgcp2	tubulin, gamma complex associated protein 2	1.76	2.73E-02	77.59	±43.22	317.95	±182.01
Rragd	Ras-related GTP binding D	1.58	1.35E-03	168.32	±76.15	563.70	±97.58
Pebp1	phosphatidylethanolamine binding protein 1	1.56	1.69E-02	443.35	±205.91	1458.52	±307.13
Sod2	superoxide dismutase 2, mitochondrial	1.46	3.04E-02	373.61	±244.44	1114.76	±240.31
Ldha	lactate dehydrogenase A	1.44	3.43E-03	1228.83	±489.57	3572.99	±1550.01
LOC101958317	phytanoyl-CoA dioxygenase, peroxisomal	1.44	2.34E-03	160.13	±50.15	454.54	±46.30
Ap1s1	adaptor protein complex AP-1, sigma 1	1.41	3.44E-02	612.75	±297.78	1800.29	±977.83
Eno1	enolase 1, alpha non-neuron	1.23	1.45E-02	2129.76	±834.45	5283.61	±1787.17
Actb	actin, beta	1.19	8.24E-03	1917.90	±621.53	4550.91	±1705.94
Tpi1	triosephosphate isomerase 1	1.05	1.35E-02	1322.76	±355.03	2808.91	±846.57
Atp5b	ATP synthase, H+ transporting mitochondrial F1 complex, beta subunit	1.04	3.79E-02	3460.23	±1218.99	7405.55	±1920.40
Prcd	NA	1.00	5.58E-04	1049.74	±192.44	2151.11	±456.44
LOC101969296	chromosome unknown C11orf58 homolog	0.90	3.94E-02	1592.15	±518.08	3032.84	±320.49
Oaz1	ornithine decarboxylase antizyme 1	0.90	1.35E-03	4456.48	±856.87	8393.27	±1525.99
H3f3b	H3 histone, family 3B	0.84	9.09E-03	5237.36	±1310.20	9499.05	±1044.16
Atp5a1	ATP synthase, H+ transporting, mitochondrial F1 complex, alpha subunit 1	0.75	3.17E-02	3824.17	±716.68	6513.31	±1443.84
Gapdh	glyceraldehyde-3-phosphate dehydrogenase	0.74	1.23E-02	5979.85	±1171.97	10059.11	±1500.55

Table 6 Upregulated genes in photoreceptors of the awake squirrel.

Upregulated genes in the awake squirrel							
Gene	**Description**	**log2Fold Change**	**P_{adj}**	**Counts (mean) in awake samples**		**Counts (mean) in hibernating samples**	
Pdk4	pyruvate dehydrogenase kinase, isoenzyme 4	-3.32	3.22E-04	372.53	±216.07	4.02	±5.16
LOC101964088	WD repeat and coiled coil containing (Wdcp)	-2.83	7.42E-03	119.12	±159.27	0.86	±1.21
Slitrk3	SLIT and NTRK-like family, member 3	-2.80	8.24E-03	64.12	±56.52	0.18	±0.27
Ctnnd1	catenin (cadherin associated protein), delta 1	-2.60	8.24E-03	240.46	±179.68	15.78	±21.48
Per1	period circadian clock 1	-2.53	2.70E-02	89.21	±92.31	0.54	±1.08
Bcl6	B cell leukemia/lymphoma 6	-2.52	2.24E-02	125.99	±111.06	5.13	±4.66
P3h3	prolyl 3-hydroxylase 3	-2.43	2.70E-02	327.76	±328.62	19.44	±29.31
Grb7	growth factor receptor bound protein 7	-2.28	1.45E-02	296.53	±287.95	36.34	±30.51
Ptar1	protein prenyltransferase alpha subunit repeat containing 1	-2.27	1.91E-02	297.91	±161.82	35.48	±42.87
Mex3c	mex3 RNA binding family member C	-2.16	4.89E-02	164.80	±98.63	18.96	±26.12
Vps13b	vacuolar protein sorting 13B (yeast)	-2.03	3.46E-05	455.66	±126.45	99.29	±58.73
Clk1	CDC-like kinase 1	-1.83	2.18E-02	884.43	±452.32	199.46	±109.49
Timm10b	translocase of inner mitochondrial membrane 10B	-1.71	1.21E-03	289.41	±86.62	80.08	±34.17
Plekhf2	pleckstrin homology domain containing, family F (with FYVE domain) member 2	-1.68	4.17E-02	1008.01	±570.06	260.32	±74.07
Abcb1	ATP binding cassette subfamily B member 1	-1.65	2.34E-03	1118.73	±538.75	321.38	±83.46
LOC101962669	chromosome unknown C21orf91 homolog (CUNH21orf91)	-1.59	1.06E-02	2183.11	±671.63	647.47	±448.06
Psme4	proteasome (prosome, macropain) activator subunit 4	-1.57	7.07E-03	968.73	±445.80	297.85	±99.16
Pnrc1	proline-rich nuclear receptor coactivator 1	-1.56	1.69E-02	525.81	±230.33	158.68	±79.29
LOC106145000	small EDRK-rich factor 1	-1.49	2.30E-02	510.03	±189.00	162.69	±87.51
Mllt6	myeloid/lymphoid or mixed-lineage leukemia; translocated to, 6	-1.42	2.18E-02	609.27	±300.39	208.75	±78.61
G0s2	G0/G1 switch gene 2	-1.41	3.22E-04	5240.90	±1660.42	1886.47	±499.31
Btbd3	BTB (POZ) domain containing 3	-1.34	8.45E-06	3970.41	±1014.21	1528.09	±263.04
Cpsf6	cleavage and polyadenylation specific factor 6	-1.28	2.64E-02	1543.38	±593.55	595.67	±253.38

LOC101971023	uncharacterized LOC101971023	-1.25	4.70E-02	336.63	±126.58	134.43	±43.65

4 Discussion

4.1 Development of the tree shrew retina

4.1.1 Morphology of the developing tree shrew retina

In this work, I investigated the development of the retina of the tree shrew, a diurnal mammal with cone-dominated vision. I explored morphological and transcriptomic changes at different embryonic and postnatal stages.

The development of the mouse retina, which is rod-dominated, has been described before and the general progression in both animals was comparable. Birthdating studies of retinal neurons in mouse have shown that ganglion cells, amacrine cells, horizontal cells and cones are generated during the embryonic stages, whereas bipolar and Müller cells follow after birth. Rods are generated both pre- and postnatally (Cepko et al., 1996).

Sharma et al. did a comparable morphological study of the mouse retina in 2003. At E18.5, recoverin staining of the mouse retina resembled my findings at E30 in tree shrew. The authors observed a patchy staining pattern of cells in the distal-most layer of the neuroblastic layer. At birth, they saw recoverin-positive fibers extending far into the neuroblastic layer. It has been reported that in ferrets, the photoreceptors extend their processes into the inner plexiform layer (IPL) at P1. Later during development, they form contacts within both ChAT-positive laminae of the IPL, before they eventually retract and contact bipolar cells (Johnson et al., 1999). I did not make this observation in tree shrew; neither the recoverin- (figure 9), nor the opsin-antibodies (figure 10) labeled processes that extended beyond the forming outer plexiform layer. It is unclear, whether this a specific characteristic of the tree

shrew, or if I was unable to visualize these contacts. Further confirmation would be required.

Looking at the other end of the photoreceptor, my opsin-antibodies gave further insights into outer segment development. In 1989, Foelix et al. studied the postnatal development of tree shrew photoreceptors using electron microscopy. There, they saw first signs of outer segments (OS) between P6 and P9. They described "small elongated evagination[s] representing the future OS". My findings support this observation: as early as P6, all opsins in figure 11 were highly concentrated at the tip of the photoreceptor inner segments, which could hint to outer segment development. However, the first disk-like structures Foelix et al. found, appeared at P10.

In addition to recoverin, I also labeled the sections with PKCα-antibody to detect bipolar cells during development. Compared to a study by Haverkamp et al. (2000) in mouse, my PKCα-antibody labeled a different subset of bipolar cells. Their antibody labeled exclusively rod bipolar cells and a layer close to the inner border of the IPL. My results were more similar to their PKCβ stainings which labeled at least three types of bipolar cells in mouse. It is possible that my α-antibody stained the β-isoform, they are 80 % identical in tree shrew (sequences were aligned with the NCBI blast suite). On the other hand, the expression of PKCα in tree shrew may be different than in mouse. In primate, PKCα stains also DB4 cone bipolar cells (Grünert et al., (1994). In human, S-cone bipolar cells are also PKCα-positive (Kolb et al., 1993). The signal at the inner border of the IPL in my sample could be an indicator for this type, because S-cone bipolar cells laminate in this position. For further clarification, additional cell markers would need to be tested. At least in primate, an antibody against a precursor of cholecystokinin (G6-gly), specifically labels S-cone bipolar cells and dendrites of midget ON bipolar cells (Wässle et al., 1994).

The final antibody I used was against ChAT (choline acetyltransferase), which labeled subsets of amacrine and ganglion cells. Kim et al. (2000) investigated ChAT-immunoreactive cells in the developing rat retina. They first detected

positive cells at E17, located in the zone between the neuroblastic layer and the future ganglion cell layer (GCL). This agreed with my findings at E40 (compare figure 10). Three days later (rat E20), they located ChAT-immunoreactive cells exclusively in the GCL, which was comparable to tree shrew P0. ChAT-bands appeared at P3 in rat and P6 in tree shrew. At this stage, I also observed ChAT-signals in the photoreceptor layer. In rat, immunoreactivity was detected in the outer plexiform layer (OPL). This has been shown to originate from horizontal cells (Kim et al., 1998). The ChAT-expression in the tree shrew has been described before (Knabe et al., 2007). In that study, ChAT-expression could be detected as early as P1 in the OPL and at the top of the photoreceptor layer. In all described studies, the signal in the outer retina vanished or became very faint during later development. At this point, only the OPL-staining is consistent (in addition to the well-known expression in amacrine cells). It is not clear, whether ChAT is truly expressed in tree shrew photoreceptors or if it was a cross-reaction of the antibody. I should test additional antibodies, directed against different epitopes of ChAT, before making conclusions about possible implications this would have for tree shrew photoreceptors.

4.1.2 Transcription factors in photoreceptor development

In addition to my morphological studies, I collected RNA-seq data from tree shrew retinas at different stages of development. The analysis showed that my samples were well-separated in an unsupervised MDS-plot, which sorted all samples based on similarity. The clustering of the samples indicated that my transcriptomic data could reflect the developmental progression of the retina.

At first, I evaluated the expression of the three opsin genes. S-opsin and Rhodopsin showed the earliest onset in tree shrew, with S-opsin showing a slightly higher expression after birth. In mouse, there was a much earlier expression of S-opsin (before birth) and a much longer delay before rhodopsin expression began. Interestingly, the transcription factors Otx2, Nrl, Rorβ and Nr2e3 peaked much

earlier in tree shrew compared to mouse. Maybe S-cone and rod genesis in tree shrew happens earlier but they require more time to maturate (relative to birth).

M-opsin was, as expected (Swaroop et al., 2010), the last opsin to be expressed. On RNA-level, I detected a mild onset at P6. This was interesting when compared to my immunohistochemical data. The M-opsin staining in figure 10 was already very strong at this time point. Trβ2 is the key factor for M-cone development and its importance has been described by Ng et al. in 2001. Trβ2 and a different splice isoform, Trβ1, are encoded by the gene Thrb. In my data, I observed two waves of Thrb expression in both mouse and tree shrew. At the first stages, the expression values were very high, before they declined and peaked a second time, days after birth. Ng et al. (2009) developed a Trβ2-specific antibody for mouse tissue, which labeled only developing M-cones. In their paper, they described the two waves of Trβ2-expression in Western blots and immunohistochemical stainings. The authors observed the first peak between E15 and E18, followed by the second peak after P10. This correlates with my RNA-seq findings in mouse. The first wave appeared at the stage when cones are generated in mice. Ng et al. hypothesized this could be necessary to prime cones for the later expression of opsins. The second, postnatal wave correlates with the onset of M-opsin expression (compare figure 12), which indicates that the fate of these cells has been decided at this point.

4.1.3 Differentially expressed genes in retinal tree shrew development

In the next part I explored genes that showed a highly significant change in expression after birth. The goal was to identify new genes that might be important during retinal development.

Most of the genes which were downregulated after birth, have various functions in the cell cycle. Upregulated genes included cone phototransduction genes, e.g., Pde6c, Pde6h, Opn1sw and Opn1mw. Furthermore, I found a number of known

transcription factors, e.g., Foxn4, which is involved in the differentiation of amacrine and horizontal cells. Other upregulated genes were known genes involved in synaptic processes, which indicated formation of synaptic connections at that time point.

The most interesting find was Wif1, because it had been described as a regulator of rod production (Hunter et al., 2004). Wif1 is expressed in the ONL, INL, GCL and the extracellular matrix (ECM) of human retina (Yang et al., 2008) and in the ECM, OPL, INL and GCL in mouse. Hang et al. demonstrated in their paper, that it regulates the production of rod photoreceptors. In one experiment, the authors dissociated mouse retinae and incubated the cells with recombinant Wif1 or Wif1 antibody. After the incubation, they labeled the cells with rhodopsin antibodies and counted the number of rods. They found that Wif1 reduced the number of rods, whereas Wif1-antibody, which they used to inhibit Wif1 activity, upregulated the rod production. In the developing mouse retina, Wif1 expression was detected at very low levels throughout all time points. In the tree shrew RNA-seq data, the expression of Wif1 correlated with the onset of M-opsin expression. It could be that Wif1 suppresses rod production in the tree shrew after P9, which could lead to the observed cone-dominance in this animal. Tree shrews have a rod density of 500–3,500 rods/mm^2. In mice, the density is 437,000 rods/mm^2. In contrast, cone densities are 14,300-35,300 cones/mm^2 in tree shrews and 12,100 cones/mm^2 in mice (Petry et al., 1993; Ortín-Martínez et al., 2014). So the largest difference between these animals is the rod abundance, whereas the cone density is similar. Maybe the suppression of rod genesis is a key factor in determining the rod- or cone-dominance of the retina.

Unfortunately, the authors of the Wif1 study did not test the effect on cone photoreceptors. This should be the next step to explore its function. In further studies, it would be interesting to create a Wif1 knockout or knockdown (using CRISPR/Cas9, shRNA or morpholinos) in a cone-dominated retina. If Wif1 plays the assumed role, I would expect to see a larger number of rods in these animals.

4.2 Genetic profiling cone photoreceptor subtypes

In this part, I investigated differences in gene expression of M- and S-cone photoreceptors in the cone-dominated retina of the thirteen-lined ground squirrel. Despite their similar morphology and function, as well as their same set of phototransduction proteins, I hypothesized that there could be more differences between those cells. In mammals, the blue pathway is different compared with the green pathway (Haverkamp et al., 2005; Chen and Li, 2012). This allows processing of different color information through the retina before integration and further processing in ganglion cells, which send the information to the higher visual cortex. Therefore, both cone types form different synaptic connections potentially regulated by a different subset of genes.

First, I demonstrated that labeling live cells is a powerful tool to purify specific cells in suspension. I developed a method to label and manually collect live S-cones, a relatively rare cell type in the ground squirrel retina (~6% of photoreceptors; Kryger et al., 1998; Sajdak et al., 2016). The goal was to identify an extracellular target, in this case S-opsin, to which an antibody could bind in a live, unperforated cell. This method eliminates the need to create a transgenic reporter animal, which therefore saves time, resources and avoids possible off-target effects caused by genetic modifications. Most importantly, the use of this method is not limited to cone photoreceptors. Potentially, any cell with a cell type-specific antigen on its surface could be targeted for downstream applications that require live cells.

My gene expression analysis revealed numerous genes that are either uniquely expressed or highly differentially expressed in one of the two cone types. These findings suggested that S- and M-cones do have their own molecular identity, although the majority of expressed genes are the same (figure 18). This was expected because they are highly related and, e.g., have been shown to use the same set of genes for phototransduction (Lamb, 2007 & 2013). As a tool to verify the expression of highly interesting genes I chose immunohistochemistry. This would add a much higher level of confidence in their expression, since it would prove actual protein expression. I found this approach more valuable than *in situ*

hybridizations which would only provide a second confirmation for RNA expression.

Ccdc136

According to the RNA-seq experiment, this gene is highly enriched in S-cone photoreceptors. Its function is not known, but previous studies have found a high expression of Ccdc136 in mouse testes (Geng et al., 2016). The authors performed Western blots on many different tissues (heart, lung, kidney, spleen, liver, epididymis, bladder, brain), but only testes were positive. They did not test the retina. In the KO-mouse, all males were infertile.

Very recently, a different publication introduced Ccdc136 as novel marker for S-cones and mixed M/S-cones that co-express both opsins (Smiley et al., 2016). In this study, the authors generated a Ccdc136-GFP reporter line. Rods and “true” M-cones were not or only weakly labeled in this mouse, whereas S- and M/S-cones showed strong GFP-expression.

Mixed cones are thought to be M-cones (that additionally express S-opsin), because they do not contact the S-cone specific bipolar cell (Haverkamp et al., 2005). The findings suggested that Ccdc136 may not be a marker for “true” S-cones in mice, but it may be coupled to S-opsin expression. However, this publication supported my RNA-seq results, as it confirmed an S-cone specific, or at least S-opsin-coupled, gene which I identified in my data.

Cadm1

Cadm1 (cell adhesion molecule 1) was predicted to be expressed in S-cones, although the overall number of reads was low: 198 reads in S-cones compared to 11 reads in M-cones. This gene was discovered independently by many groups of different fields. This is reflected in the many names the molecule was given: immunoglobulin superfamily 4 (IGSF4), tumor-suppressor in lung cancer-1 (TSLC1), RA175, synapse cell adhesion molecule-1 (SynCAM1), spermatogenic immunoglobulin, Superfamily (SgIGSF) and nectin-like molecule-2 (Necl-2) (Shingai et al., 2003). Since 2008, its official name is adhesion molecule-1 (Cadm1).

Cadm1 plays a role in synapse formation in the brain (Biederer et al., 2002). In 2014, Ribic et al. studied its function in the retina of a Cadm1-KO-mouse. They found that horizontal cells sprouted into the outer nuclear layer. This result suggested that Cadm1 is important for synapse formation in the retina.

My RNA-seq data suggested an S-cone specific role for Cadm1. The antibody-staining showed mixed results (figure 22). All cell bodies of the retina were labeled. It is not clear if this was a cross-reaction, because rods and S-cones showed a very different signal. Distinct puncta of Cadm1 were observed in the inner and outer segments of these cells. If this was true, it would still be puzzling. Based on its projected role in synapse formation, I would have expected labeling of the outer plexiform layer. Ribic et al. (2014) immunolabeled the retina of a mouse. Their antibody detected Cadm1 in all nuclear and plexiform layers, and only a very sparse labeling of inner and outer segments.

I suggest to specifically test if the wiring of S-cones is affected. Alterations in S-cone to S-cone bipolar cell synapses may have been overlooked in Ribic's study, since S-cone bipolar cells account only for 1-2% of all mouse bipolar cells (Haverkamp et al., 2005). To investigate this synapse, the Cadm1-KO mouse (Ribic et al., 2014) should be crossed with the Clomeleon-mouse, that expresses a fluorescent label in S-cone bipolar cells (Haverkamp et al., 2005). This would allow to assess possible changes in synapse formation by evaluating the co-localization of S-cone pedicles and S-cone bipolar cell dendrites (compare section 1.6).

Filamin A (Flna)

In my RNA-seq analysis, Flna was identified to be highly expressed in S-cones. When I immunolabeled ground squirrel tissue for filamin A, I observed a clear pattern of antibody signals in the outer plexiform layer and in blood vessels (figure 21). The protein has been described to help forming cell-cell contacts in the cardiovascular system in mice (Feng et al., 2006), which explains the signal in blood vessels. Most interestingly, in *Drosophila*, filamin A is involved in axon guidance of the UV-specific R7 photoreceptor (Oliva et al., 2015). In a knockdown-model, axons of this cell extended beyond their usual target layer. This finding could hint to a conserved function of this protein. Based on the signal I saw in the OPL of the

ground squirrel, it was not possible to identify which cells express the protein. Its location close to the INL could hint to an expression in horizontal cells or bipolar cells. Although its cell type-specificity in the ground squirrel could not be confirmed yet, its specific location in the OPL makes this still a highly interesting target for future studies.

Rod arrestin (Sag)

Rod arrestin is an important protein in the termination and recovery phase of the rod phototransduction cascade (Lamb, 2013). After the activation of the phototransduction cascade through light, CNG-channels close (see section 1.2) and the influx of Ca^{2+} and Na^{+} is stopped. The intracellular Ca^{2+}-concentration drops because of the continued activity of the Na^{+}/Ca^{2+}, K^{+} exchanger. The lowered Ca^{2+}-concentration leads to dissociation of Ca^{2+} from the calcium sensor protein recoverin, thus causing conformational changes in this protein which is inhibiting the rhodopsin kinase in the dark state. Because of the conformational changes, recoverin dissociates from rhodopsin kinase and lifts its inhibition. The kinase is then active and phosphorylates activated rhodopsin. Rod arrestin binds to phosphorylated rhodopsin and temporarily “arrests” it by covering the binding site for transducin. This prevents the immediate re-activation of the phototransduction cascade by rhodopsin.

In my RNA-seq results, rod arrestin was one of the most differentially expressed genes. It was predicted to be S-cone specific. Immunostaining of ground squirrel retina confirmed these results. Inner and outer segments showed a strong signal (figure 20). Expression of this protein in S-cones of different species has been reported before. In 2014, Craft et al. showed rod arrestin in S-cones of macaque, chimpanzee and marmoset (figure 28). What became obvious in their studies is that, in addition, cone arrestin showed a less intense staining in S-cones compared to M-cones. A possibly related side-effect could be seen in Li Jia’s S-cone bipolar cell connectivity study in mice (section 1.6). In figure 8, we could see a clear reduction of cone arrestin in all cones pedicles of mice with a Thrb-deletion (Thrb is important for M-cone differentiation). Taken together, it could mean that the expression of cone arrestin is biased towards M-cones, with a lower expression in S-cones.

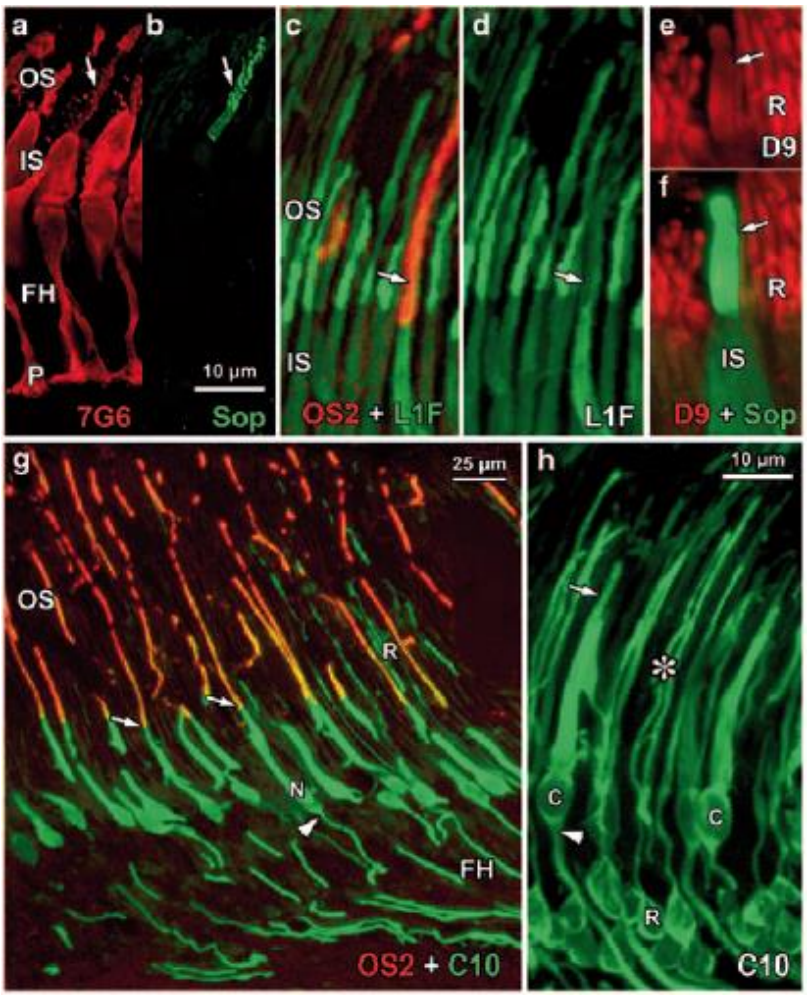

Figure 28 Primate and human retina sections stained for rod and cone arrestin. **a** Cone arrestin (7G6, red) in the periphery of a human retina. **b** S-opsin staining in the same section seen in (a). The cone-arrestin staining in the outer segment of the S-cone looked more faint compared to surrounding M&L-cones. **c, d** Cone arrestin (L1F, green) and S-opsin (OS2, red) staining in the macaque central retina. Cone arrestin staining looked also more faint in S-cone outer segments in this animal. **e, f** Rod arrestin (D9, red) and S-opsin (Sop, green) in the chimpanzee retina. In addition to the surrounding rods (R), the S-cone was also positive for rod arrestin. **g** Rod arrestin (C10, green) and S-opsin (OS2, red) in the marmoset retina (foveal edge). All S-opsin-positive cells were also labeled for rod arrestin. **h** Rod arrestin (C10, green) in the macaque retina. Both S-cone (C) outer segments (arrow) and rod (R) outer segments (asterisk) were rod arrestin-positive, as well as the cell bodies and the Fiber of Henle (FH, arrowhead).
Antibodies: 7G6: human cone arrestin hArr4; L1F: human cone arrestin CARR-LUMIf; D9: rod arrestin Arr1; C10: rod arrestin C10C10; Sop: S-opsin; OS2: S-opsin.
From: Craft et al. (2014). Reprint permission for use in this thesis was obtained from the publisher.

An interesting experiment would be to measure light-responses in S-cones that lack rod- and/or cone arrestin. This could determine if their roles are interchangeable in the squirrel and if they have additional functions. A comparable experiment was performed in mice (Brown et al., 2010). After 15 minutes of steady background illumination, rod-arrestin-KO mice showed a smaller b-wave amplitude in photopic ERG measurements. The cone arrestin-KO showed a response similar to wild type mice. In cone flicker response, only double-KO mice showed a decrease in their response. In addition to these results, they found that rod-arrestin-KO mice suffer from light-independent cone dystrophy. Taken together, this suggests that rod arrestin has an important role for cones in mice. But this raises a different question: ground squirrels do not express rod arrestin in M-cones. How is this compatible with Brown et al.'s findings? To answer this question, it would be necessary to repeat this study in the ground squirrel. Methods on how to achieve genetically altered ground squirrels are discussed in section 4.3.

4.3 AAV mediated GFP-expression in the ground squirrel

Here, I explored tools to enable genetic modifications in the ground squirrel retina. Both adeno-associated virus serotypes (AAV2 and 8) proved to successfully transduce retinal cells as demonstrated by the expression of GFP. For my cone project, AAV8 was especially valuable, because its subretinal injection specifically targeted photoreceptors. Further experiments would be required to develop strategies to target individual photoreceptor types. This could be achieved by identifying promoter regions of cell type-specific genes.

Besides for the delivery of a GFP reporter protein, the AAV system could be used for the delivery of CRISPR/Cas9 to photoreceptors (Yu et al., 2017). In the recent years, CRSIPR/Cas9 (Clustered Regularly Interspaced Short Palindromic Repeats/Cas9) has been identified as a powerful tool for genome editing with relatively low effort (Jinek et al., 2012; Cong et al., 2013; Mali et al., 2013; Jinek et al., 2013). To knockdown the expression of a gene in the squirrel, an AAV vector containing the sequences for the endonuclease Cas9 and a gene-specific guide RNA

(gRNA) would be required. The gRNA must contain a sequence of approx. 20 bp that is homologous to the target gene. Cas9 and the gRNA form a complex in the cell, and when the gRNA anneals to the target, Cas9 cuts the DNA-strand at a nearby PAM sequence (e.g. 5′-NGG-3′ for *Streptococcus pyogenes* Cas9). Errors in the repair mechanisms of a cell could result in deletions or insertions that lead to a frameshift or a premature stop codon, thus preventing the cell from expressing the functional protein.

Functional analysis in animal models has yet to confirm the exact role of the genes I identified in my RNA-seq experiment. Applying the CRISPR/Casp system would allow me to perform functional studies in the ground squirrel or the tree shrew, animals which previously had only a limited set of genetic tools available compared to mice or zebrafish (Kardash, 2017).

4.4 Targeting rod photoreceptors for genetic profiling

In my RNA-seq experiment that determined differences in cone photoreceptors, I observed a high expression of rod arrestin in S-cones. I hypothesized that rods may share more genes with S-cones than we previously thought (section 1.4). I tried to identify rods by using human GRK1 promoter-controlled GFP-expression in rods. My results revealed that the cells I collected did not express any rod genes, instead I found high expression of M-cone specific genes. I concluded that I collected M-cones instead of rods.

It is possible that the human GRK1 promoter might be closer related to the squirrel Grk7 promoter (cone-specific) than to the squirrel Grk1 promoter (rod-specific). But in this case I would have expected that S-cones would be labeled as well. My data suggested that the sample did not contain significant amounts of S-cone specific RNA. However, this can be explained by the M- to S-cone ratio. If both cone types would express the same label, the likelihood to collect an M-cone would be much higher because of the lower abundance of S-cones (6%) compared to M-cones (80%). To investigate if S-cones were labeled as well, I could use an S-opsin-

antibody to co-stain these cells. A different option would be to avoid pooling cells, and instead collecting and sequencing true single cells.

I further wanted to investigate and compare the promoter regions of Grk1 and 7 in human and squirrel. I compared the regions upstream of the transcription start site (TSS) of human GRK1, human GRK7, squirrel Grk1 and squirrel Grk7. The promoter sequence I used for the vector has been described (Yu et al., 2017; suppl. 6.2.2) and starts 112 bp before the TSS and ends 180 bp after the TSS of human GRK1. I aligned the sequences of all Grk genes (+/- 300 bp of their respective TSS) with the NCBI alignment tool (blast.ncbi.nlm.nih.gov). No significant similarities were found.

A different way to identify the promoter regions would be to find so-called CpG islands, areas with a high frequency of the 5'-CG-3'-sequence. Approximately 70% of gene promoters in human are associated with a CpG island (Saxony et al., 2006). I analyzed my genes of interest using the UCSC Genome Browser (Kent et al., 2002). There were no CpG islands in the regions 10 kb upstream of the transcription start sites of these genes.

To conclude, I have no evidence that supports my hypothesis that the GFP-expression was under the control of the Grk7 promoter instead of the Grk1 promoter in the ground squirrel. Since the human GRK1 promoter was not sufficient in targeting rods, and the CpG analysis for Grk1 was negative, the squirrel Grk1 promoter would need to be identified experimentally. I could clone and replace the human GRK1 promoter sequence with the upstream region of squirrel Grk1 or other rod-specific genes, e.g., Gnat1 (rod transducin) or Rho (rhodopsin) and monitor the expression of GFP.

4.5 Effects of hibernation on the transcriptome of squirrel photoreceptors

The retina of the ground squirrel is subject to different morphological and physiological changes during hibernation. Reports described dramatically smaller or detached ribbons, shortened outer segments, a reduced number of synaptic vesicles, and a reduced number and size of ellipsoid mitochondria (Kuwabara, 1975; Gruber et al., 2006, Mehta et al, 2013; Merriman et al., 2016). To study the genetic mechanisms behind these adaptive changes, I analyzed the single cell photoreceptor data regarding effects of hibernation. I compared the expression of phototransduction genes in both conditions. I did not find a significant difference in any of these genes, despite the changed morphology of outer segments. These findings agreed with electrophysical recordings in retinal samples from hibernating animals: the cone membrane resting potential was unchanged, and they generally show light responses after a short period of warming (Mehta et al., 2013; personal communication by Juan Angueyra, NEI/NIH). On the other hand, the smaller or detached ribbons in hibernating animals are reflected by a reduced frequency of mlEPSCs (miniature-like evoked postsynaptic currents) in recordings from postsynaptic OFF cone bipolar cells (Mehta et al., 2013).

Other genes I detected could be related to the observed changes in morphology during hibernation. I identified two genes that encode synaptic proteins, Slitrk3 and Ctnnd1 (Takahashi et al., 2012; Yuan et al., 2017). Both are downregulated during hibernation. They may not be associated with changes in the ribbon structure, but they could hint to additional changes in photoreceptor synapses that have not been discovered yet.

A highly upregulated gene during hibernation was Pebp1. Overexpression of this gene has been reported to lead to abnormalities in outer segment development. In a recent study with zebrafish that overexpressed Pebp1, outer segments appeared dramatically smaller compared to wild type zebrafish (Murga-Zamalloa et al., 2011). This phenotype could correspond to the observed changes in outer segment length in the hibernating squirrel (Kuwabara, 1975; Gruber et al., 2006). Further studies would be required to determine its function in the squirrel outer segments.

4.6 Conclusions and outlook

In this thesis, I investigated characteristics of cone-dominated retinae and the genetic profile of cone photoreceptor subtypes. In tree shrew, I described morphological and transcriptomic changes during development. Compared to mice, the general morphology of the developing retina was similar. There were subtle differences in the onset of transcription factors and in the relative timepoints of photoreceptor genesis. In the transcriptomic analysis, I identified the expression of the gene Wif1 that may suppress rod development shortly after birth of the tree shrew. Future studies should examine if the deletion of this gene could lead to a higher abundance of rods in a cone-dominated animal. At the same time, a transgenic mouse that overexpresses Wif1 should be examined, to test how a rod-dominated retina would be affected.

Furthermore, I investigated differences in gene expression of M- and S-cone photoreceptors in the ground squirrel. My gene expression analysis revealed numerous genes that were highly differentially expressed. The findings suggested that S- and M-cones do have their own molecular identity. I confirmed that rod arrestin was highly expressed in S-cones of the ground squirrel. Questions arose whether it is part of the phototransduction cascade in S-cones or if it has a different function. Studies in mouse revealed a high importance of rod arrestin-expression for cone survival (Brown et al., 2010). It would be interesting to study the effects of a rod arrestin-knockdown on cones in the ground squirrel

I identified two molecules, that could be involved in the specific formation of S-cones synapses. Filamin A, which was highly S-cone-specific in the transcriptome data, was confirmed to be exclusively expressed in the outer plexiform layer of the retina. Taken together with its known axon guidance role in other model organisms (Oliva et al., 2015), it would be a highly interesting candidate for knockdown studies in the squirrel. The second gene with a role in synapse formation was the cell adhesion molecule Cadm1. I suggest additional studies on the function of this gene in mice. An existing Cadm1-KO mouse (Ribic et al., 2014) could be crossed with an S-cone bipolar cell reporter mouse to identify changes at the synapse.

Furthermore, I reported a successful GFP-expression after delivery via AVV8. Further experiments are required to identify cell-specific promoters. I was unable to use the human GRK1-promoter to label rods in the squirrel retina for RNA-seq studies. In the future, an AAV could be used to deliver CRISPR/Cas9-constructs for gene-knockdowns in the squirrel. This would allow to functionally study genes that I described in this thesis.

At last, I analyzed differences in mRNA expression in photoreceptors of the hibernating ground squirrel. I concluded that the expression of phototransduction genes was not affected by hibernation, despite the known morphological changes in outer segments of hibernating animals (Merriman et al., 2016). However, I identified differentially expressed genes that may play roles in the adaptive changes of the photoreceptor outer segment and synapse during hibernation.

5 References

Allocca M, Mussolino C, Garcia-Hoyos M, Sanges D, Iodice C, Petrillo M, Vandenberghe LH, Wilson JM, Marigo V, Surace EM, Auricchio A (2007) Novel adeno-associated virus serotypes efficiently transduce murine photoreceptors. J Virol. 81(20):11372-80.

Anders S, Pyl PT, Huber W (2015) HTSeq--a Python framework to work with high-throughput sequencing data. Bioinformatics. 31(2):166-9. doi: 10.1093/bioinformatics/btu638.

Applebury ML, Antoch MP, Baxter LC, Chun LL, Falk JD, Farhangfar F, Kage K, Krzystolik MG, Lyass LA, Robbins JT (2000) The murine cone photoreceptor: a single cone type expresses both S and M opsins with retinal spatial patterning. Neuron. 27(3):513-23.

Biederer T, Sara Y, Mozhayeva M, Atasoy D, Liu X, Kavalali ET, Südhof TC. (2003) SynCAM, a synaptic adhesion molecule that drives synapse assembly. Science.297(5586):1525-31.

Bowmaker JK (2008) Evolution of vertebrate visual pigments. Vision Res. 2008 Sep;48(20):2022-41. doi: 10.1016/j.visres.2008.03.025.

Bray NL, Pimentel H, Melsted P, Pachter L (2016) Near-optimal probabilistic RNA-seq quantification. Nat Biotechnol. 34(5):525-7. doi: 10.1038/nbt.3519.

Bruce M. Brown, Teresa Ramirez, Lawrence Rife, Cheryl M. Craft (2010) Visual Arrestin 1 Contributes to Cone Photoreceptor Survival and Light Adaptation Invest Ophthalmol Vis Sci. 51(5): 2372–2380. doi: 10.1167/iovs.09-4895

Centanin L, Wittbrodt J (2014) Retinal neurogenesis. Development. 141(2):241-4. doi: 10.1242/dev.083642. Review.

Cepko CL, Austin CP, Yang X, Alexiades M, Ezzeddine D (1996) Cell fate determination in the vertebrate retina. Proc Natl Acad Sci U S A 93: 589–595

Chen J, Rattner A, Nathans J (2005) The rod photoreceptor-specific nuclear receptor Nr2e3 represses transcription of multiple cone-specific genes. J Neurosci. 25(1):118-29.

Chen S, Li W (2012) A color-coding amacrine cell may provide a blue-off signal in a mammalian retina. Nat Neurosci. 15(7):954-6. doi: 10.1038/nn.3128.

Cho Y, Park D, Cavalli V. (2015) Filamin A is required in injured axons for HDAC5 activity and axon regeneration. J Biol Chem. 290(37):22759-70. doi: 10.1074/jbc.M115.638445.

Cong L, Ran FA, Cox D, Lin S, Barretto R, Habib N, Hsu PD, Wu X, Jiang W, Marraffini LA, Zhang F (2013) Multiplex genome engineering using CRISPR/Cas systems. Science. 339(6121):819-23. doi: 10.1126/science.1231143.

Craft CM, Huang J, Possin DE, Hendrickson A (2014) Primate short-wavelength cones share molecular markers with rods. Adv Exp Med Biol. 2014;801:49-56. doi: 10.1007/978-1-4614-3209-8_7.

Dean C, Scholl FG, Choih J, DeMaria S, Berger J, Isacoff E, Scheiffele P (2003) Neurexin mediates the assembly of presynaptic terminals. Nat Neurosci 6(7):708-16.

Dobin A, Davis CA, Schlesinger F, Drenkow J, Zaleski C, Jha S, Batut P, Chaisson M, Gingeras TR (2013) STAR: ultrafast universal RNA-seq aligner. Bioinformatics. 29(1):15-21. doi: 10.1093/bioinformatics/bts635.

Dowling JE (1987) The retina. An approachable part of the brain. Belknap Press of Harvard Univ. Press. Cambridge, Mass., USA

Fan Y, Huang ZY, Cao CC, Chen CS, Chen YX, Fan DD, He J, Hou HL, Hu L, Hu XT, Jiang XT, Lai R, Lang YS, Liang B, Liao SG, Mu D, Ma YY, Niu YY, Sun XQ, Xia JQ, Xiao J, Xiong ZQ, Xu L, Yang L, Zhang Y, Zhao W, Zhao XD, Zheng YT, Zhou JM, Zhu YB, Zhang GJ, Wang J, Yao YG (2013) Genome of the Chinese tree shrew. Nat Commun. 2013;4:1426. doi: 10.1038/ncomms2416.

Feng Y, Chen MH, Moskowitz IP, Mendonza AM, Vidali L, Nakamura F, Kwiatkowski DJ, Walsh CA (2006) Filamin A (FLNA) is required for cell-cell contact in vascular development and cardiac morphogenesis. Proc Natl Acad Sci U S A. 2006 Dec 26;103(52):19836-41.

Foelix RF, Kretz R, Rager G (1987) Structure and postnatal development of photoreceptors and their synapses in the retina of the tree shrew (Tupaia belangeri). Cell Tissue Res. 1987 Feb;247(2):287-97.

Forrest D, Swaroop A (2009) Minireview: the role of nuclear receptors in photoreceptor differentiation and disease. Mol Endocrinol. 26(6):905-15. doi: 10.1210/me.2012-1010.

Freeman M (2016) Rhomboids, signalling and cell biology. Biochem Soc Trans. 44(3):945-50. doi: 10.1042/BST20160035.

Fu Y, Yau KW (2007) Phototransduction in mouse rods and cones. Pflügers Arch. 454(5):805-19.

Fuchs E and Corbach-Söhle S (2010) Chapter 20: Tree Shrews. The UFAW Handbook on the Care and Management of Laboratory and Other Research Animals 8th Edition. Editors: Hubrecht RC, Kirkwood J. Wiley-Blackwell. New Jersey, USA

Fujitani Y, Fujitani S, Luo H, Qiu F, Burlison J, Long Q, Kawaguchi Y, Edlund H, MacDonald RJ, Furukawa T, Fujikado T, Magnuson MA, Xiang M, Wright CV (2006) Ptf1a determines horizontal and amacrine cell fates during mouse retinal development. Development. 133(22):4439-50.

Furukawa T, Morrow EM, Li T, Davis FC, Cepko CL (1999) Retinopathy and attenuated circadian entrainment in Crx-deficient mice. Nat Genet. 23(4):466-70.

Geng Q, Ni L, Ouyang B, Hu Y, Zhao Y, Guo J (2016) A Novel Testis-Specific Gene, Ccdc136, Is Required for Acrosome Formation and Fertilization in Mice. Reprod Sci. 23(10):1387-96. doi: 10.1177/1933719116641762.

Gentleman RC, Carey VJ, Bates DM, Bolstad B, Dettling M, Dudoit S, Ellis B, Gautier L, Ge Y, Gentry J, Hornik K, Hothorn T, Huber W, Iacus S, Irizarry R, Leisch F, Li C, Maechler M, Rossini AJ, Sawitzki G, Smith C, Smyth G, Tierney L, Yang JY, Zhang J (2004) Bioconductor: open software development for computational biology and bioinformatics. Genome Biol. 5(10):R80.

Greferath U, Grünert U, Wässle H (1990) Rod bipolar cells in the mammalian retina show protein kinase C-like immunoreactivity. J Comp Neurol. 301(3):433-42.

Griffiths AJ et al. (2005) Chapter 3 - The Chromosomal Basis of Inheritance. An Introduction to Genetic Analysis. 8th ed. W.H. Freeman and Company. New York, USA p. 82

Gruber AR, Betts KE, Lewis GP, Fisher SK, Vaughan DK (2006) Photoreceptor antigens are altered during season hibernation of a cone-dominant rodent. Invest. Ophthalmol. Vis. Sci. 47, p a2845

Güler AD, Ecker JL, Lall GS, Haq S, Altimus CM, Liao HW, Barnard AR, Cahill H, Badaea TC, Zhao H, Hankins MW, Berson DM, Lucas RJ, Yau KW, Hattar S (2008) Melanopsin cells are the principal conduits for rod-cone input to non-image-forming vision. Nature. 453(7191):102-5. doi: 10.1038/nature06829.

Grünert U, Martin PR, Wässle H (1994) Immunocytochemical analysis of bipolar cells in the macaque monkey retina. J Comp Neurol. 348(4):607-27.

Hatori M, Le H, Vollmers C, Keding SR, Tanaka N, Buch T, Waisman A, Schmedt C, Jegla T, Panda S (2008) Inducible ablation of melanopsin-expressing retinal ganglion cells reveals their central role in non-image forming visual responses. PLoS One. 3(6):e2451. doi: 10.1371/journal.pone.0002451.

Haverkamp S, Wässle H (2000) Immunocytochemical analysis of the mouse retina. J Comp Neurol. 424(1):1-23

Haverkamp S, Ghosh KK, Hirano AA, Wässle H (2003) Immunocytochemical description of five bipolar cell types of the mouse retina. J Comp Neurol. 455(4):463-76.

Haverkamp S, Wässle H, Duebel J, Kuner T, Augustine GJ, Feng G, Euler T (2005) The primordial, blue-cone color system of the mouse retina. J Neurosci. 25(22):5438-45.

Hlawatsch J, Karlstetter M, Aslanidis A, Lückoff A, Walczak Y, Plank M, Böck J, Langmann T (2013) Sterile alpha motif containing 7 (samd7) is a novel crx-regulated transcriptional repressor in the retina. PLoS One. 8(4):e60633. doi: 10.1371/journal.pone.0060633.

Huber W, Carey VJ, Gentleman R, Anders S, Carlson M, Carvalho BS, Bravo HC, Davis S, Gatto L, Girke T, Gottardo R, Hahne F, Hansen KD, Irizarry RA, Lawrence M, Love MI, MacDonald J, Obenchain V, Oleś AK, Pagès H, Reyes A, Shannon P, Smyth GK, Tenenbaum D, Waldron L, Morgan M (2015) Orchestrating high-throughput genomic analysis with Bioconductor. Nat Methods. 12(2):115-21. doi: 10.1038/nmeth.3252.

Hunter DD, Zhang M, Ferguson JW, Koch M, Brunken WJ (2004) The extracellular matrix component WIF-1 is expressed during, and can modulate, retinal development. Mol Cell Neurosci. 27(4):477-88.

Hume DA, Perry VH, Gordon S (1983) Immunohistochemical localization of a macrophage-specific antigen in developing mouse retina: phagocytosis of dying neurons and differentiation of microglial cells to form a regular array in the plexiform layers. J Cell Biol. 97(1):253-7.

Ichtchenko K, Hata Y, Nguyen T, Ullrich B, Missler M, Moomaw C, Südhof TC (1995) Neuroligin 1: a splice site-specific ligand for beta-neurexins. Cell. 81(3):435-43.

Jadhav AP, Mason HA, Cepko CL (2006) Notch 1 inhibits photoreceptor production in the developing mammalian retina. Development. 133(5):913-23.

Jagadish N, Rana R, Mishra D, Kumar M, Suri A (2005) Sperm associated antigen 9 (SPAG9): a new member of c-Jun NH2 -terminal kinase (JNK) interacting protein exclusively expressed in testis. Keio J Med. 54(2):66-71.

Jia L, Oh EC, Ng L, Srinivas M, Brooks M, Swaroop A, Forrest D (2009) Retinoid-related orphan nuclear receptor RORbeta is an early-acting factor in rod photoreceptor development. Proc Natl Acad Sci USA. 106(41):17534-9. doi: 10.1073/pnas.0902425106.

Jinek M, Chylinski K, Fonfara I, Hauer M, Doudna JA, Charpentier E (2012) A programmable dual-RNA-guided DNA endonuclease in adaptive bacterial immunity. Science. 337(6096):816-21. doi: 10.1126/science.1225829.

Jinek M, East A, Cheng A, Lin S, Ma E, Doudna J (2013) RNA-programmed genome editing in human cells. Elife. 2:e00471. doi: 10.7554/eLife.00471.

Johnson PT, Williams RR, Cusato K, Reese BE (1999) Rods and cones project to the inner plexiform layer during development. J Comp Neurol. 414(1):1-12.

Johnson J, Fremeau RT Jr, Duncan JL, Rentería RC, Yang H, Hua Z, Liu X, LaVail MM, Edwards RH, Copenhagen DR (2007) Vesicular glutamate transporter 1 is required for photoreceptor synaptic signaling but not for intrinsic visual functions. J Neurosci. 27(27):7245-55.

Jones BW, Kondo M, Terasaki H, Watt CB, Rapp K, Anderson J, Lin Y, Shaw MV, Yang JH, Marc RE (2011) Retinal remodeling in the Tg P347L rabbit, a large-eye model of retinal degeneration. J Comp Neurol. 519(14):2713-33. doi: 10.1002/cne.22703.

Kardash E (2017) Current Methods in Zebrafish Research. MATER METHODS 2012;2:109. dx.doi.org/10.13070/mm.en.2.109

Kefalov VJ, Estevez ME, Kono M, Goletz PW, Crouch RK, Cornwall MC, Yau KW (2005) Breaking the covalent bond--a pigment property that contributes to desensitization in cones. Neuron. 46(6):879-90.

Kent WJ, Sugnet CW, Furey TS, Roskin KM, Pringle TH, Zahler AM, Haussler D (2002) The human genome browser at UCSC. Genome Res. 12(6):996-1006

Khani SC, Pawlyk BS, Bulgakov OV, Kasperek E, Young JE, Adamian M, Sun X, Smith AJ, Ali RR, Li T (2007) AAV-mediated expression targeting of rod and cone photoreceptors with a human rhodopsin kinase promoter. Invest Ophthalmol Vis Sci. 48(9):3954-61.

Kim IB, Park DK, Oh SJ, Chun MH (1998) Horizontal cells of the rat retina show choline acetyltransferase- and vesicular acetylcholine transporter-like immunoreactivities during early postnatal developmental stages. Neurosci Lett. 253(2):83-6.

Kim IB, Lee EJ, Kim MK, Park DK, Chun MH (2000) Choline acetyltransferase-immunoreactive neurons in the developing rat retina. J Comp Neurol. 427(4):604-16.

Knabe W, Washausen S, Happel N, Kuhn HJ (2007) Development of starburst cholinergic amacrine cells in the retina of Tupaia belangeri. J Comp Neurol. 502(4):584-97.

Kolb H, Zhang L, Dekorver L (1993) Differential staining of neurons in the human retina with antibodies to protein kinase C isozymes. Vis Neurosci. 10(2):341-51.

Kolb H (2005) Photoreceptors. In: Webvision: The Organization of the Retina and Visual System [Internet]. Editors: Kolb H, Fernandez E, Nelson R. Salt Lake City (UT): University of Utah Health Sciences Center [updated 2007 May 01].

Kolb H (2005b) Outer Plexiform Layer. In: Webvision: The Organization of the Retina and Visual System [Internet]. Editors: Kolb H, Fernandez E, Nelson R. Salt Lake City (UT): University of Utah Health Sciences Center [updated 2012 Feb 28].

Korenbrot JI (2012) Speed, sensitivity, and stability of the light response in rod and cone photoreceptors: facts and models. Prog Retin Eye Res. 31(5):442-66. doi: 10.1016/j.preteyeres.2012.05.002.

Kouyama N, Marshak DW (1992) Bipolar cells specific for blue cones in the macaque retina. J Neurosci. 12(4):1233-52.

Kraft TW (1988) Photocurrents of cone photoreceptors of the golden-mantled ground squirrel. J Physiol. 404:199-213.

Kryger Z, Galli-Resta L, Jacobs GH, Reese BE (1998) The topography of rod and cone photoreceptors in the retina of the ground squirrel. Vis Neurosci. 15(4):685-91.

Kuner T, Augustine GJ (2000) A genetically encoded ratiometric indicator for chloride: capturing chloride transients in cultured hippocampal neurons. Neuron. 27(3):447-59.

Kuwabara T (1975) Cytologic changes of the retina and pigment epithelium during hibernation. Invest Ophthalmol. 1975 Jun;14(6):457-67.

Lamb TD, Collin SP, Pugh EN Jr (2007) Evolution of the vertebrate eye: opsins, photoreceptors, retina and eye cup. Nat Rev Neurosci. 8(12):960-76.

Lamb TD (2013) Evolution of phototransduction, vertebrate photoreceptors and retina. Prog Retin Eye Res. 2013 Sep;36:52-119. doi: 10.1016/j.preteyeres.2013.06.001.

Law CW, Chen Y, Shi W, Smyth GK (2014) Voom: Precision weights unlock linear model analysis tools for RNA-seq read counts. Genome Biol. 15(2):R29. doi: 10.1186/gb-2014-15-2-r29.

Law CW, Alhamdoosh M, Su S et al. (2016) RNA-seq analysis is easy as 1-2-3 with limma, Glimma and edgeR [version 2; referees: 3 approved]. F1000Research. 5:1408 doi: 10.12688/f1000research.9005.2

Liu P, Osawa S, Weiss ER (2005) M opsin phosphorylation in intact mammalian retinas. J Neurochem. 93(1):135-44.

Liu PC, Chiao CC (2007) Morphologic identification of the OFF-type blue cone bipolar cell in the rabbit retina. Invest Ophthalmol Vis Sci. 48(7):3388-95.

Love MI, Huber W and Anders S (2014) Moderated estimation of fold change and dispersion for RNA-seq data with DESeq2. Genome Biology, 15, pp. 550. doi: 10.1186/s13059-014-0550-8.

Love MI, Anders S, Huber W (2017) Analyzing RNA-seq data with DESeq2. Bioconductor. bioconductor.org/packages/devel/bioc/vignettes/DESeq2/inst/doc/DESeq2.html

Luo DG, Xue T, Yau KW (2008) How vision begins: an odyssey. Proc Natl Acad Sci U S A. 105(29):9855-62. doi: 10.1073/pnas.0708405105.

Mali P, Yang L, Esvelt KM, Aach J, Guell M, DiCarlo JE, Norville JE, Church GM (2013) RNA-guided human genome engineering via Cas9. Science. 339(6121):823-6. doi: 10.1126/science.1232033.

Mariani AP (1984) Bipolar cells in monkey retina selective for the cones likely to be blue-sensitive. Nature. 308(5955):184-6.

Marini F (2017) pcaExplorer: Interactive Visualization of RNA-seq Data Using a Principal Components Approach. R package version 2.2.1, https://github.com/federicomarini/pcaExplorer.

Matsumoto A, Arcaroli J, Chen Y, Gasparetto M, Neumeister V, Thompson DC, Singh S, Smith C, Messersmith W, Vasiliou V (2017) Aldehyde dehydrogenase 1B1: a novel immunohistological marker for colorectal cancer. Br J Cancer. doi: 10.1038/bjc.2017.304. [Epub ahead of print]

Mears AJ, Kondo M, Swain PK, Takada Y, Bush RA, Saunders TL, Sieving PA, Swaroop A (2001) Nrl is required for rod photoreceptor development. Nat Genet. 29(4):447-52.

Mehta B, Snellman J, Chen S, Li W, Zenisek D (2013) Synaptic ribbons influence the size and frequency of miniature-like evoked postsynaptic currents. Neuron. 77(3):516-27. doi: 10.1016/j.neuron.2012.11.024.

Merriman DK, Sajdak BS, Li W, Jones BW (2016) Seasonal and post-trauma remodeling in cone-dominant ground squirrel retina. Exp Eye Res. 150:90-105. doi: 10.1016/j.exer.2016.01.011

Migdale K, Herr S, Klug K, Ahmad K, Linberg K, Sterling P, Schein S (2003) Two ribbon synaptic units in rod photoreceptors of macaque, human, and cat. J Comp Neurol.455(1):100-12.

Milam AH, Dacey DM, Dizhoor AM (1993) Recoverin immunoreactivity in mammalian cone bipolar cells. Vis Neurosci. 10(1):1-12.

Morgans CW (1999) Calcium channel heterogeneity among cone photoreceptors in the tree shrew retina. Eur J Neurosci. ;11(8):2989-93.

Müller B, Peichl L, De Grip WJ, Gery I, Korf HW. (1989) Opsin- and S-antigen-like immunoreactions in photoreceptors of the tree shrew retina. Invest Ophthalmol Vis Sci. 30(3):530-5.

Murga-Zamalloa CA, Ghosh AK, Patil SB, Reed NA, Chan LS, Davuluri S, Peränen J, Hurd TW, Rachel RA, Khanna H (2011) Accumulation of the Raf-1 kinase inhibitory protein (Rkip) is associated with Cep290-mediated photoreceptor degeneration in ciliopathies. J Biol Chem.286(32):28276-86. doi: 10.1074/jbc.M111.237560.

Mustafi D, Engel AH, Palczewski K (2009) Structure of cone photoreceptors. Prog Retin Eye Res.28(4):289-302. doi: 10.1016/j.preteyeres.2009.05.003. Review.

Negishi K, Kato S, Teranishi T (1988) Dopamine cells and rod bipolar cells contain protein kinase C-like immunoreactivity in some vertebrate retinas. Neurosci Lett. 94(3):247-52.

Ng L, Hurley JB, Dierks B, Srinivas M, Saltó C, Vennström B, Reh TA, Forrest D (2001) A thyroid hormone receptor that is required for the development of green cone photoreceptors. Nat Genet. 27(1):94-8.

Ng L, Ma M, Curran T, Forrest D (2009) Developmental expression of thyroid hormone receptor beta2 protein in cone photoreceptors in the mouse. Neuroreport. 20(6):627-31. doi: 10.1097/WNR.0b013e32832a2c63.

Ng L, Liu H, St Germain DL, Hernandez A, Forrest D (2017) Deletion of the Thyroid Hormone-Activating Type 2 Deiodinase Rescues Cone Photoreceptor Degeneration but Not Deafness in Mice Lacking Type 3 Deiodinase. Endocrinology.158(6):1999-2010. doi: 10.1210/en.2017-00055.

Nork TM, McCormick SA, Chao GM, Odom JV (1990) Distribution of carbonic anhydrase among human photoreceptors. Invest Ophthalmol Vis Sci. 31(8):1451-8.

Nishida A, Furukawa A, Koike C, Tano Y, Aizawa S, Matsuo I, Furukawa T (2003) Otx2 homeobox gene controls retinal photoreceptor cell fate and pineal gland development. Nat Neurosci. 6(12):1255-63. Epub 2003 Nov 16.

Omori Y, Kubo S, Kon T1, Furuhashi M, Narita H, Kominami T, Ueno A, Tsutsumi R, Chaya T, Yamamoto H, Suetake I, Ueno S, Koseki H, Nakagawa A, Furukawa T (2017) Samd7 is a cell type-specific PRC1 component essential for establishing retinal rod photoreceptor identity. Proc Natl Acad Sci U S A. 114(39):E8264-E8273. doi: 10.1073/pnas.1707021114.

Okano T, Kojima D, Fukada Y, Shichida Y, Yoshizawa T (1992) Primary structures of chicken cone visual pigments: vertebrate rhodopsins have evolved out of cone visual pigments. Proc Natl Acad Sci U S A. 89(13):5932-6.

Oliva C, Molina-Fernandez C, Maureira M, Candia N, López E, Hassan B, Aerts S, Cánovas J, Olguín P, Sierralta J (2015) Hindsight regulates photoreceptor axon targeting through transcriptional control of jitterbug/Filamin and multiple genes involved in axon guidance in Drosophila. Dev Neurobiol. 2015 Sep;75(9):1018-32. doi: 10.1002/dneu.22271. Epub 2015 Feb 18.

Ortín-Martínez A, Nadal-Nicolás FM, Jiménez-López M, Alburquerque-Béjar JJ, Nieto-López L, García-Ayuso D, Villegas-Pérez MP, Vidal-Sanz M, Agudo-Barriuso M (2014) Number and distribution of mouse retinal cone photoreceptors: differences between an albino (Swiss) and a pigmented (C57/BL6) strain. PLoS One. 9(7):e102392. doi: 10.1371/journal.pone.0102392..

Peng YW1, Robishaw JD, Levine MA, Yau KW (1992) Retinal rods and cones have distinct G protein beta and gamma subunits. Proc Natl Acad Sci U S A. 89(22):10882-6.

Perestenko PV, Pooler AM, Noorbakhshnia M, Gray A, Bauccio C, Jeffrey McIlhinney RA (2010) Copines-1, -2, -3, -6 and -7 show different calcium-dependent intracellular membrane translocation and targeting. FEBS J. 277(24):5174-89. doi: 10.1111/j.1742-4658.2010.07935.x.

Petrenko AG, Ullrich B, Missler M, Krasnoperov V, Rosahl TW, Südhof TC (1996) Structure and evolution of neurexophilin. J Neurosci. 16(14):4360-9.

Petry HM, Erichsen JT, Szél A (1993) Immunocytochemical identification of photoreceptor populations in the tree shrew retina. Brain Res. 616(1-2):344-50.

Petry HM, Murphy HA (1995) Differentiation of short-wavelength-sensitive cones by NADPH diaphorase histochemistry. Proc Natl Acad Sci U S A. 92(11):5121-3.

Puller C, Ondreka K, Haverkamp S (2011) Bipolar cells of the ground squirrel retina. J Comp Neurol. 519(4):759-74. doi: 10.1002/cne.22546.

Reichenbach and Robinson (1995) The involvement of Müller cells in the outer retin. In: Neurobiology and Clinical Aspects of the Outer Retina. Editors: Djamgoz MBA, Archer SN, Vallerga S. Springer, Dordrecht. pp 395-416

Ribic A, Liu X, Crair MC, Biederer T (2014) Structural organization and function of mouse photoreceptor ribbon synapses involve the immunoglobulin protein synaptic cell adhesion molecule 1. J Comp Neurol.522(4):900-20. doi: 10.1002/cne.23452.

Riesenberg AN, Liu Z, Kopan R, Brown NL (2009) Rbpj cell autonomous regulation of retinal ganglion cell and cone photoreceptor fates in the mouse retina. J Neurosci. 29(41):12865-77. doi: 10.1523/JNEUROSCI.3382-09.2009.

Ritchie ME, Phipson B, Wu D, Hu Y, Law CW, Shi W and Smyth GK (2015) Limma powers differential expression analyses for RNA-sequencing and microarray studies. Nucleic Acids Research, 43(7), pp. e47.

Robinson MD, McCarthy DJ, Smyth GK (2010). edgeR: a Bioconductor package for differential expression analysis of digital gene expression data. Bioinformatics, 26(1), pp. 139-140.

Sajdak B, Sulai YN, Langlo CS, Luna G, Fisher SK, Merriman DK, Dubra A (2016) Noninvasive imaging of the thirteen-lined ground squirrel photoreceptor mosaic. Vis Neurosci. 33:e003. doi: 10.1017/S0952523815000346.

Saxonov S, Berg P, Brutlag DL (2006) A genome-wide analysis of CpG dinucleotides in the human genome distinguishes two distinct classes of promoters. Proc Natl Acad Sci U S A. 103(5):1412-7.

Schindelin J, Arganda-Carreras I, Frise E et al. (2012) Fiji: an open-source platform for biological-image analysis. Nature methods 9(7): 676-682. PMID 22743772

Schindelin J, Rueden, CT, Hiner MC et al. (2015) The ImageJ ecosystem: An open platform for biomedical image analysis. Molecular Reproduction and Development. PMID 26153368

Shanker S, Paulson A, Edenberg HJ, Peak A, Perera A, Alekseyev YO, Beckloff N, Bivens NJ, Donnelly R, Gillaspy AF, Grove D, Gu W, Jafari N, Kerley-Hamilton JS, Lyons RH, Tepper C, Nicolet CM (2015) Evaluation of commercially available RNA amplification kits for RNA sequencing using very low input amounts of total RNA. J Biomol Tech. 26(1):4-18. doi: 10.7171/jbt.15-2601-001.

Sharma RK, O'Leary TE, Fields CM, Johnson DA (2003) Development of the outer retina in the mouse. Brain Res Dev Brain Res. 145(1):93-105.

Shekhar K, Lapan SW, Whitney IE, Tran NM, Macosko EZ, Kowalczyk M, Adiconis X, Levin JZ5, Nemesh J, Goldman M, McCarroll SA, Cepko CL, Regev A, Sanes JR (2016) Comprehensive Classification of Retinal Bipolar Neurons by Single-Cell Transcriptomics. Cell. 166(5):1308-1323.e30. doi: 10.1016/j.cell.2016.07.054.

Shilatifard A, Duan DR, Haque D, Florence C, Schubach WH, Conaway JW, Conaway RC (1997) ELL2, a new member of an ELL family of RNA polymerase II elongation factors. Proc Natl Acad Sci U S A.94(8):3639-43.

Shingai T, Ikeda W, Kakunaga S, Morimoto K, Takekuni K, Itoh S, Satoh K, Takeuchi M, Imai T, Monden M, Takai Y (2003) Implications of nectin-like molecule-2/IGSF4/RA175/SgIGSF/TSLC1/SynCAM1 in cell–cell adhesion and transmembrane protein localization in epithelial cells. J Biol Chem 278:35421–35427

Sidman RL (1961) Histogenesis of mouse retina studied with thymidine-H3. In: The Structure of the Eye. pp. 487-505. Editor: Smelser GK, Academic Press, New York

Smiley S, Nickerson PE, Comanita L, Daftarian N, El-Sehemy A, Tsai EL, Matan-Lithwick S, Yan K1, Thurig S, Touahri Y, Dixit R, Aavani T, De Repentingy Y, Baker A, Tsilfidis C, Biernaskie J, Sauvé Y, Schuurmans C, Kothary R, Mears AJ, Wallace VA (2017) Establishment of a cone photoreceptor transplantation platform based on a novel cone-GFP reporter mouse line. Sci Rep. 6:22867. doi: 10.1038/srep22867.

Soneson C, Love MI, Robinson MD (2015). Differential analyses for RNA-seq: transcript-level estimates improve gene-level inferences. F1000Research, 4. doi: 10.12688/f1000research.7563.1.

Springer MS, Gatesy J (2016) The gene tree delusion. Mol Phylogenet Evol. 94(Pt A):1-33. doi: 10.1016/j.ympev.2015.07.018.

Surace EI, Strickland A, Hess RA, Gutmann DH, Naughton CK (2006) Tslc1 (nectin-like molecule-2) is essential for spermatozoa motility and male fertility. J Androl. 2006 Nov-Dec;27(6):816-25.

Swaroop A, Kim D, Forrest D (2010) Transcriptional regulation of photoreceptor development and homeostasis in the mammalian retina. Nat Rev Neurosci. 11(8):563-76. doi: 10.1038/nrn2880.

Tachibanaki S, Tsushima S, Kawamura S (2001) Low amplification and fast visual pigment phosphorylation as mechanisms characterizing cone photoresponses. Proc Natl Acad Sci U S A. 98(24):14044-9.

Takahashi H, Katayama K, Sohya K, Miyamoto H, Prasad T, Matsumoto Y, Ota M, Yasuda H, Tsumoto T, Aruga J, Craig AM (2012) Selective control of inhibitory synapse development by Slitrk3-PTPδ trans-synaptic interaction. Nat Neurosci. 15(3):389-98, S1-2. doi: 10.1038/nn.3040.

Tran TL, Hamann S, Heegaard S (2017) Aquaporins in the Eye. Adv Exp Med Biol. 969:193-198. doi: 10.1007/978-94-024-1057-0_12.

Van Breukelen F, Martin SL (2015) The Hibernation Continuum: Physiological and Molecular Aspects of Metabolic Plasticity in Mammals. Physiology (Bethesda). 30(4):273-81. doi: 10.1152/physiol.00010.2015.

Wang H, Wan H, Li X, Liu W, Chen Q, Wang Y, Yang L, Tang H, Zhang X, Duan E, Zhao X, Gao F, Li W (2014) Atg7 is required for acrosome biogenesis during spermatogenesis in mice. Cell Res. 24(7):852-69. doi: 10.1038/cr.2014.70. Epub 2014 May 23.

Warnes GR, Bolker B, Bonebakker L, Gentleman R, Huber W, Liaw A, Lumley T, Maechler M, Magnusson A, Moeller S, Schwartz M, Venables B (2016) gplots: Various R programming tools for plotting data. R package. cran.r-project.org/

Wässle H, Grünert U, Martin PR, Boycott BB (1994) Immunocytochemical characterization and spatial distribution of midget bipolar cells in the macaque monkey retina. Vision Res.34(5):561-79.

Yang J, Pawlyk B, Wen XH, Adamian M, Soloviev M, Michaud N, Zhao Y, Sandberg MA, Makino CL, Li T (2007) Mpp4 is required for proper localization of plasma membrane calcium ATPases and maintenance of calcium homeostasis at the rod photoreceptor synaptic terminals. Hum Mol Genet. 16(9):1017-29.

Yang J, Zhao JJ, Zhu Y, Xiong W, Lin JY, Ma X (2008) Identification of candidate cancer genes involved in human retinoblastoma by data mining. Childs Nerv Syst. 24(8):893-900. doi: 10.1007/s00381-008-0595-7.

Yaron O, Farhy C, Marquardt T, Applebury M, Ashery-Padan R (2006) Notch1 functions to suppress cone-photoreceptor fate specification in the developing mouse retina. Development. 133(7):1367-78.

Young RW (1985) Cell differentiation in the retina of the mouse. Anat Rec. 212(2):199-205.

Yu W, Mookherjee S, Chaitankar V, Hiriyanna S, Kim JW, Brooks M, Ataeijannati Y, Sun X, Dong L, Li T, Swaroop A, Wu Z (2017) Nrl knockdown by AAV-delivered CRISPR/Cas9 prevents retinal degeneration in mice. Nat Commun. 8:14716. doi: 10.1038/ncomms14716.

Yuan L, Arikkath J (2017) Functional roles of p120ctn family of proteins in central neurons. Semin Cell Dev Biol. 69:70-82. doi: 10.1016/j.semcdb.2017.05.027. Review.

Additional resources

Mouse RNA-seq data: Forrest D, accession number GSE95016. NCBI Gene Omnibus (GEO). ncbi.nlm.nih.gov/geo/

NIH Biowulf2 computer cluster. hpc.nih.gov

NCBI BLST - Basic Local Alignment Search Tool blast.ncbi.nlm.nih.gov/

Protein and mRNA expression profiles in *Homo sapiens*: The Human Protein Atlas. proteinstlas.org/

UCSC Genome Browser. genome.ucsc.edu/

6 Supplement

6.1 False alignments (3.2.4)

Calu and Tex28, genes that seemed to be highly expressed in my database, were identified as false-positives. By visualizing the individual reads of these genes, I observed that these reads most likely belonged to S-opsin, respectively M-opsin. Both 3' ends of Calu and Tex28 overlap with one of the opsin genes on the genome. The reads that were assigned to these genes only appeared in these overlapping areas, no other exon was covered. A strong indication for the false assignment was the shape of coverage in these areas (figure 29). The poly A-based enrichment method that was used to generate cDNA has been reported to show a significant 3′ bias (Shanker et al., 2015). An additional factor are partially degraded mRNA fragments. This means, the cDNA libraries are enriched for 3'-ends of each transcript. When looking at the aligned reads, this looks like a wave-shaped coverage, with the peak of the wave at the very end of the last exon of a given gene. With this in mind, I can assign all reads in these overlapping areas to the opsin genes and remove Calu and Tex28 from my list of genes. All genes at the top of my list were manually checked to rule out other false alignments.

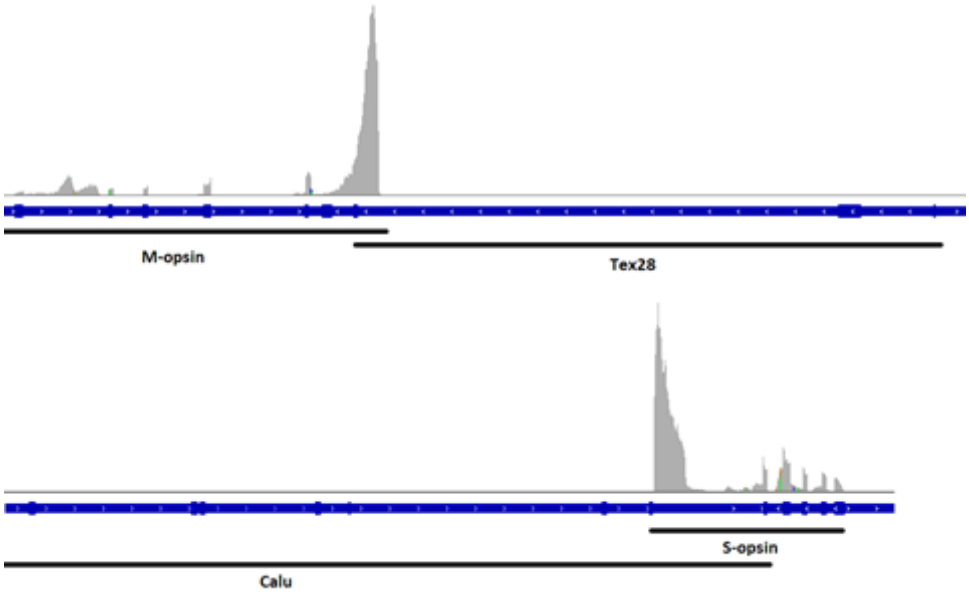

Figure 29 S-opsin and M-opsin reads aligned to the squirrel genome.

6.2 AAV inserts

6.2.1 CMV-eGFP insert

CMV-eGFP (eGFP with an upstream CMV-promoter) sequence that was delivered via AAV2 or AAV8. The AAV vectors and sequence information were kindly provided by Zhijian Wu (NEI/NIH). Highlighted are the CMV-promoter and the start codon of eGFP.

GGCCGCACGCGTGGAGCTAGTTATTAATAGTAATCAATTACGGGGTCATTAGTTCATAGC
CCATATATGGAGTTCCGCGTTACATAACTTACGGTAAATGGCCCGCCTGGCTGACCGCCC
AACGACCCCCGCCCATTGACGTCAATAATGACGTATGTTCCCATAGTAACGCCAATAGGG
ACTTTCCATTGACGTCAATGGGTGGAGTATTTACGGTAAACTGCCCACTTGGCAGTACAT
CAAGTGTATCATATGCCAAGTACGCCCCCTATTGACGTCAATGACGGTAAATGGCCCGCC
TGGCATTATGCCCAGTACATGACCTTATGGGACTTTCCTACTTGGCAGTACATCTAGTAT
TAGTCATCGCTATTACCATGGTGATGCGGTTTTGGCAGTACATCAATGGGCGTGGATAGC
GGTTTGACTCACGGGGATTTCCAAGTCTCCACCCCATTGACGTCAATGGGAGTTTGTTTT
GGCACCAAAATCAACGGGACTTTCCAAAATGTCGTAACAACTCCGCCCCATTGACGCAAA
TGGGCGGTAGGCGTGTACGGTGGGAGGTCTATATAAGCAGAGCTCGTTTAGTGAACCGTC
AGATCGCCTGGAGACGCCATCCACGCTGTTTTGACCTCCATAGAAGACACCGGGACCGAT
CCAGCCTCCGCGGCCGGGAACGGTGCATTGGAACGCGGATTCCCCGTGCCAAGAGTGACG
TAAGTACCGCCTATAGAGTCTATAGGCCCACCCCCTTGCTTTTATTTTTTGGTTGGGATA
AGGCTGGATTATTCTGAGTCCAAGCTAGGCCCTTTTGCTAATCATCTTCATACCTCTTAT
CTTCCTCCCACAGCTCCTGGGCAACGTGCTGGTCTGTGTGCTGGCCCATCACTTTGGCAA
AGAATTATCGATAGCCACCATGGTGAGCAAGGGCGAGGAGCTGTTCACCGGGGTGGTGCC
CATCCTGGTCGAGCTGGACGGCGACGTAAACGGCCACAAGTTCAGCGTGTCCGGCGAGGG
CGAGGGCGATGCCACCTACGGCAAGCTGACCCTGAAGTTCATCTGCACCACCGGCAAGCT
GCCCGTGCCCTGGCCCACCCTCGTGACCACCCTGACCTACGGCGTGCAGTGCTTCAGCCG
CTACCCCGACCACATGAAGCAGCACGACTTCTTCAAGTCCGCCATGCCCGAAGGCTACGT
CCAGGAGCGCACCATCTTCTTCAAGGACGACGGCAACTACAAGACCCGCGCCGAGGTGAA
GTTCGAGGGCGACACCCTGGTGAACCGCATCGAGCTGAAGGGCATCGACTTCAAGGAGGA
CGGCAACATCCTGGGGCACAAGCTGGAGTACAACTACAACAGCCACAACGTCTATATCAT
GGCCGACAAGCAGAAGAACGGCATCAAGGTGAACTTCAAGATCCGCCACAACATCGAGGA

CGGCAGCGTGCAGCTCGCCGACCACTACCAGCAGAACACCCCCATCGGCGACGGCCCCGT
GCTGCTGCCCGACAACCACTACCTGAGCACCCAGTCCGCCCTGAGCAAAGACCCCAACGA
GAAGCGCGATCACATGGTCCTGCTGGAGTTCGTGACCGCCGCCGGGATCACTCTCGGCAT
GGACGAGCTGTACAAGTAACTCGAGAGATCTAATCTCGCTTTCTTGCTGTCCAATTTCTA
TTAAAGGTTCCTTTGTTCCCTAAGTCCAACTACTAAACTGGGGGATATTATGAAGGGCCT
TGAGCATCTGGATTCTGCCTAATAAAAAACATTTATTTTCATTGCAATGATGTATTTAAA
TTATTTCTGAATATTTTACTAAAAAGGGAATGTGGGAGGTCAGTGCATTTAAAACATAAA
GAAAGTAGGG

6.2.2 RK-eGFP insert

RK-eGFP (Rhodopsin kinase-promoter and eGFP) sequence that was delivered via AAV8. The AAV vector and sequence information were kindly provided by Zhijian Wu (NEI/NIH). Highlighted are the RK-promoter and the start codon of eGFP.

GGCCGCTGGGCCCCAGAAGCCTGGTGGTTGTTTGTCCTTCTCAGGGGAAAAGTGAGGCGG
CCCCTTGGAGGAAGGGGCCGGGCAGAATGATCTAATCGGATTCCAAGCAGCTCAGGGGAT
TGTCTTTTTCTAGCACCTTCTTGCCACTCCTAAGCGTCCTCCGTGACCCCGGCTGGGATT
TAGCCTGGTGCTGTGTCAGCCCCGGGCTCCCAGGGGCTTCCCAGTGGTCCCCAGGAACCC
TCGACAGGGCCAGGGCGTCTCTCTCGTCCAGCAAGGGCAGGGACGGGCCACAGGCCAAGG
GCCGCGGCCGGGAACGGTGCATTGGAACGCGGATTCCCCGTGCCAAGAGTGACGTAAGTA
CCGCCTATAGAGTCTATAGGCCCACCCCCTTGCTTTTATTTTTTGGTTGGGATAAGGCTG
GATTATTCTGAGTCCAAGCTAGGCCCTTTTGCTAATCATCTTCATACCTCTTATCTTCCT
CCCACAGCTCCTGGGCAACGTGCTGGTCTGTGTGCTGGCCCATCACTTTGGCAAAGAATT
ATCGATAGCCACCATGGTGAGCAAGGGCGAGGAGCTGTTCACCGGGGTGGTGCCCATCCT
GGTCGAGCTGGACGGCGACGTAAACGGCCACAAGTTCAGCGTGTCCGGCGAGGGCGAGGG
CGATGCCACCTACGGCAAGCTGACCCTGAAGTTCATCTGCACCACCGGCAAGCTGCCCGT
GCCCTGGCCCACCCTCGTGACCACCCTGACCTACGGCGTGCAGTGCTTCAGCCGCTACCC
CGACCACATGAAGCAGCACGACTTCTTCAAGTCCGCCATGCCCGAAGGCTACGTCCAGGA
GCGCACCATCTTCTTCAAGGACGACGGCAACTACAAGACCCGCGCCGAGGTGAAGTTCGA
GGGCGACACCCTGGTGAACCGCATCGAGCTGAAGGGCATCGACTTCAAGGAGGACGGCAA
CATCCTGGGGCACAAGCTGGAGTACAACTACAACAGCCACAACGTCTATATCATGGCCGA

CAAGCAGAAGAACGGCATCAAGGTGAACTTCAAGATCCGCCACAACATCGAGGACGGCAG
CGTGCAGCTCGCCGACCACTACCAGCAGAACACCCCCATCGGCGACGGCCCCGTGCTGCT
GCCCGACAACCACTACCTGAGCACCCAGTCCGCCCTGAGCAAAGACCCCAACGAGAAGCG
CGATCACATGGTCCTGCTGGAGTTCGTGACCGCCGCCGGGATCACTCTCGGCATGGACGA
GCTGTACAAGTAACTCGAGAGATCTAATCTCGCTTTCTTGCTGTCCAATTTCTATTAAAG
GTTCCTTTGTTCCCTAAGTCCAACTACTAAACTGGGGGATATTATGAAGGGCCTTGAGCA
TCTGGATTCTGCCTAATAAAAAACATTTATTTTCATTGCAATGATGTATTTAAATTATTT
CTGAATATTTTACTAAAAAGGGAATGTGGGAGGTCAGTGCATTTAAAACATAAAGAAAGT
AGGGG

Acknowledgments

I would like to thank my mentors and academic supervisors Wei Li and Karl Koch, and the most supportive co-worker one can wish for, Juan Angueyra, for their support and guidance. I thank my family for all their help and my friends who accompanied me through the years.

Further, I would like to thank the people who supported me on the path towards this thesis, both before and during my time at the NIH: Alex Scholten, David Schneeweis, Douglas Forrest, Eileen Nguyen, Fengyu Qiao, Francisco Nadal, Fritz and Viola Kretschmer, Gail Seabold, Hong Liu, Jacob Nellissery, Jennifer Zhu, Jingxing Ou, John Ball, Jutta Appelt, Jutta Kretzberg, Karin Dedek, Katherine Chuang, Li Jia, Matthew Brooks, Michael Müller, Michihiko Arakami , Shan Chen, Susan Dailey, Szilard Sajgo, Tantai Zhao, Thad Whitaker, Werner Säftel, Xuefeng Wu, Yizhen Zhang, Yong-Gang Yao, Yufeng Xu, Zhi Xie, Zhijian Wu.

List of most frequently used words; wordcloud.com

Curriculum vitae

Vincent P. Kunze

EDUCATION

2014– present National Eye Institute (NIH), USA. Graduate student (Graduate Partnerships Program) in cooperation with Prof. Dr. Karl-Wilhelm Koch (Biochemistry group, University of Oldenburg, Germany). Lab: Retinal Neurophysiology Section (Wei Li).

2010– 2013 Master of Science in biology. Carl von Ossietzky University of Oldenburg, Germany. Master thesis: "The cone-specific guanylate cyclase 3 of the zebrafish retina" (in German language) in the lab of Prof. Dr. Koch (Biochemistry, University of Oldenburg).

2007– 2010 Bachelor of Science in biology. Carl von Ossietzky University of Oldenburg, Germany. Bachelor thesis: "Signaling proteins in the outer plexiform layer of the vertebrate retina" (in German language) in the lab of Prof. Dr. Koch (Biochemistry, University of Oldenburg).

1999– 2006 High school - Ubbo-Emmius-Gymnasium Leer (Ostfriesland)

1997– 1999 Orientation stage - Carl-Goerdeler-school Jemgum

1993– 1997 Primary school Jemgum-Ditzum

ADVANCED EDUCATION

2015 - 2017 Leadership Series. Lori Conlan. Office of Intramural Training & Education (OITE), NIH campus Bethesda.

- Workplace Dynamics I/II: Self-Awareness, the key to professional success
- Workplase Dynamics III: Conflict & Feedback
- Workplace Dynamics IV: Team Skills
- Workplace Dynamics V: Diversity in a Multicultural Society

2016 GRAD 500 Writing and Publishing a Scientific Paper Workshop. Marguerite Meitzler Foundation for Advanced Education in the Sciences (FAES), NIH campus Bethesda

2015 Scientists Teaching Science. Barbara Houtz. Office of Intramural Training & Education (OITE), NIH campus Bethesda

RESEARCH AND TEACHING EXPERIENCE

2017 Supervised a summer student in Dr. Wei Li's lab (Retinal Neurophysiology Section, NEI, NIH). Project: Cone-specific gene expression in the vertebrate retina

2016 Supervised a summer student in Dr. Wei Li's lab (Retinal Neurophysiology Section, NEI, NIH). Project: Morphological changes during development of the cone-dominated retina of the tree shrew.

2013 Co-supervised an undergraduate student's bachelor thesis under Prof. Dr. Kretzberg (Computational Neuroscience, University of Oldenburg). Topic: Optomotor responses of GluR4 deficient mice.

2011 – 2013 Research assistant for Prof. Dr. Kretzberg (Computational Neuroscience, University of Oldenburg). Tasks: Behavioral experiments with mice using the optomotor response arena by Dr. Kretschmer.

2011 – 2013 Graduate teaching assistant in principles of biochemistry (Prof. Dr. Koch, Biochemistry, University of Oldenburg). Tasks: Taught undergraduate students in biochemical calculations and revised lectures.

2011 – 2012 Graduate teaching assistant in neurobiology lab courses: "Electrical signals of nerve cells" (Prof. Dr. Ammermueller, Neurobiology, University of Oldenburg) and "G protein coupled receptors and G proteins" (Prof. Dr. Koch, Biochemistry, University of Oldenburg).

2012 Internship in the Molecular and Industrial Biotechnology Group of Pere Garriga at the UPC (Universitat de Polytèchnica de Catalunya) in Terrassa (Spain), funded by the EU ("ERASMUS Student mobility for placements").

2010 Undergraduate teaching assistant in multiple lab courses

- Principles of biochemistry (Prof. Dr. Koch, Biochemistry, University of Oldenburg)
- Principles of neurobiology lab course: "G protein coupled receptors and G proteins" (Prof. Dr. Koch, Biochemistry, University of Oldenburg)

RESEARCH SKILLS

- Single cell RNA-sequencing and data analysis
- Single cell isolation
- Heterologous protein expression
- Cell culture
- FPLC
- SDS-PAGE
- UV/VIS-Spectroscopy measurements
- Mouse colony management
- In situ hybridization
- Immunohistochemistry
- Molecular cloning
- Handling of radiolabeled substances
- HPLC
- Western blotting
- Mouse optomotor response

AWARDS

2017 NIH FARE award winner. Fellows' award for research excellence. Bethesda, Maryland, USA

2017 Travel award, FASEB research conference The Biology & Chemistry of Vision. Steamboat Springs, Colorado, USA

2016 Award for best contribution at the 2nd European Meeting on Phototransduction. Congressi Stefano Franscini, ETH Zürich, Monte Verita, Switzerland.

PUBLICATIONS AND PRESENTATIONS

2017 Kunze VP, Angueyra JM, Li J, Puller C, Li W. Genetic Profiling of Photoreceptors – Determination of S- and M-Cone Identity. Selected data blitz presentation at the FASEB conference on the Biology & Chemistry of Vision. Steamboat Springs, Colorado, USA

2017 Luan Y, Ou J, Kunze VP, Qiao F, Wang Y, Wei L, Li W, Xie Z. Integrated transcriptomic and metabolomic analysis reveals adaptive changes of hibernating retinas. J Cell Physiol. doi: 10.1002/jcp.26030.

2016 Kunze VP, Angueyra JM, Li J, Puller C, Li W. Genetic Profiling of Sensory Neurons – Determination of S- and M-Cone Identity. Talk at the National Eye Institute Focus on Fellows, NIH, Bethesda, Maryland, USA.

2016 Kunze VP, Angueyra JM, Li J, Puller C, Li W. Determination of S- and M-Cone Identity -Genetic Profiling of Cone Types in the Ground Squirrel Retina. Selected talk at the 2nd European Meeting on Phototransduction, Congressi Stefano Franscini, ETH Zürich, Monte Verita, Switzerland. Keystone, Colorado, USA

2013 Kretschmer F, Kretschmer V, Kunze VP, Kretzberg J. OMR-Arena: Automated Measurement and Stimulation System to Determine Mouse Visual Thresholds Based on Optomotor Responses. PLoS ONE 8(11): e78058. doi:10.1371/journal.pone.0078058

2013 Kunze VP, Fries R, Koch KW. Cone specific guanylate cyclase 3 of the zebrafish retina –heterologous expression in mammalian cells. Conference poster at the European Meeting on Phototransduction, Delmenhorst, Germany.

2010 Müller M, Kunze VP, Koch KW. Signaling components of the mGluR6 pathway in on-bipolar cells of the bovine retina. Conference poster at the 5th Westerberg meeting on Molecular Neurobiology: Pathways in Health and Disease, Osnabrueck, Germany.

Erklärung

Hiermit versichere ich, dass ich diese Arbeit selbstständig verfasst und keine anderen als die angegebenen Quellen und Hilfsmittel verwendet habe. Außerdem versichere ich, dass ich die allgemeinen Prinzipien wissenschaftlicher Arbeit und Veröffentlichung, wie sie in den Leitlinien guter wissenschaftlicher Praxis der Carl von Ossietzky Universität Oldenburg festgelegt sind, befolgt habe.